Modeling the Impact of Irrigation on Precipitation over the Great Plains

A THESIS
SUBMITTED TO THE FACULTY OF THE GRADUATE SCHOOL
OF THE UNIVERSITY OF MINNESOTA
BY

Keith John Iliff Harding

IN PARTIAL FULFILLMENT OF THE REQUIREMENTS
FOR THE DEGREE OF
MASTER OF SCIENCE

Peter Snyder

August 2011

Acknowledgments

I would like to thank everyone in my research group for providing a very enjoyable and productive environment. The light-hearted nature of everyone in the group provided a good environment in which to thrive. Thank you to Dr. Peter Snyder and Dr. Tracy Twine for helping me on this project. I would especially like to thank Dr. Snyder for his guidance as my advisor. It has been extremely enjoyable to work with him on this project and I look forward to working with him in the future. I would also like to thank Jarod Bryant, Hong Xu, and Stefan Liess for being supportive, helpful, and enjoyable to be around. Your help on a daily basis regarding large and small problems kept me on track and guided me through my studies.

I would like to thank Dr. Francina Dominguez for providing programming code for use in precipitation recycling calculations and for general guidance at AGU 2011 in San Francisco. Thank you to Dr. Mutlu Ozdogan for providing the MODIS fractional irrigation dataset.

Thank you to my committee for providing me with assistance in writing my thesis and guiding me through this process. I appreciate all of your help. Thank you Dr. Snyder, Dr. Twine, and Dr. Jason Hill.

On a personal note, I would like to thank my wife, Kelly, for her never-ending support and love through this project and all of my scholarly endeavors. Thank you to my daughter Jade, whose arrival near the end of this project has given me plenty of wonderful and peaceful moments. I would to thank my family, Loretta, Ian, and Gillian Harding for their support and everything they have done for me through the years.

Abstract

Since World War II, the rapid expansion of irrigation throughout the Great Plains has threatened the sustainability of the Ogallala Aquifer. Irrigation has been shown to modify the surface energy and water budgets over the Great Plains by altering the partitioning of latent and sensible heating. An increase in latent heating from irrigation contributes to a cooler and more humid surface, which has competing impacts on convection. In this study, the Weather Research and Forecasting model was modified to simulate the effects of irrigation at sub-grid scales. Nine April-October simulations were completed for different hydrologic conditions over the Great Plains. Data from these simulations was assimilated into a back-trajectory analysis to identify where evapotranspired moisture from irrigated fields predominantly falls out as precipitation. May through September precipitation increased on average over the Great Plains by 4.97 mm (0.91%), with the largest increases during wet years (6.14 mm; 0.98%) and the smallest increases during drought years (2.85 mm; 0.63%). Large precipitation increases occurred over irrigated areas during normal and wet years, with decreases during drought years. On average, only 15.8% of evapotranspired moisture from irrigated fields fell out as precipitation over the Great Plains, resulting in 5.11 mm of May-September irrigation-induced precipitation. The heaviest irrigation-induced precipitation occurred over north-central Nebraska, coincident with simulated and observed precipitation increases. While irrigation resulted in localized and region-wide increases in precipitation, large evapotranspiration increases suggest that irrigation contributes to a net loss of water in the Great Plains.

Table of Contents

Acknowledgments i
Abstract ii
List of Tables v
List of Figures vii
1. Introduction 1
2. General Impacts of Irrigation on Precipitation and the Energy Budget 7
2.1 Overview 8
2.2 Introduction 9
2.3 Methods 15
2.3.1 WRF/Noah Model Description 15
2.3.2 Irrigation Representation 16
2.3.3 Experimental Design 18
2.3.4 Statistical Significance 20
2.4 Results 21
2.4.1 Model Validation 21
2.4.2 Overall Model Results 22
2.4.3 Comparison of Precipitation Regimes 24
2.4.4 Comparison of ENSO Regimes 27
2.4.5 Sensitivity Simulations from time-decay irrigation technique 28
2.5 Discussion 29
2.5.1 Comparison to previous studies 29
2.5.2 Comparison with Offline Simulations 31
2.5.3 Overall Impact of Irrigation on Great Plains Precipitation 32
2.6 Conclusions 35
2.7 Acknowledgments 37
3. The Precipitation of Irrigated Water and Changes in Precipitation Recycling 38
3.1 Overview 39
3.2 Introduction 40
3.3 Methods 45

3.3.1 WRF/Noah LSM Model Description **45**
3.3.2 Irrigation Representation **45**
3.3.3 Determination of Irrigation-Induced Precipitation from Backward Trajectory Analysis **46**
3.3.4 Precipitation Recycling **48**
3.3.5 Experimental Design **51**
3.3.6 Statistical Significance **53**
3.4 Results **53**
3.4.1 Irrigation-Induced Precipitation **53**
3.4.2 Precipitation Recycling **57**
3.5 Discussion **60**
3.5.1 Comparison to previous studies **60**
3.5.2 Discussion of Model Results **62**
3.6 Conclusions **67**
3.7 Acknowledgments **69**
4. Conclusion **70**
4.1 Future Work **74**
Tables **77**
Figures **85**
Bibliography **104**

List of Tables

Table 1. Summary of simulated years, precipitation regimes, and ENSO regimes. 77

Table 2. May-September and June-July-August (JJA) weighted averages of differences between control and irrigated simulations for all simulated years. Weighted averages were calculated for the region of study and for grid cells with at least 10% irrigation within the region of study. Significance values for paired t-tests are as follows: * ($p < 0.1$), ** ($p < 0.05$), *** ($p < 0.01$). 78

Table 3. May-September weighted averages of differences between control and irrigated simulations for all, drought, normal, and pluvial years. Weighted averages were calculated for the region of study and for grid cells with at least 10% irrigation within the region of study. Significance values for paired t-tests are as follows: * ($p < 0.1$), ** ($p < 0.05$), *** ($p < 0.01$). 79

Table 4. May-September weighted averages of differences between control and irrigated simulations for all, El Niño, neutral, and La Niña years. Weighted averages were calculated for region of study and for grid cells with at least 10% irrigation within region of study. Significance values for paired t-tests are as follows: * ($p < 0.1$), ** ($p < 0.05$), *** ($p < 0.01$)..... 80

Table 5. Weighted area average of irrigation-induced precipitation (mm) over the region of study from grid cells with at least 10% irrigation fraction. Significance values for paired t tests are as follows: * ($p < 0.1$), ** ($p < 0.05$), *** ($p < 0.01$). 81

Table 6. Recycling ratio calculated from control simulations using the approach of Dominguez et al. (2006). Recycling ratio calculated for the domain shown in Figure 3b..... 81

Table 7. Recycling ratio calculated from control simulations using the approach of Brubaker et al. (2001). Recycling ratio calculated for the domain shown in Figure 3b..... 82

Table 8. Difference in recycling ratio (Irrigation (IRRIG) minus control (CONTROL)) using the approach of Dominguez et al. (2006). Recycling ratio calculated for the domain shown in Figure 3b. Significance values for paired t tests are as follows: * ($p < 0.1$), ** ($p < 0.05$), *** ($p < 0.01$). 82

Table 9. Difference in recycling ratio (IRRIG minus CONTROL) using the approach of Brubaker et al. (2001). Recycling ratio calculated for the domain shown in Figure 3b. Significance values for paired t tests are as follows: * ($p < 0.1$), ** ($p < 0.05$), *** ($p < 0.01$)..... 83

Table 10. Difference (IRRIG minus CONTROL) in simulated precipitation, irrigation-induced precipitation, recycled precipitation, and ET averaged over June-August and May-September. All values are calculated over the recycling region as depicted in Figure 3b. Recycled precipitation change is the average recycled precipitation change based on approaches from Dominguez et al. (2006) and Brubaker et al. (2001). Significance values for paired t tests are as follows: * ($p < 0.1$), ** ($p < 0.05$), *** ($p < 0.01$). 84

List of Figures

Figure 1. Groundwater pumpage for irrigation from 1949 to 1995 in the Great Plains states (McGuire et al. 2003). 85

Figure 2. Water level changes in the Ogallala Aquifer, predevelopment to 2005 (McGuire 2007). 86

Figure 3. (a) MODIS Land Use Category that is input to WRF model and (b) irrigated fraction from Ozdogan and Gutman (2008) for WRF Model Domain. The region of study, shown in (b), is a subset of the WRF domain to minimize model edge effects and concentrate the impacts of irrigation. 87

Figure 4. Irrigation representation in the WRF Model. 88

Figure 5. (a) Average May-September simulated precipitation from WRF for all simulated years. (b) As (a) but for NARR observed precipitation. 89

Figure 6. (a) Latent heat flux observed at Ameriflux Mead Rainfed Site and simulated from WRF Model for 2008. (b) As (a) but observed at Ameriflux Mead Irrigated Rotation Site and simulated by WRF Model with irrigation. (c) Latent heat flux difference between Ameriflux Mead Irrigated Rotation and Rainfed sites (blue) and WRF irrigated and control simulations (red) for 2008. 90

Figure 7. (a) Average May-September irrigated (IRRIG) minus control (CTRL) simulated latent heat flux for all years. (b) As (a) but for sensible heat flux. (c) As (a) but for 2-m dew point temperature. (d) As (a) but for 2-m temperature. Differences are shown only for grid cells found to be significant using a two-tailed paired t-test at the 95% confidence level. 91

Figure 8. (a) Average May-September IRRIG minus CTRL simulated convective available potential energy (CAPE) for all years. (b) As (a) but for convective inhibition (CIN). (c) As (a) but for planetary boundary layer (PBL) height. (d) As (a) but for column precipitable water. Differences are shown only for grid cells found to be significant using a two-tailed, paired t-test at the 95% confidence level. 92

Figure 9. (a) Weighted average of IRRIG minus CTRL simulated precipitation (mm) in region of study (defined in Figure 3b) during JJA and May-September for drought, normal, pluvial, and all years. Error bars denote 95% confidence interval. (b) Average May-September CTRL simulated precipitation for all years. (c) Average May-September IRRIG minus CTRL simulated precipitation for all years. No differences in (c) were found to be statistically significant with 95% confidence from a two-tailed, paired t-test. 93

Figure 10. Weighted average of IRRIG minus CTRL simulated (a) volumetric soil moisture content, (b) latent heat flux, (c) sensible heat flux, (d) 2-m temperature, (e) 2-m dew point, (f) convective available potential energy (CAPE), (g) convective inhibition (CIN) (h) planetary boundary layer (PBL) height, (i) 10-m convergence, (j) column precipitable water, and (k) precipitation as a function of grid cell irrigation fraction. Drought, normal, pluvial (flood), and all years are plotted as described in (a). Levels of statistical significance are noted on bars above each plot as described in (a). Only grid cells within the region of study were considered. 94

Figure 11. Weighted average of IRRIG minus CTRL simulated (a) volumetric soil moisture content, (b) latent heat flux, (c) sensible heat flux, (d) 2-m temperature, (e) 2-m dew point, (f) CAPE, (g) CIN, (h) planetary boundary layer height, (i) 10-m convergence, (j) column precipitable water, and (k) precipitation as a function of grid cell irrigation fraction. El Niño, neutral, La Niña, and all years are plotted as described in (a). Levels of statistical significance are noted on bars above each plot as described in (a). Only grid cells within the region of study were considered. 95

Figure 12. Weighted average of IRRIG minus CTRL simulated (a) volumetric soil moisture within the region of study for simulations of original irrigation method (ORIGINAL) and time-decay irrigation method (DECAY). (b) As (a) but for latent heat flux with the inclusion of offline simulations as described in section 2.5.2. (c) As (a) but for planetary boundary layer (PBL) height. (d) As (a) but for precipitation. 96

Figure 13. Average May-September IRRIG minus CTRL simulated latent heat flux for all simulated years using offline simulations that employed (a) the DECAY irrigation technique from section 2.4.5 and (b) the ORIGINAL irrigation technique from section 2.3.2. 97

Figure 14. Average May-September irrigation-induced precipitation (mm) from grid cells with at least 10% irrigation fraction for (a) all simulated years, (b) drought years, (c) normal precipitation years, (d) pluvial years, (e) La Niña years, (f) neutral years, and (g) El Niño years. Hatched areas represent locations where irrigation-induced precipitation is significantly different than zero at the 95% confidence level. 98

Figure 15. May-September average moisture-weighted wind vectors and average irrigation-induced precipitation (mm) that originated from grid cells with at least 10% irrigation for all simulated years within the regions outlined in black in (a) through (e). Hatched areas represent locations where irrigation-induced precipitation is significantly different than zero at the 95% confidence level. 99

Figure 16. Average May-September 850 hPa wind speed (filled; ms^{-1}), geopotential height (contours; meters), and wind vectors (ms^{-1}) from irrigation simulations of (a)

all, (b) drought, (c) normal, (d) pluvial, (e) La Niña, (f) neutral, and (g) El Niño years. 100

Figure 17. Average 850 hPa wind speed (filled; ms^{-1}), geopotential height (contours; meters), and wind vectors (ms^{-1}) from irrigation simulations of all years for (a) May, (b) June, (c) July, (d) August, (e) September. 101

Figure 18. (a) Weighted average of the *origin* of irrigation-induced precipitation (mm) over the region of study as a function of grid cell irrigation percentage during May-September for all, drought, normal, and pluvial years. Values from each range of irrigation percentages represent the amount of precipitation that originated from ET in grid cells within that irrigation percentage range. Precipitation values are shown per 1000 grid cells to normalize values for each irrigation percentage group and give equal weight to groups with fewer grid cells. (b) Weighted average of the amount of irrigation-induced precipitation *received* as a function of grid cell irrigation percentage during May-September for all, drought, normal, and pluvial years. 102

Figure 19. (a) May-September average irrigation-induced precipitation over Nebraska (areal average of 9.11 mm over outlined area). (b) Simulated May-September average irrigated minus control precipitation over Nebraska (areal average of 8.96 mm over outlined area). (c) North-central Nebraska analysis region for COOP observed precipitation comparisons. The shaded region represents counties where the 1951-2000 precipitation is larger than the 1901-1950 precipitation using the COOP precipitation dataset from NCDC. The hatched regions represent counties where the difference is statistically significant at the 95% confidence level. 103

Chapter 1

Introduction

Since World War II, the rapid expansion of irrigation in the Great Plains has rapidly increased groundwater extraction in the region (Figure 1) (McGuire et al. 2003), resulting in significant stress on the Ogallala Aquifer – a vast, yet shallow, aquifer situated throughout much of the Great Plains. Water table declines of over 40 m (Figure 2) (McGuire 2007) have contributed to an increase in the cost of groundwater extraction (McGuire et al. 2003), jeopardizing the future ability of the Ogallala Aquifer to support agriculture. Future projections of increased drought prevalence and intensity in the Great Plains (Gregory et al. 1997; IPCC 2007; Kumar 2007; Manabe et al. 2004; Rind et al. 1990; Wang 2005; Wetherald and Manabe 1995, 1999) suggest the possibility of accelerated stress on the Ogallala Aquifer with continued irrigation. The fact that the Great Plains is part of the world's most productive agricultural region implies the need for sophisticated water management. Achieving more sophisticated water management in the Great Plains necessitates knowledge of the full impact that irrigation has on the hydrologic cycle. This study aims to better explain the impact that irrigation has on precipitation and the atmospheric branch of the hydrologic cycle, thereby allowing more sophisticated water management of the Ogallala Aquifer.

Numerous studies have attempted to determine the impact of irrigation on precipitation in the Great Plains through use of observational and modeling approaches. While observational studies have the advantage of not relying on simulated data to

explain mechanisms, the impact of irrigation cannot be fully isolated from climatic variations without using numerical models. Since the impact of irrigation on precipitation is non-local, a vast observational network is needed to capture changes in precipitation from irrigation over a large area. Because of the large inter-annual variability of regional precipitation over the Great Plains during the warm season, observed precipitation changes over this area cannot be explicitly attributed to irrigation. On the other hand, while modeling studies can hold otherwise varying climate factors constant and completely isolate the impact of irrigation, results tend to be highly dependent on model physics and parameterizations. Therefore, a combination of modeling and observational approaches is necessary to quantify the impact of irrigation on precipitation and the mechanisms responsible. While previous modeling studies have been broadly consistent in their findings, these studies relied on models that were not run at sufficiently high spatial resolution to adequately resolve small-scale land-atmosphere processes or were not implemented over a sufficiently long duration to determine the atmospheric impact of irrigation. This study uses a high-resolution coupled land-atmosphere model that can resolve precipitation processes and land-atmosphere interactions at a high spatial resolution. Simulations were completed over different years during the growing season and represent a range of climate conditions necessary for determining the impact of irrigation on the atmospheric branch of the hydrologic cycle in the Great Plains.

Irrigation primarily affects the hydrologic cycle of the Great Plains by enhancing evapotranspiration (ET) over irrigated fields, which modifies the atmospheric conditions that drive the development of convective precipitation. The rapid increase in irrigation

over the Great Plains in the 20th century has roughly doubled the amount of water that is available for ET within the domain of the Ogallala Aquifer (Moore and Rojstaczer 2001), resulting in considerable alteration of the surface energy budget (Pielke 2001). Large increases in latent heating (due to increases in ET) are compensated by decreases in sensible heating, contributing to changes in the surface temperature and moisture fields (Barnston and Schickedanz 1984; DeAngelis et al. 2010; Kueppers et al. 2007; Ozdogan et al. 2010; Pielke 2001; Sacks et al. 2009). Increases in latent heating at the expense of sensible heating result in a decrease in surface air temperature and an increase in surface humidity (Adegoke et al. 2003; Baidya Roy et al. 2003; Kueppers et al. 2007; Lobell et al. 2006; Mahmood et al. 2004; Mahmood et al. 2006; Sacks et al. 2009). Modification of the surface temperature and moisture fields from irrigation has competing effects on the development of convective precipitation. While increases in surface humidity enhance convective available potential energy (CAPE) and act to enhance convection (DeAngelis et al. 2010; Pielke 2001; Segal et al. 1998), surface cooling decreases the height on the planetary boundary layer (PBL) and suppresses convection (Barnston and Schickedanz 1984; Boucher et al. 2004; De Ridder and Gallee 1998; DeAngelis et al. 2010; Sacks et al. 2009). The net effect that irrigation has on convection is determined by the relative size of both forcings. A high-resolution coupled land-atmosphere model was used in this study to determine whether irrigation results in the enhancement or suppression of convection over the Great Plains. Simulations using the Weather Research and Forecasting (WRF) model (Skamarock et al. 2008) were completed both with and without irrigation for a suite of years representing different precipitation and El Niño-

Southern Oscillation (ENSO) regimes. Simulations were completed for the full spectrum of precipitation and ENSO conditions to determine the general impact of irrigation on the energy budget and hydrologic cycle in the Great Plains.

While the overall impact that irrigation has on precipitation is an important aspect of the hydrologic cycle, it is crucial to determine the amount of irrigated water that falls out as local precipitation, restoring groundwater supplies. This is especially vital because *most* of the water that is applied to irrigated fields is evapotranspired into the atmosphere rather than being lost through drainage (DeAngelis et al. 2010; Moore and Rojstaczer 2001). Data from the WRF simulations were used in coordination with a backward trajectory technique from Brubaker et al. (2001) to trace the path of irrigated water through the atmosphere and to quantify the distribution of precipitation that results from ET over irrigated fields (i.e. irrigation-induced precipitation). In doing so, the amount of irrigated water that returns to the region as precipitation can be identified. Similarly, the overall pattern of irrigation-induced precipitation and how it varies for different precipitation and ENSO regimes adds insight into the impact of irrigation on the hydrologic cycle. The methods used here provide for examination of exactly where water from irrigated fields in the Great Plains eventually falls as precipitation.

The backward trajectory technique used in this study traces the path of all evapotranspired water from the region of study, enabling the determination of recycled precipitation, which describes precipitation that falls within the same region in which it was originally evapotranspired (Brubaker et al. 1993; Brubaker et al. 2001; Dirmeyer et al. 2009; Dominguez et al. 2006; Zangvil et al. 2004). In this study, the impact of

irrigation on precipitation recycling will be examined to quantify the amount of local moisture that returns to the region as precipitation, a key component of the regional hydrologic cycle. Quantifying the impact of irrigation on precipitation recycling and determining the distribution of irrigation-induced precipitation allows for better understanding of the water cycle in the Great Plains, laying the groundwork for sophisticated water management of the Ogallala Aquifer in the 21st century. In providing a unique look at irrigation-induced precipitation and the impact of irrigation on precipitation recycling in the Great Plains, this study aims to improve understanding of the hydrologic cycle and offer improved management strategies for sustaining the Ogallala Aquifer, a critical source of groundwater in the region.

Chapter 2

General Impacts of Irrigation on Precipitation and the Energy Budget

Harding, K. J. and P. K. Snyder, *Journal of Hydrometeorology,* to be submitted

2.1 Overview

Since World War II, the expansion of irrigation throughout the Great Plains has resulted in a significant decline in the water table of the Ogallala Aquifer, threatening its long-term sustainability. The addition of near-surface water for irrigation has previously been shown to impact the surface energy and water budgets by modifying the partitioning of latent and sensible heating. A strong increase in latent heating drives near-surface cooling and an increase in humidity, which has competing impacts on the development of convective precipitation. In this study, the Weather Research and Forecasting (WRF) model was modified to simulate the effects of irrigation on precipitation. Using a satellite-derived fractional irrigation dataset, grid cells were divided into irrigated and non-irrigated segments and the near-surface soil layer within irrigated segments was held at saturation. Nine April through October periods (three drought, three normal, and three pluvial) were simulated over the Great Plains. May-September precipitation increased by 4.97 mm (0.91%), with localized increases of up to 20%. The largest precipitation increases occurred during pluvial years (6.14 mm; 0.98%) and the smallest increases occurred during drought years (2.85 mm; 0.63%). Over irrigated areas, precipitation increased by 7.86 mm (1.61%). Large precipitation increases occurred over irrigated areas during normal and pluvial years, while decreases occurred during drought years. This suggests the presence of a soil moisture threshold whereby irrigation results in the suppression of convection over irrigated areas when antecedent soil moisture is extremely low and the enhancement of convection when antecedent soil moisture is relatively high.

2.2 Introduction

The expansion of irrigation in the Great Plains since World War II has significantly affected the Ogallala Aquifer, jeopardizing the future viability of regional groundwater extraction. Large groundwater withdrawals from the Ogallala Aquifer have resulted in steep declines in the water table by more than 40 m (McGuire 2007), making water extraction for municipal and agricultural uses significantly more expensive (McGuire et al. 2003). Irrigation is heavily concentrated within and adjacent to the Ogallala Aquifer as identified by United States Department of Agriculture (USDA) and satellite-derived irrigation estimates (Ozdogan and Gutman 2008). In some areas within this region, up to 80% of the land has been changed from non-irrigated natural vegetation to irrigated agriculture since pre-development (Mahmood et al. 2006). This change has roughly doubled the amount of surface water available for evapotranspiration (ET) within the domain of the Ogallala Aquifer (Moore and Rojstaczer 2001). Most of the water applied to the surface through irrigation is evapotranspired to the atmosphere rather than running off the surface or being lost through drainage (DeAngelis et al. 2010; Moore and Rojstaczer 2001). Irrigation results in significant changes to the atmospheric branch of the hydrologic cycle as the evapotranspired water eventually falls out as precipitation. The goal of this study is to further explore the impact that irrigation has on the hydrologic cycle using a high-resolution coupled land-atmosphere model. Simulations using the Weather Research and Forecasting (WRF) model (Skamarock et al. 2008) were performed both with and without irrigation for a suite of years from different precipitation and El Niño-Southern Oscillation (ENSO) regimes. The simulated years

were chosen to capture the atmospheric response to irrigation over a wide range of climatic conditions that are experienced over the Great Plains.

The availability of such a large quantity of water available for ET has a sizeable effect on surface energy and water budgets (Pielke 2001). Increases in latent heating with additional water are offset by decreases in sensible heating, resulting in changes to the surface temperature and moisture fields (Barnston and Schickedanz 1984; DeAngelis et al. 2010; Kueppers et al. 2007; Ozdogan et al. 2010; Pielke 2001; Sacks et al. 2009). The repartitioning of sensible heating into latent heating decreases the surface air temperature and increases the surface dew point temperature as shown by numerous modeling and observational studies (Adegoke et al. 2003; Baidya Roy et al. 2003; Kueppers et al. 2007; Lobell et al. 2006; Mahmood et al. 2004; Mahmood et al. 2006; Sacks et al. 2009). Mahmood et al. (2006) noted a surface temperature decrease of approximately 1°C for heavily irrigated sites in Nebraska during the second half of the 20th century using observations from NCDC's Cooperative Weather Observation Network and the Historical Climate Network dataset. Baidya Roy et al. (2003) used a regional model to show that a simulated cooling of up to 1°C in surface temperature over the Great Plains and Midwest from irrigation could be expected. Similarly, Mahmood et al. (2006) observed a 4-5°C dew point temperature difference between irrigated and non-irrigated sites in Nebraska while Adegoke et al. (2003) found a dew point increase of 2.6°C from weeklong simulations of irrigation over Nebraska.

Convective precipitation develops when sufficient quantities of convective available potential energy (CAPE), precipitable water, and low-level convergence occur

in the presence of a sufficiently thick planetary boundary layer (PBL) and relatively small amounts of convective inhibition (CIN). Changes in the surface temperature and moisture fields with irrigation have competing effects on the development of convective precipitation, Additional near-surface moisture from irrigation enhances convection by changing the amount of CAPE present, despite the decrease in surface temperatures with irrigation (Pielke 2001; Segal et al. 1998). However, the decrease in surface temperature and enhanced cloud cover from irrigation also decrease the height of the PBL and increase CIN, acting to inhibit the development of deep convection (Barnston and Schickedanz 1984; Boucher et al. 2004; De Ridder and Gallee 1998; DeAngelis et al. 2010; Sacks et al. 2009). Over irrigated areas where localized cooling occurs, the suppression of convection from decreased PBL height and increased CIN is especially magnified (DeAngelis et al. 2010; Sacks et al. 2009). Locations downwind of irrigated areas experience increases in CAPE without increases in CIN because while additional moisture is advected in from irrigated regions, temperature decreases do not occur where there is no increase in latent heating (DeAngelis et al. 2010). When synoptic conditions are favorable for the forcing of convection, CAPE increases downwind of irrigated locations result in enhanced convection. Because a large percentage of precipitation over the Great Plains is driven by convection [80% of July and August precipitation over the Ogallala Aquifer domain (Changnon 2001)], it is reasonable to assume that increases in CAPE with irrigation will contribute to an increase in precipitation.

The addition of low-level moisture from irrigation increases precipitation not only through enhanced convection, but also through an increase in the amount of precipitable

water. For example, Koster et al. (2004) noted that soil moisture is positively correlated with precipitation over the Great Plains. Enhancement in soil moisture drives an increase in ET, thereby providing the atmosphere with additional precipitable water, which has been shown to be positively correlated with precipitation at both global and regional scales (Trenberth et al. 2003). Because CAPE and precipitable water increase due to irrigation, precipitation increases are expected to occur downwind of irrigated areas provided the forcing for convection (i.e., low-level convergence) is unchanged (DeAngelis et al. 2010).

Numerous observational studies have attempted to determine the impact of irrigation on precipitation, with generally contradictory results. Barnston and Schickedanz (1984) observed an increase in precipitation of up to 20% over the Texas Panhandle from 1930-70, coincident with the rapid adoption of irrigation. Contrarily, Moore and Rojstaczer (2001) were unable to attribute changes in precipitation to irrigation over the Great Plains from 1950-1982 using an EOF analysis of precipitation. DeAngelis et al. (2010) observed a downwind enhancement of July precipitation over the Great Plains and Midwest during years with higher ET over the Ogallala Aquifer, suggesting that ET from irrigation has a significant impact on precipitation over the Great Plains. Similarly, Jódar et al. (2010) observed orographic precipitation increases downwind of irrigated areas in Spain over long periods when irrigation was prevalent.

Observational studies have generally yielded contradictory results because they have been conducted for periods when changes in irrigation were insufficient at influencing precipitation or they took place over small areas where downwind effects

cannot be realized (DeAngelis et al. 2010). While observational studies have the advantage of using observed rather than simulated data, the exact impact of irrigation cannot be isolated from numerous compounding climatic factors. Modeling studies can remove climatic factors and isolate the impact of irrigation on precipitation, but results can be highly dependent on model physics. Regardless, an analysis of the results from a wide array of modeling studies enables a comprehensive understanding of how irrigation affects precipitation. Previous modeling studies have included the use of mesoscale models (Pielke et al. 1997; Segal et al. 1998), regional atmospheric models (Adegoke et al. 2003; Baidya Roy et al. 2003; De Ridder and Gallee 1998), global climate models (GCMs) (Lee et al. 2011; Puma and Cook 2010; Sacks et al. 2009), and off-line land-surface models (LSMs) (Ozdogan et al. 2010), producing results that have been broadly consistent in determining the impact of irrigation on precipitation. Segal et al. (1998) simulated a slight overall increase in precipitation over North America, with most increases downwind of heavily irrigated areas and differing impacts for drought and pluvial periods. Using a coupled land-atmosphere GCM, Sacks et al. (2009) simulated a 1.24% June-August increase in precipitation globally over land for irrigation simulations. De Ridder and Gallee (1998) simulated conditions that favored increased moist convective development in southern Israel due to irrigation.

Limited computational resources have prevented many of these models from being run at sufficiently high spatial resolutions to adequately resolve small scale land-atmosphere interactions and mesoscale convection (Segal et al. 1998). Modeling studies at coarse spatial resolutions and run over large areas provide a good sense of the general

impacts of irrigation on precipitation, but higher resolutions are needed to fully resolve the processes that influence precipitation in regions dominated by convection. Similarly, studies that were run at high spatial resolution were implemented over small domains for short time periods, yielding results that do not include downwind effects or are not applicable outside of the simulated periods.

While a wide array of different models have been implemented in irrigation modeling studies, techniques with varying levels of complexity have been used to represent irrigation. Using a regional climate model, Kueppers et al. (2007) held the soil at field capacity for all irrigated grid cells in California. Adegoke et al. (2003) saturated all irrigated grid cells once daily at 0000 UTC using a regional atmospheric model for sub-monthly simulations over Nebraska. Sacks et al. (2009) applied water to the cropland fraction of grid cells equally when the Leaf Area Index reached 80% of the annual maximum for 30-year coupled simulations with a GCM. Using a similar approach, Puma and Cook (2010) applied soil moisture to the vegetated portion of irrigated grid cells whenever soil moisture dropped below crop-dependent thresholds in a GCM. Ozdogan et al. (2010) used a daily irrigation trigger to determine whether to apply water to sub-grid scale irrigation in offline simulations using the Noah LSM.

In this study, WRF was run over the Great Plains domain at a 10 km spatial resolution while holding the irrigated portion of grid cells constantly at saturation, an approach similar to that used by Adegoke et al. (2003) but with the addition of a sub-grid scale irrigation representation similar to Puma and Cook (2010) and Sacks et al. (2009). The nature of this experimental design allows for determination of the upper limits of the

impact that irrigation has on precipitation and the energy and water budgets over the Great Plains. Various climatic regimes were chosen to represent the full gamut of precipitation and El Niño-Southern Oscillation (ENSO) conditions that influence the climate of the Great Plains. In taking this comprehensive approach, we can assess the general impact that irrigation has on the climate of the Great Plains and whether these impacts vary with different precipitation and ENSO regimes.

2.3 Methods

2.3.1 WRF/Noah Model Description

The regional WRF model version 3.2 (Skamarock et al. 2008) was used in this study to simulate the atmospheric response to irrigation. WRF is a mesoscale and non-hydrostatic atmospheric model that can be used both for research and operational forecasting. The model uses a terrain-following vertical coordinate system that extends from the surface to 50 hPa. Coupled to WRF is the Noah LSM, which was used to provide surface fluxes of energy, momentum, and mass to the WRF Model.

The Noah LSM, which has been coupled to the WRF Model, has four soil layers (10, 30, 60, and 100 cm), one canopy layer, and one snow layer (when applicable). Vegetation and soil parameters and land cover data were assimilated into Noah from the 20-category, 30-arc-second resolution MODerate Resolution Imaging Spectroradiometer (MODIS) land use dataset (Friedl et al. 2002). In Noah, ET is calculated as the sum of direct ground and canopy evaporation, transpiration from vegetation, and sublimation from snowpack (Chen and Dudhia 2001; Hong et al. 2009). The components of ET are

calculated through simple linear methods using soil and vegetation parameters based on MODIS soil and vegetation types (Betts et al. 1997; Friedl et al. 2002; Jacquemin and Noilhan 1990; Noilhan and Planton 1989).

2.3.2 Irrigation Representation

Areal irrigation datasets are available at high spatial resolution (500 m), which provides more detail than current mesoscale and regional atmospheric models require. Irrigation was represented on a sub-grid cell basis in this study in order to capture the small-scale heterogeneity of irrigation without being computationally prohibitive or resulting in the breakdown of the model physics. The fraction of irrigation in each grid cell was obtained from the 500 m resolution MODIS-derived fractional irrigation dataset from Ozdogan and Gutman (2008) and aggregated to a 10 km domain in WRF (Figure 3). The MODIS irrigation dataset from Ozdogan and Gutman (2008) represents the fractional irrigation area from 2001 and is highly correlated to the 2002 USDA-NASS irrigation dataset on a state-level (R^2 = 0.8833) (NASS 2002). The MODIS-derived dataset was chosen because it is based on observed irrigation whereas the USDA-NASS dataset was compiled from county-level reports of irrigation that may be subject to more errors or missing data.

To represent irrigation in WRF, the Noah LSM was modified to calculate surface fluxes based on the soil moisture in the irrigated and non-irrigated parts of each grid cell (Figure 4). The soil moisture in the irrigated portion of a grid cell was held constant at saturation to a depth of 2 m, while the soil moisture in the non-irrigated portion was controlled by the unmodified physics of the Noah LSM. MODIS land use categories were

left unchanged and irrigation was applied based on the fractional irrigation dataset from Ozdogan and Gutman (2008). Surface fluxes and variables for each grid cell were calculated separately for the irrigated and non-irrigated portions of a grid cell at each time step and were weighted based on the irrigated fraction as shown in (Eq. 1):

$$H = f_i H_{irrigated} + (1 - f_i) H_{non-irrigated} \qquad (1)$$

where H is the sensible heat flux for a grid cell, f_i is the irrigated fraction, $H_{irrigated}$ is the sensible heat flux over the irrigated portion of a grid cell, and $H_{non-irrigated}$ is the sensible heat flux over the non-irrigated portion. The areal extent and amount of irrigation were kept constant for all simulations, which overlapped the period of heaviest annual irrigation in the Great Plains (DeAngelis et al. 2010). Since the soil moisture was kept at saturation for all simulations, this resulted in the overuse of irrigated water as compared to reality. For example, for Colorado, Kansas, and Nebraska, water use for irrigation for May-September 2000 in WRF was 7.06 x 10^{10} m^3, compared with 3.3 x 10^{10} m^3 from USDA annual irrigation surface and ground water withdrawals (Hutson et al. 2004). Therefore, this method of irrigation added slightly more than double the amount of water that was actually applied to the soil for irrigation. The simplistic temporal application of irrigated water warrants further improvement, but is deemed adequate for this study. Simulated latent heat flux values from WRF compared reasonably well with observations from an irrigated field in Nebraska (section 2.4.1) and comparison of 2-m temperature and latent heating changes between observational studies and the irrigation method in this study are in general agreement (section 2.5.1). Sensitivity simulations that set the soil

moisture at saturation in irrigated portions of grid cells when it dropped below 50% of capacity showed similar effects on precipitation as shown in section 2.4.5.

2.3.3 Experimental Design

This study includes a range of precipitation and ENSO regimes for the purpose of representing the broad range of climatic conditions observed over the Great Plains. An array of precipitation regimes were chosen to represent the various antecedent soil moisture conditions in the Great Plains, while ENSO regimes were chosen to represent the array of external climate forcings. The characterization of drought, normal, and pluvial years was determined by first calculating the 1980-2008 average May-September precipitation for an area centered over the Great Plains region (30.5° to 44.5° N, 91.5° to 105.5° W) using the North American Regional Reanalysis (NARR) dataset (Mesinger et al. 2006). Drought years had May-September precipitation at least one standard deviation below the 1980-2008 mean, while pluvial years were classified as at least one standard deviation above the mean. Normal years were within one standard deviation of the mean. El Niño/La Niña years were determined from May-September averages of the bimonthly ranks of the Multivariate ENSO Index (MEI) Wolter and Timlin (1998). El Niño, La Niña, and neutral years were determined using guidelines from Wolter and Timlin (1998), except that terciles (33rd percentiles) were used instead of the lowest and highest 30th percentiles. Selection of simulated years was done through the identification of nine different years that represent all combinations of the three precipitation and three ENSO regimes (Table 1).

WRF was initialized using 3-hourly data from the North American Regional

Reanalysis (NARR) for all identified years in Table 1 (Mesinger et al. 2006; Skamarock et al. 2008). All model simulations were completed using the same 180 x 195 grid with a 10 km horizontal resolution, 38 vertical levels, 4 soil layers (to a depth of 2 m), and a 30-second time step (except for 2007, which had a 25-second time step due to instabilities with the forcing dataset during that year). Control (CTRL) and Irrigation (IRRIG) simulations were run for each year from April 1 to October 1, overlapping the period of heaviest annual irrigation in the Great Plains (DeAngelis et al. 2010). The Morrison 2-moment Microphysics scheme, YSU Planetary Boundary Layer (PBL) Scheme, RRTM long wave radiation scheme, Dudhia shortwave radiation scheme, and Monin-Obukhov surface-layer scheme were used. The modified Noah Land-Surface Model was run with the new irrigation sub-model. No cumulus parameter was employed because sensitivity runs of WRF using a cumulus parameter (and without irrigation) showed a dramatic overestimation of precipitation over long periods of time when compared with precipitation estimates from NARR and NCEP's National Stage IV datasets (Lin and Mitchell 2005; Mesinger et al. 2006).

Determination of the model parameters as listed above was based on the performance and feasibility of fourteen sensitivity simulations of WRF without irrigation from June 1-30, 2005, a normal precipitation and neutral ENSO year. Simulations incorporated a variety of resolutions, domain sizes, and model parameters to achieve a suitable array of possible model configurations. Ultimately, the model configuration used in this study was based on the performance of the simulated precipitation compared to NCEP Stage IV precipitation (Lin and Mitchell 2005), the computational efficiency of

the model, and the capability of the model to resolve physical processes between the land surface and the atmosphere. No cumulus parameter was used because all sensitivity simulations that included a cumulus parameter dramatically overestimated the precipitation as compared to NARR and Stage IV observed precipitation estimates. For example, sensitivity simulations of WRF from April-October 1997 with a cumulus parameter overestimated precipitation by 102.3% compared with NARR, while simulations without a cumulus parameter resulted in an overestimation of only 30.3% (not shown). Comparison of the average precipitation for all simulated years over the domain using the selected model configuration shows an overestimation when compared to the NARR dataset (Figure 5). Considering the precipitation that fell within the region of study as shown in Figure 3b (33.65°N-45.16°N, 91.77°W-103.2°W) for May-September of all simulated years, WRF overestimated precipitation by 33.2% when using the selected model configuration (Figure 5). While WRF overestimated precipitation throughout the Great Plains, the model simulated the general pattern of precipitation that is present in the NARR data. Since this overestimation was constant for irrigation and control simulations of WRF, it did not lead to any systematic bias for irrigation or control simulations.

2.3.4 Statistical Significance

To determine whether statistical significance was achieved when comparing variables between control and irrigation simulations, t-tests using a matched pairs design were employed. In a matched pairs design, the control and treatment (irrigated) groups share the same variance between individual samples and only the variance of the

difference between the groups is considered. In this study, the set of differences is considered to be the set of control simulations subtracted from the set of irrigation simulations, unless otherwise noted. All t-tests were performed using two tails with a 95% confidence level, unless otherwise noted.

2.4 Results

All results are reported for the region of study (as shown in Figure 3b) using averages of all simulated years from May-September unless otherwise noted.

2.4.1 Model Validation

The comparison of WRF simulated latent heat flux with two Ameriflux field stations from May-September 2008, a wet period, showed a general overestimation of latent heating by WRF. Control simulations of WRF overestimated the latent heat flux by 17.5% when compared with the Ameriflux Mead Rainfed Site (41.1797°N 96.4396°W; Figure 6a) (Verma et al. 2005). Irrigation simulations of WRF overestimated the latent heat flux by 22.7% compared with the Ameriflux Mead Irrigated Rotation Site (41.1649°N 96.4701°W; Figure 6b) (Verma et al. 2005). When considering that eddy-covariance methods generally underestimate latent heating due to a mean surface energy imbalance on the order of 20% (Twine et al. 2000; Wilson et al. 2002), it is reasonable to assume that the overestimation of latent heat flux by WRF was considerably smaller. Overall, WRF simulated the seasonality of latent heating at these locations with a reasonable degree of accuracy. WRF also simulated the seasonality of the difference

between the observed latent heat flux at the Mead Irrigated Rotation Site and the Mead Rainfed Site reasonably well (Figure 6c).

2.4.2 Overall Model Results

In the following sections, "overall" results refer to May-September weighted averages over the entire region of study, while results for "irrigated grid cells" refer to May-September weighted averages of grid cells with at least 10% irrigation within the region of study.

Soil moisture increases of 27% in irrigated grid cells (Table 2) drove statistically significant increases in latent heating (Figure 7a) and decreases in sensible heating (Figure 7b). Latent heat flux increases of 20.7 W m^{-2} (22.6%) and sensible heat flux decreases of 14.5 W m^{-2} (-30.2%) occurred in irrigated grid cells (Table 2). The increase in latent heating drove statistically significant increases in the 2-m dew point temperature over much of the Great Plains (Figure 7c), with an increase of 0.79°C for irrigated grid cells and 0.30°C overall (Table 2). Similarly, decreases in sensible heating were coincident with statistically significant decreases in the 2-m temperature in the vicinity of irrigated grid cells (Figure 7d), with 0.49°C temperature decreases over irrigated grid cells and 0.16°C overall (Table 2). Increased low-level moisture resulted in statistically significant CAPE increases throughout much of the Great Plains (Figure 8a) with an amplified response over irrigated grid cells [16.0% increase for irrigated grid cells compared with 5.0% overall (Table 2)]. The addition of low-level moisture from irrigation increased low-level cloud cover adjacent to irrigated areas (not shown), but net radiation increased slightly (Table 2) due to decreases in upwelling long wave radiation.

Enhancement of low-level moisture also led to statistically significant increases in the column precipitable water (Figure 8d), which increased by 0.74% over irrigated grid cells and 0.50% overall (Table 2). However, low-level cooling from irrigation also decreased the PBL height over much of the Great Plains (Figure 8c), partially counteracting the enhancement of convection from increased CAPE. CIN increases of 5.7% were simulated for irrigated grid cells compared to 0.6% increases overall (Table 2). Only a small number of irrigated grid cells had statistically significant CIN increases (Figure 8b). Low-level cooling also resulted in decreased surface convergence over irrigated grid cells (-84.2%), with smaller decreases overall (-4.75%; Table 2). Statistically significant average precipitation increases of 4.97 mm (0.91%) and 4.25 mm (1.29%) were observed overall for May-September and June-August respectively (Figure 9a), with localized precipitation increases of up to 20% over parts of Nebraska, Kansas, and Oklahoma (Figure 9c). The average overall May-September precipitation increase was smaller than the increase in evapotranspiration (22.70 mm), meaning that irrigation resulted in a net loss of water of 17.73 mm. On average, precipitation increases were larger for irrigated grid cells compared with the entire region of study during May-September and June-August (Table 2). No individual months had statistically significant changes in precipitation. When considering the spatial pattern of precipitation changes from irrigation (Figure 9c), no individual grid cells had statistically significant changes in precipitation.

The effects of irrigation were clearly amplified with increasing irrigation fraction as shown in Figure 10. Stronger soil moisture enhancement with increasing irrigation

fraction (Figure 10a) resulted in greater partitioning of net radiation into latent heating for heavily irrigated grid cells (Figure 10b), at the expense of sensible heating (Figure 10c). As a result, surface cooling (Figure 10d) and dew point enhancement (Figure 10e) intensified as irrigation became more concentrated. Greater increases in 2-m dew point temperature with increasing irrigation fraction drove larger CAPE increases for heavily irrigated grid cells (Figure 10f). However, stronger surface cooling with increasing irrigation fraction resulted in greater CIN increases (Figure 10g), greater PBL height decreases (Figure 10h), and stronger decreases in convergence (Figure 10i) with increasing irrigation intensity. Greater latent heating with increasing irrigation intensity contributed to the enhancement of column precipitable water with increasing irrigation fraction until about 25% irrigation fraction, but decreases in column precipitable water occurred at higher irrigation concentrations (Figure 10j). Slight increases in precipitation occurred with increasing irrigation fraction, but these increases were not statistically significant due to the small number of heavily irrigated grid cells (Figure 10k).

2.4.3 Comparison of Precipitation Regimes

Because drought years had the lowest antecedent soil moisture, the largest soil moisture changes occurred both for irrigated grid cells and overall during drought years (Table 3). Therefore, drought years had the greatest changes in latent and sensible heating for irrigated grid cells and overall (Table 3). Strong latent heating enhancement during drought years drove the greatest 2-m dew point temperature increase for irrigated grid cells (Table 3). Similarly, the strong decrease in sensible heating was coincident with the largest 2-m temperature decrease overall and for irrigated grid cells (Table 3). The fact

that dew points increased the most during drought years meant that CAPE increases were also the largest during drought years for irrigated grid cells and overall (Table 3). However, precipitable water increases were the lowest for drought years overall. Greater temperature decreases during drought years led to the greatest decrease in PBL height overall and for irrigated grid cells (Table 3). Because of strong PBL height decreases, the smallest increase in precipitation occurred over the region of study during drought years [2.85 mm (0.63%)] when considering all precipitation regimes. Meager precipitation increases during drought years were coincident with the greatest increase in ET (23.84 mm), meaning that irrigation resulted in the largest loss of water (20.99 mm) during drought years over the region of study. Similarly, very strong PBL height decreases over irrigated grid cells resulted in precipitation decreases of 1.26 mm (-0.31%) over irrigated grid cells during drought years, in contrast with increases of 14.87 mm (3.01%) and 9.97 mm (1.77%) during normal and pluvial years, respectively. These precipitation decreases were coincident with the largest increase in ET (115.56 mm) over irrigated grid cells, meaning that irrigation resulted in the largest loss of water (116.82 mm) over irrigated grid cells during drought years.

The impacts of irrigation were also the most amplified with increasing irrigation fraction during drought years. The strongest amplification of changes in latent (Figure 10b) and sensible heating (Figure 10c) with increasing irrigation intensity occurred during drought years, driving the greatest changes in 2-m temperature (Figure 10d) and dew point (Figure 10e) with increasing irrigation fraction. Greater dew point increases for heavily irrigated grid cells during drought years resulted in greater CAPE increases with

increasing irrigation fraction (Figure 10f). However, strong temperature decreases over heavily irrigated grid cells led to greater PBL height decreases (Figure 10h) and stronger CIN increases (Figure 10g; not significant) with increasing irrigation fraction. Total column precipitable water increases also sharply declined with increasing irrigation fraction (Figure 10j) likely because of the decreased PBL height over heavily irrigated grid cells. The fact that heavily irrigated grid cells had the most amplified PBL height decreases and the smallest increases in precipitable water resulted in a decrease in precipitation with increasing irrigation intensity during drought years (Figure 10k), despite strong CAPE increases.

While strong amplification of the effects of irrigation occurred during drought years, rather ambiguous effects occurred during normal and pluvial years. The smallest changes in latent (Figure 10b) and sensible heating (Figure 10c) occurred in heavily irrigated grid cells during normal years, which resulted in the smallest changes in 2-m temperature with increasing irrigation fraction (Figure 10d). The reduced surface cooling resulted in the smallest decrease in PBL height with increasing irrigation fraction (Figure 10h) and overall for normal years (Table 3). Despite the small CAPE increase (Figure 10f) and the large CIN increase (Figure 10g) with increasing irrigation fraction, precipitation increased with increasing irrigation intensity during normal years (Figure 10k) because of reduced PBL height decreases (Figure 10h) and enhanced precipitable water over heavily irrigated grid cells (Figure 10j). Precipitation increased by 5.94 mm (1.06%) overall and by 14.87 mm (3.01%) for irrigated grid cells during normal years.

Pluvial years had the greatest precipitation increase when considering the entire region of study [6.14 mm (0.98%)], and even greater increases over irrigated grid cells [9.97 mm (1.77%)]. This was coincident with the smallest decrease in convergence overall and the smallest percentage decrease for irrigated grid cells (Table 3). CIN decreases occurred overall and the smallest increases in CIN occurred for irrigated grid cells during pluvial years (Table 3).

2.4.4 Comparison of ENSO Regimes

The impact of irrigation on the energy budget was the largest during neutral ENSO years, when soil moisture changes were the largest (Figure 11a; Table 4). As a result, the largest changes in latent and sensible heating occurred during neutral years overall (Table 4) and with increasing irrigation fraction (Figures 11b; 11c). This led to the strongest temperature decreases (Figure 11d) and dew point temperature increases (Figure 11e) with increasing irrigation fraction. Large 2-m temperature decreases during neutral years resulted in strong PBL height decreases overall (Table 4) and with increasing irrigation fraction (Figure 11h). Strong dew point increases during neutral years drove the strongest increases in CAPE and column precipitable water overall (not significant) (Table 4), which counteracted PBL height decreases. As a result, the largest precipitation increases occurred overall (5.78 mm) and for irrigated grid cells (12.20 mm) during neutral years (Table 4). Precipitation generally increased with increasing irrigation fraction (not significant) during neutral years (Figure 11k), coincident with strong CAPE and precipitable water increases with increasing irrigation fraction.

While neutral years exhibited the strongest irrigation signal, El Niño years exhibited the weakest irrigation signal. The smallest soil moisture change occurred during El Niño years (because precipitation was the highest of all ENSO regimes), which led to the weakest changes in latent heating, sensible heating, and 2-m dew point temperature (Table 4). Despite relatively weak PBL height decreases (Table 4, Figure 11h), the smallest precipitation increases occurred for irrigated grid cells and overall during El Niño years because of weak increases in CAPE overall and over irrigated grid cells combined with rather large decreases in convergence over irrigated grid cells (Table 4, Figure 11f).

2.4.5 Sensitivity Simulations from time-decay irrigation technique

Since the approach used to simulate intensive irrigation described in section 2.3.2 (ORIGINAL) used approximately twice as much water used as USDA estimates, sensitivity simulations with a time-decay irrigation (DECAY) scheme were conducted to determine whether the overuse of water in this study exaggerated the atmospheric impact of irrigation. In these simulations, the soil moisture in the irrigated portion of grid cells was set at saturation whenever it dropped below 50% of saturation. Results from simulations of four years show relatively the same May-September precipitation difference between irrigated and control simulations [4.71 mm for the DECAY method compared to 4.95 mm for the ORIGINAL method] despite the fact that soil moisture changes in the DECAY scheme were only 41% as large as the ORIGINAL scheme (Figure 12a). Overall changes in latent heating were only 36% as large as the ORIGINAL method (Figure 12b), which drove dew point temperature changes only 39% as large.

Reduced irrigation-induced cooling led to PBL height decreases only 35% as large as the ORIGINAL scheme (Figure 12c). Despite the fact that CAPE increases were only 35% as large, simulations using the DECAY scheme resulted in only slightly smaller increases in precipitation (Figure 12d) compared to simulations with the ORIGINAL technique (1.02% compared with 1.07%). Changes in latent heating and temperature from the ORIGINAL approach were similar to results from previous observational and modeling studies as discussed in section 2.5.1, while changes in temperature and latent heating from the DECAY approach were significantly smaller. WRF simulations using the ORIGINAL approach also reasonably simulated latent heat flux changes over irrigated fields in Nebraska (section 2.4.1). Based on these findings, the ORIGINAL approach was determined to be a more accurate representation of the atmospheric effect on irrigation in WRF despite overusing water. Because the ORIGINAL technique more accurately represented the atmospheric impact of irrigation while overusing water suggests possible deficiencies in the representation of crops in the Noah LSM when coupled to WRF.

2.5 Discussion

2.5.1 Comparison to previous studies

Overall, simulated latent heat flux changes from irrigation compared reasonably well with previous studies despite the overuse of water by the irrigation technique used in this study. June-August average simulated latent heating increases of up to ~47 W m^{-2} occurred over heavily irrigated areas of Nebraska, compared with simulated increases of up to 30 W m^{-2} over Nebraska as reported by Sacks et al. (2009). Simulated latent heating

increases averaged over Nebraska were only 6.53 W m^{-2} (5.9%) for the period of 7-15 July, 1997 (not shown) compared with 27 W m^{-2} (35%) over the same period as Adegoke et al. (2003), which used a regional model and saturated the entire irrigated grid cell once a day. August latent heating increases of up to ~35 W m^{-2} occurred over heavily irrigated grid cells in Nebraska (not shown), compared with up to 100 W m^{-2} in offline simulations from Ozdogan et al. (2010).

Latent heating increases over irrigated grid cells in this study drove dew point temperature changes that were smaller than previous studies. Mahmood et al. (2006) observed 4-5°C growing season dew point temperature differences between irrigated and non-irrigated sites in Nebraska, well above the 1.5°C differences that occurred over similar heavily irrigated grid cells in this study. Adegoke et al. (2003) simulated 2.6°C dew point temperature increases over Nebraska, compared with 0.53°C increases from the same period in this study (not shown). Decreases in sensible heating were coincident with similar surface temperature decreases when compared to previous studies. Simulated 2-m temperature decreases of up to 0.9°C from May-September occurred for all simulated years over the heaviest irrigated areas in the model domain, compared with observed growing season temperature decreases of ~1°C for heavily irrigated sites in Nebraska during the second half of the twentieth century (2006). June-August simulated temperature decreases of up to 0.9°C over the heaviest irrigated grid cells in Nebraska were smaller than 2°C temperature decreases reported by Sacks et al. (2009).

In this study, modifications to the low-level temperature and moisture fields had a significant influence on the development of convective precipitation. Small, but

statistically significant, precipitation increases of 1.29% occurred for June-August, compared with a 1.24% June-August increase in precipitation globally over land for irrigated GCM simulations reported by Sacks et al. (2009). DeAngelis et al. (2010) observed a larger precipitation increase of approximately 1.7% over the Great Plains and Midwest [Regions 1-3 in DeAngelis et al. (2010)] for May-September due to irrigation, while Segal et al. (1998) simulated a smaller 0.68% continentally-averaged increase over the United States using a low-resolution mesoscale model. In general, precipitation changes in this study were similar to previous studies despite the fact that latent heat flux and dew point temperature changes were generally smaller than previous studies. Despite the overuse of water by the irrigation technique used in this study, the simulated effects of irrigation were of similar magnitude to previous studies.

2.5.2 Comparison with Offline Simulations

Because of the large difference between latent heat flux changes in this study and those from Ozdogan et al. (2010), offline simulations of the Noah LSM were conducted to assess the validity of using offline simulations to simulate the impacts of irrigation on the energy and water budgets. Offline simulations were conducted using the High Resolution Land Data Assimilation System (HRLDAS) for all identified years (Chen et al. 2004). Separate offline irrigation simulations were run using the irrigation technique described in section 2.3.2 (ORIGINAL) and the time-decay irrigation technique described in section 2.4.5 (DECAY). Offline simulations of the Noah LSM using the ORIGINAL technique showed an even larger overestimation of latent heating from irrigation compared with Ozdogan et al. (2010). Over the region of study, May-September latent

heating changes from offline simulations of four individual years using the ORIGINAL irrigation technique were 388% larger than when using the same technique in WRF (Figure 12b). Offline simulations using the ORIGINAL technique resulted in May-September latent heat flux changes of up to 280 Wm^{-2} for heavily irrigated grid cells averaged over all simulated years (Figure 13b), compared with up to 47 Wm^{-2} from WRF simulations using the same technique. Using the DECAY technique in offline simulations resulted in up to 95 Wm^{-2} increases in latent heating (Figure 13a), significantly smaller than offline simulations using the ORIGINAL technique. However, overall latent heating changes from the offline DECAY simulations were still 29.7% larger than values from WRF simulations that used the ORIGINAL technique. These results suggest that overestimation of the latent heating change in offline simulations likely occurs because uncoupled LSMs do not simulate the enhanced low-level moisture that occurs over irrigated fields. Therefore, uncoupled LSMs tend to underestimate low-level moisture in the presence of irrigation, thus creating an unrealistic water vapor gradient that drives exaggerated latent heat flux values over irrigated fields.

2.5.3 Overall Impact of Irrigation on Great Plains Precipitation

Simulation of irrigation altered the energy budget over the Great Plains by partitioning net radiation into additional latent heating at the expense of sensible heating. Modifications to latent and sensible heating over irrigated fields drove significant changes in the surface temperature and moisture fields. These changes had competing effects on the development of precipitation and the forcing of convection. When considering how irrigation impacted the development of convection, only changes in

CAPE and the PBL height appeared to play a leading role. CAPE enhancement led to precipitation increases overall and over irrigated grid cells for the average of all simulated years despite strong PBL height decreases. Because precipitation increases occurred overall and for irrigated grid cells, the enhancement of convection due to increased surface moisture from irrigation generally overwhelmed the suppression of convection from irrigation-induced cooling over the Great Plains. While even larger PBL height decreases occurred over irrigated grid cells, precipitation increases were larger over irrigated areas compared with the region of study because of stronger CAPE increases, similar to results as reported by Sacks et al. (2009). Despite the fact that irrigation resulted in precipitation increases in this study, ET increases were much larger, thereby confirming that irrigation results in a net loss of water over the Great Plains.

In this study, the impact of irrigation clearly intensified with increasing irrigation fraction. As the grid cell irrigation fraction increased, greater changes in latent and sensible heating resulted in stronger temperature and dew point temperature modifications. Despite the increase in 2-m dew point temperature with increasing irrigation intensity, total column precipitable water decreased with increasing irrigation fraction for heavily irrigated grid cells. This occurred because declines in the height of the moist PBL increased the thickness of the relatively drier free troposphere, which reduced the column-integrated precipitable water. Regardless, large 2-m dew point temperature increases over heavily irrigated grid cells drove strong enhancement in CAPE with increasing irrigation intensity. Similarly, stronger irrigation-induced cooling with increasing irrigation fraction resulted in greater PBL height decreases over heavily

irrigated grid cells. The enhanced PBL height decreases with increasing irrigation fraction were more than offset by strong CAPE increases. As a result, a slight increase in precipitation occurred on average for all simulated years as irrigation intensity increased. While not significant, this result warrants further investigation.

Factors that affect the suppression and enhancement of convection from irrigation were not constant when considering variations in antecedent soil moisture. Irrigation clearly had a stronger impact on the surface energy and moisture budgets during periods with low antecedent soil moisture. Greater water vapor deficits over irrigated fields during drought years resulted in larger latent heating increases over irrigated areas, at the expense of greater reductions in sensible heating. As a result, generally stronger irrigation-induced cooling and greater enhancement of surface moisture occurred during drought years. While CAPE increases were the largest during drought years, precipitation decreased over irrigated grid cells because of strong PBL height decreases. Similarly, precipitation decreased with increasing irrigation intensity during drought years because of strong PBL height decreases with increased irrigation fraction.

The fact that precipitation decreased over irrigated grid cells during drought years suggests that the level of antecedent soil moisture is a control for whether irrigation results in suppression or enhancement of convection. For periods when the antecedent soil moisture was extremely low, irrigation suppressed convection over irrigated areas. During these times, PBL height decreases from irrigation-induced cooling overwhelmed the enhancement of CAPE from increases in surface moisture. By contrast, irrigation enhanced convection over irrigated areas (and overall) when antecedent soil moisture

levels were reasonably high because the enhancement in CAPE overwhelmed the weaker decreases in PBL height. This is supported by the fact that precipitation increases occurred over irrigated grid cells in the region of study for normal and pluvial years, but not for drought years. Because irrigation had opposing effects on precipitation over irrigated areas at low and high antecedent soil moisture levels, an antecedent soil moisture threshold likely exists where the competing effects of irrigation are cancelled. During periods when the antecedent soil moisture is below the threshold, irrigation suppresses the development of convective precipitation over irrigated areas. For years with antecedent soil moisture above the threshold, irrigation enhances convective precipitation over irrigated areas. Determination of the presence and magnitude of an antecedent soil moisture threshold warrants further exploration.

While antecedent soil moisture played a large role in determining the impact of irrigation on the energy budget and precipitation, variations in ENSO did not. Irrigation had the greatest impact during neutral years, likely because antecedent soil moisture was the lowest. El Niño years had the most dampened irrigation signal because of high antecedent soil moisture during those years. The fact that irrigation had a greater impact during neutral years because of the low level of antecedent soil moisture suggests that ENSO is simply a secondary factor in influencing the impact of irrigation.

2.6 Conclusions

Irrigation has greatly expanded over the Great Plains since World War II, threatening the sustainability of regional groundwater supplies. Because of large groundwater withdrawals from irrigation, steep declines in the water table have driven up

costs for agricultural and municipal water use (McGuire et al. 2003). In this paper, irrigation has been shown to have a significant impact on the water cycle over the Great Plains by enhancing evapotranspiration and precipitation. Increases in evapotranspiration were much larger than increases in precipitation, confirming that irrigation enhances the net loss of water over the Great Plains. The effects of irrigation have also been shown to be dependent on the level of antecedent soil moisture in this study. Irrigation enhanced precipitation over irrigated areas during periods with high antecedent soil moisture and suppressed precipitation over irrigated areas during periods with low antecedent soil moisture. Therefore, an antecedent soil moisture threshold has been identified as separating conditions where irrigation results in either the enhancement or the suppression of convective precipitation. Knowledge of possible conditions when irrigation suppresses precipitation is critical to the management of regional groundwater supplies. Years with low antecedent soil moisture require the largest volume of water for irrigation while at the same time experiencing decreases in precipitation over irrigated areas. For these reasons, irrigation potentially has the most negative impact on groundwater supplies during drought years. The combination of high drought sensitivity and future projections of increased drought likelihood with climate change over the Great Plains (Gregory et al. 1997; IPCC 2007; Kumar 2007; Manabe et al. 2004; Rind et al. 1990; Wang 2005; Wetherald and Manabe 1995, 1999) suggest that irrigation might result in increased future stress to groundwater supplies in the region. In a region where drought severity and prevalence are expected to increase due to climate change, it is crucial that we understand the full impact that irrigation has on the water cycle in order to

effectively manage water for future agricultural and municipal uses. In Chapter 3, an examination of where water that is added to irrigated fields eventually falls as precipitation will be completed, allowing for additional understanding of the impact that irrigation has on the water budget. Gaining a more complete understanding of this impact improves the potential for more sophisticated water management and conservation in the Great Plains, helping to reverse recent depletion of groundwater supplies and ensure a more economically viable supply of groundwater in one of the world's most crucial agricultural regions.

2.7 Acknowledgments

Support for this project was provided by the University of Minnesota Grant-in-Aid Program (#21601). This work was carried out in part using computing resources at the University of Minnesota Supercomputing Institute. We thank Dr. Mutlu Ozdogan for providing the fractional irrigation dataset and Dr. Stefan Liess for aid with the coupled model enhancements.

Chapter 3

The Precipitation of Irrigated Water and Changes in Precipitation Recycling

Harding, K. J. and P. K. Snyder, *Journal of Hydrometeorology,* to be submitted

3.1 Overview

The rapid expansion of irrigation in the Great Plains since World War II has resulted in significant water table declines, threatening the long-term sustainability of the Ogallala Aquifer. As discussed in Chapter 2 of this paper, the Weather Research and Forecasting (WRF) model was modified to simulate the effects of irrigation at sub-grid scales. Simulations of nine April-October periods (three drought, three normal, and three pluvial) over the Great Plains were completed to determine the full impact of irrigation on the water budget. The application of water for irrigation over the Great Plains contributes to an increase in May-September evapotranspiration by approximately 4% and precipitation by 1%, with localized increases of up to 20%. Data from these WRF simulations were used along with a backward trajectory analysis to identify where evapotranspired moisture from irrigated fields falls as precipitation (i.e. irrigation-induced precipitation) and how irrigation impacts precipitation recycling. On average, only 15.8% of evapotranspired moisture from irrigated fields fell as precipitation over the Great Plains, resulting in 5.11 mm of May-September irrigation-induced precipitation and contributing to 6.71 mm of recycled precipitation. Reductions in non-recycled precipitation suggest that irrigation reduces precipitation of advected moisture. The heaviest irrigation-induced precipitation was coincident with simulated and observed precipitation increases, suggesting that observed precipitation increases in north-central Nebraska are strongly related to evapotranspiration of irrigated water. Water losses due to evapotranspiration were much larger than irrigation-induced precipitation and recycled

precipitation increases, confirming that irrigation results in a net water loss over the Great Plains.

3.2 Introduction

Irrigation in the Great Plains has rapidly increased since World War II (McGuire et al. 2003), jeopardizing the future viability of the Ogallala Aquifer as evidenced by water table declines of over 40 m in some areas (McGuire 2007). Currently, irrigation is heavily concentrated within and adjacent to the Ogallala Aquifer as documented by United States Department of Agriculture and satellite-derived irrigation estimates (Ozdogan and Gutman 2008). The doubling of available water for evapotranspiration (ET) in the Great Plains (Moore and Rojstaczer 2001) has significantly altered the Bowen Ratio (Pielke 2001), driving additional partitioning of energy into latent heating at the expense of sensible heating (Barnston and Schickedanz 1984; DeAngelis et al. 2010; Kueppers et al. 2007; Ozdogan et al. 2010; Pielke 2001; Sacks et al. 2009). Modifications to latent and sensible heating result in a cooler and more humid surface (Adegoke et al. 2007; Adegoke et al. 2003; Baidya Roy et al. 2003; Kueppers et al. 2007; Lobell et al. 2008; Mahmood et al. 2004; Mahmood et al. 2006; Sacks et al. 2009), which drives competing impacts on convection. Overall, increases in convective available potential energy (CAPE) due to the increase in surface humidity generally overwhelm the suppression of convection that results from decreases in planetary boundary layer (PBL) height from surface cooling (DeAngelis et al. 2010; Pielke 2001; Segal et al. 1998). Numerous studies have shown that irrigation enhances precipitation (DeAngelis et al. 2010; Jódar et al. 2010; Sacks et al. 2009; Segal et al. 1998). DeAngelis et al. (2010)

observed increases in precipitation downwind of irrigated areas over the Ogallala Aquifer for years with high ET, suggesting that irrigation results in downwind precipitation increases. Similarly, Jódar et al. (2010) observed orographically enhanced precipitation downwind of irrigated areas in southern Spain. Segal et al. (1998) simulated slight continent-wide increases in precipitation over North America using a regional climate model, while Sacks et al. (2009) simulated slight global precipitation increases over land due to irrigation. Using a mesoscale atmospheric model in Chapter 2 of this study, precipitation increases of 1% were simulated region-wide over the northern Great Plains and Midwest due to irrigation, with up to 20% increases at individual locations.

While irrigation has been shown to influence the spatial distribution of precipitation over the Great Plains and Upper Midwest, identification of the relative quantity of irrigated water that falls as precipitation within the region allows for a better understanding of how irrigation affects the regional water budget. DeAngelis et al. (2010) employed a backward trajectory technique based on Dominguez et al. (2006) using data from the North American Regional Reanalysis (NARR) to show that evapotranspired water from an area over the Ogallala Aquifer falls as precipitation primarily over the Great Plains and Upper Midwest. This study uses a backward trajectory method based on the approach of Brubaker et al. (2001) with data generated from simulations of the Weather Research and Forecasting (WRF) model that include a spectrum of antecedent soil moisture and El Niño-Southern Oscillation (ENSO) conditions. Performing a backward trajectory analysis on model data from irrigated and control simulations allows for the isolation of ET resulting from irrigation. In this manner, an estimate of

precipitation that results exclusively from ET over irrigated fields, hereafter referred to as "irrigation-induced precipitation," can be determined and placed in context with previous observational and modeling studies.

The tracing of irrigated water from evapotranspiration to precipitation also allows for additional insight into the role that irrigation plays on precipitation recycling, a critical component of the atmospheric branch of the hydrologic cycle (Dirmeyer et al. 2009). Recycled precipitation is defined as water that is evapotranspired within the same region that it eventually falls out as precipitation (Brubaker et al. 1993; Brubaker et al. 2001; Dirmeyer et al. 2009; Dominguez et al. 2006; Zangvil et al. 2004). The recycling ratio is simply the ratio of recycled precipitation to total precipitation within a region. The size of the precipitation recycling ratio is dependent on the size of the basin that is considered because larger areas have more opportunity for locally evapotranspired water vapor to fall as precipitation (Brubaker et al. 2001; Dirmeyer and Brubaker 1999; Dominguez et al. 2006). Recycling ratios can range from zero for an infinitely small area to one for the entire planet (Brubaker et al. 1993; Brubaker et al. 2001; Eltahir and Bras 1994). When considering the domain over which to quantify the amount of precipitation recycling, previous studies (Dominguez et al. 2006; Rasmusson 1968) have determined that an area of at least ~1.0 x 10^6 km^2 is required because it is large enough to capture mesoscale and synoptic moisture transport while also capturing small-scale variability. In this study, precipitation recycling was calculated over the region outlined in Figure 3b, which will be referred to as the "region of study." The region of study is approximately

1.25 x 10^6 km^2 in size, roughly consistent with the size of ideal recycling basins as defined by Dominguez et al. (2006) and Rassmusson (1968).

To determine the precipitation recycling ratio, numerous methods including isotope tracers, analytical models, and numerical tracing experiments have been applied (Dominguez et al. 2006). Here emphasis is placed on studies using analytical models and numerical tracing experiments. Using a simple analytical recycling model on radiosonde data over a large portion of the central United States, Brubaker et al. (1993) observed May-September monthly-averaged recycling ratios of approximately 0.28 for the period of 1963-73, with monthly recycling ratios of up to 0.22 in June and 0.34 in July (Brubaker et al. 1993; Zangvil et al. 2004). Bosilovich and Schubert (2001) calculated monthly-averaged May-August recycling ratios of 0.27 using a bulk recycling method from Eltahir and Bras (1994) over the same region as Brubaker et al. (1993) for the years 1980-94.

Early analytical precipitation recycling model studies assumed that moisture storage in the atmospheric column is negligible, restricting recycling calculations to monthly time scales where this assumption is approximately valid. To capture higher temporal precipitation recycling variability, models that do not assume negligible moisture storage must be used. To correct this problem, Zangvil et al. (2004) developed a bulk-recycling model that does not assume negligible moisture storage, allowing for recycling calculations on a daily basis. Using this model, Zangvil et al. (2004) calculated May-August recycling ratios of approximately 0.20 over the Midwest for four different years.

While analytical precipitation recycling models without negligible moisture storage allow for recycling calculations on short times scales, backward trajectory methods have the advantage of being able to trace the source of precipitation instead of using time-averaged variables that may not be representative of conditions during generally short precipitation events (Brubaker et al. 2001). Brubaker et al. (2001) used a three-dimensional, quasi-isentropic backward trajectory (QIBT) technique to trace precipitation to its evaporative source, allowing for simple determination of whether precipitation had its evaporative source within the same area. Using NARR data from 1963-1998, Brubaker et al. (2001) observed June-August recycling ratios of 0.22 over the northern Great Plains [Missouri Region in Brubaker et al. (2001)]. In a similar study, Dominguez et al. (2006) used the two-dimensional, Dynamic Recycling Model (DRM) with backward trajectories to calculate recycling ratios along the path of the moisture source. June-August recycling ratios over the Great Plains from Dominguez et al. (2006) were approximately 0.12 to 0.14 for 1979-2000 when using DRM with NARR data (Mesinger et al. 2006).

In this study, precipitation recycling ratios were calculated using the backward trajectory recycling techniques from Brubaker et al. (2001) and Dominguez et al. (2006) with model output from simulations using the WRF model. Precipitation recycling ratios were calculated for irrigated and control cases with WRF for a suite of simulations representing antecedent soil moisture and ENSO conditions. Comparison of recycling ratios from irrigated and control simulations allows for the determination of the impact that irrigation has on precipitation recycling over the Great Plains.

3.3 Methods

3.3.1 WRF/Noah LSM Model Description

For this study the regional WRF model version 3.2 (Skamarock et al. 2008) was run with the coupled Noah Land Surface Model (LSM) (Chen and Dudhia 2001). WRF is a non-hydrostatic mesoscale meteorological model, while the Noah LSM is the coupled land-surface model that provides surface fluxes of energy, momentum, and mass to the WRF model. The 20-category, 30-arc-second resolution MODIS land use dataset (Figure 3a) was assimilated into the Noah LSM and WRF. Additional information on WRF and the Noah LSM is available in Section 2.3.1.

3.3.2 Irrigation Representation

Irrigation was represented on a sub-grid cell basis using the high-resolution (500 m) irrigation fraction dataset from Ozdogan and Gutman (2008). Fractional irrigation data was aggregated to the 10 km WRF domain shown in Figure 3b. To represent irrigation, grid cells were divided into irrigated and non-irrigated segments and the near-surface soil layer within irrigated segments was held at saturation to a depth of 2 m (Figure 4). Surface fluxes and variables for each grid cell were calculated separately for the irrigated and non-irrigated segments at each time step and were weighted based on the irrigated fraction. A more detailed description of the process of applying irrigation in WRF is available in Section 2.3.2.

3.3.3 Determination of Irrigation-Induced Precipitation from Backward Trajectory Analysis

To determine the distribution of irrigation-induced precipitation, a backward trajectory technique was employed to establish the source of precipitation for each grid cell within the model domain (Figure 3a). This technique is based on the quasi-isentropic backward trajectory (QIBT) technique of Brubaker et al. (2001) and further discussed in Dirmeyer and Brubaker (2007). Trajectory calculations were based on the Lagrangian Trajectory Analysis from Merrill et al. (1986) and were performed with a time step of ten minutes using hourly WRF output that was linearly interpolated to ten-minute intervals.

Backward trajectories were calculated for each pentad (five-day period) to capture synoptic scale variability of precipitation (Dirmeyer and Brubaker 2007). For each pentad from May 4th to September 30th, the total precipitation was calculated for each grid cell using hourly WRF output. To track the source of precipitation in each grid cell, one hundred parcels were launched from each grid cell within a pentad, with each parcel representing a hundredth of the total pentad precipitation for each grid cell. Parcels were launched at the time that precipitation occurred, meaning that most parcels were launched at approximately the same time due to the highly convective nature of precipitation in the Great Plains (Changnon 2001). As parcels were tracked backwards, a fraction of the original precipitation of each parcel was attributed to local ET over the grid cells that the parcel passed over. The fraction of precipitation attributed to ET (the evaporative source) for each grid cell the parcel passed over was equal to the ET divided by the total column precipitable water of the grid cell the parcel was over. This approach assumes that water

vapor from surface ET mixes uniformly throughout the tropospheric column. While this assumption is not entirely realistic, errors are generally small for high ET rates since mixing is generally larger during high ET conditions (Dirmeyer and Brubaker 2007). As each parcel was tracked backwards, the evaporative source at each time step was deducted from the total precipitation. Parcels were tracked backwards until all the precipitation in the parcel was accounted for, it reached the boundary of the domain, or it was tracked for more than seven days. At the end of being tracked, each parcel had a unique distribution of the evaporative source of the precipitation that occurred at the time the parcel was launched. The combination of all one hundred parcels from a grid cell gave the origin of the precipitation that fell in the starting grid cell during a given pentad. Every grid cell within the model domain had 100 parcel launches for each pentad from May 4th through September 30th (unless no precipitation occurred).

Since the back-trajectory technique described above links precipitation over one grid cell to ET in grid cells upstream, data from this technique was used to determine the precipitation field that results from ET over each grid cell. Grid cells that had an irrigation fraction above a certain threshold had their precipitation distribution aggregated to give the distribution of precipitation that resulted from ET over all grid cells with a certain level of irrigation. This aggregation occurred for both control and irrigation simulations and allowed for calculation of the difference in the precipitation distribution between irrigated and control simulations. This difference (irrigated minus control) will be referred to as "irrigation-induced precipitation" because it is precipitation that resulted directly from ET of irrigated water.

3.3.4 Precipitation Recycling

Two approaches were used in this study to determine the precipitation recycling ratio for the region depicted in Figure 3b, an area calculated to be 1.25 x 10^6 km^2 in size. The first approach employed the QIBT analysis from Brubaker et al. (2001) as described in section 3.3.3 to trace the evaporative source of precipitation in each grid cell for every pentad. The second approach was derived from Dominguez et al. (2006), which uses the Dynamic Recycling Model (DRM) to trace the daily evaporative source of precipitation.

As described in section 3.3.3, the first approach to calculating precipitation recycling ratios was based on the QIBT technique from Brubaker et al. (2001). Precipitation that fell and had its evaporative source within the region of study was considered to be recycled precipitation. The precipitation recycling ratio (rr) was determined by dividing the recycled precipitation by the total precipitation within the region of study:

$$rr = \frac{\mathrm{Pr}}{P} \quad (2)$$

where Pr is the precipitation of recycled origin, and P is the total precipitation. Precipitation recycling ratios were calculated for all pentads from May to September.

The second approach used the DRM from Dominguez et al. (2006), which accounts for moisture storage and assumes a well-mixed atmosphere. Accounting for moisture storage allows for the computation of recycling ratios on short time-scales (Bisselink and Dolman 2008). The well-mixed atmosphere assumption implies that the ratio of recycled precipitation to total precipitation is equal to the ratio of locally evapotranspired water vapor to total water vapor. This assumption limits the temporal

scale of the DRM to timescales that are equivalent to boundary layer mixing (Dominguez et al. 2006). The underlying principle of the DRM (and all other bulk recycling models) is the vertically integrated water vapor balance equation, which is expressed as

$$\frac{\partial w}{\partial t} + \frac{\partial (wu)}{\partial x} + \frac{\partial (wv)}{\partial y} = E - P \qquad (3)$$

where

$$w = \int_0^{p_0} \overline{q} \frac{dp}{g}; \qquad (4)$$

$$u = \frac{1}{w}\left(\int_0^{p_0} \overline{q}\,\overline{\hat{u}} \frac{dp}{g} + \int_0^{p_0} \overline{q' \hat{u}'} \frac{dp}{g} \right); \qquad (5)$$

$$v = \frac{1}{w}\left(\int_0^{p_0} \overline{q}\,\overline{\hat{v}} \frac{dp}{g} + \int_0^{p_0} \overline{q' \hat{v}'} \frac{dp}{g} \right), \qquad (6)$$

where w is the precipitable water in a column of air, E is evapotranspiration, P is precipitation; and $\overline{q}$, q', $\overline{\hat{u}}$, $\hat{u}'$, $\overline{\hat{v}}$, and $\hat{v}'$ are the time mean and transient eddy values of specific humidity as well as zonal and meridional wind components, respectively. Integrals are performed from the surface ($p = p_0$) to the top of the atmosphere ($p = 0$) and g is the acceleration due to gravity (Dominguez et al. 2006). The variables $u, v,$ and w represent the vertically integrated moisture flux vector components, which describe column-averaged, moisture-weighted wind vectors. The variables u, v, and w were calculated hourly from the WRF output.

The water vapor balance equation makes up the foundation of the dynamic recycling model. Using the assumption that the atmosphere is well mixed, the definition of the recycling ratio, and the conservation of mass, Equation (3) can be rewritten as

$$w\frac{\partial \rho}{\partial t} + wu\frac{\partial \rho}{\partial x} + wv\frac{\partial \rho}{\partial y} = E(1-\rho), \qquad (7)$$

where ρ is the local recycling ratio. A Lagrangian coordinate system (where $\chi = x - ut$, $\xi = y - vt$, $\tau = t$) that follows the movement of moisture advection is used to solve for recycling ratio. Substituting this new coordinate system yields a simple ordinary differential equation that describes the recycling ratio (R) for a single grid point within the region of study:

$$R(\chi,\xi,\tau) = 1 - \exp\left[-\int_0^{\tau} \frac{\varepsilon(\chi,\xi,\tau)}{\omega(\chi,\xi,\tau)}\partial\tau'\right], \qquad (8)$$

where $\varepsilon(\chi,\xi,\tau)$is the evapotranspiration, $R(\chi,\xi,\tau)$ is the recycling ratio, and $\omega(\chi,\xi,\tau)$ is the precipitable water. To calculate the recycling ratio from Equation (8), each grid cell had a daily backward trajectory completed to determine the source of moisture over each grid cell. Trajectories were calculated using the moisture-weighted column averages of the meridional and zonal wind velocities calculated in Equations (5-6) and the iterative backward trajectory technique from Merrill et al. (1986). Recycling ratios were calculated using integrals calculated along the path of trajectories using the Lagrangian coordinate system. Once recycling ratios were determined for individual grid cells within the region of study, the recycling ratio for the entire region of study (rr) was determined by summing the recycled precipitation from all grid cells within the region of study and dividing by the total precipitation:

$$rr = \frac{\sum_{i=1}^{n} \rho_i P_i \Delta A_i}{\sum_{i=1}^{n} P_i \Delta A_i}, \qquad (9)$$

where ρ_i is the recycling ratio for each grid cell, P_i is the precipitation from each grid cell, and ΔA_i is an area consisting of *n* grid cells (Bisselink and Dolman 2008).

The precipitation recycling methods described above from Brubaker et al. (2001) and Dominguez et al. (2006) provide similar avenues for determining the recycling ratio. Each method determines the recycling ratio by tracing the source of moisture through backward trajectories, while assuming a well-mixed atmosphere. Notable differences between the two techniques, however, generally produce different results. The technique of Brubaker et al. (2001) typically results in higher recycling ratios because the launch of one hundred trajectories per pentad from each grid cell produces shorter trajectories for low precipitation events compared with Dominguez et al. (2006) which launches a single daily backward trajectory, thereby placing the evaporative source closer to where the precipitation occurs. The inclusion of two different precipitation recycling approaches allows for a more complete look at how irrigation impacts precipitation recycling over the Great Plains while not being subject to possible biases from using a single method.

3.3.5 Experimental Design

This study included a balance of precipitation and ENSO regimes to represent the broad spectrum of climatic conditions that occur over the Great Plains. An array of precipitation regimes were chosen to represent the spectrum of antecedent soil moisture conditions, while a set of ENSO regimes were chosen to represent the spectrum of external climate forcings. Drought, normal, and pluvial years were determined based on the average 1980-2008 May-September NARR precipitation (Mesinger et al. 2006) over an area centered in the Great Plains region (30.5° to 44.5° N, 91.5° to 105.5° W).

Drought years had May-September precipitation at least one standard deviation below the 1980-2008 mean, flood years were at least one standard deviation above the mean, and normal years were any year within one standard deviation of the mean. El Niño/La Niña years were determined from May-September averages of the bimonthly ranks of the Multivariate ENSO Index (MEI) from Wolter and Timlin (1998). El Niño, La Niña, and neutral years were determined using guidelines from Wolter and Timlin (1998), except that terciles (33rd percentiles) were used instead of the lowest and highest 30th percentiles. Selection of simulated years was determined by identifying nine different years that represent all combinations of the three precipitation regimes and the three ENSO states (Table 1). For each year, simulations without irrigation (control) and with irrigation were conducted.

The WRF model (v3.2) was initialized using 3-hourly data from NARR for all identified years as listed in Table 1 (Mesinger et al. 2006; Skamarock et al. 2008). Model simulations were completed using the same 180 x 195 grid with a 10 km horizontal resolution, 38 vertical levels, 4 soil layers (to a depth of 2 m), and a 30-second time step, with the exception of 2007 which used a 25-second time step for both control and irrigation simulations because of instabilities with the forcing dataset during that year. Simulations were completed from April 1 to October 1. The Noah Land-Surface Model was modified to include irrigation (described in sections 2.3.2 and 3.3.2). No cumulus parameter was employed because sensitivity runs of WRF using a cumulus parameter (explained in section 2.3.3) showed a dramatic overestimation of precipitation over long periods of time when compared with precipitation estimates from NARR (Mesinger et al.

2006) and NCEP's National Stage IV datasets (Lin and Mitchell 2005). Additional information on the selection of model parameters is described in section 2.3.3.

3.3.6 Statistical Significance

Two-tailed t-tests using a matched pairs design at a 95% confidence level were conducted to determine whether statistically significant differences between irrigated and control simulations occurred. Unless otherwise noted, all differences are considered to be the set of control simulations subtracted from the set of irrigation simulations.

3.4 Results

All results in this section are reported for pentad groups because since the distribution of irrigation-induced precipitation was determined for pentads, calculations over calendar months were not possible. Instead, groups of six pentads (30 days) were used as proxies for months. Therefore, results reported for "May" are for the 30-day period from May 4-June 2, "June" is for June 3-July 2, "July" is for July 3-August 1, "August" is for August 2-31, and "September" is for September 1-30. All numerical values of irrigation-induced precipitation describe weighted area averages of irrigation-induced precipitation that originated from grid cells with at least 10% irrigation within the region of study (defined in Figure 3b), unless otherwise noted. All discussed values are for the period of May-September unless otherwise noted.

3.4.1 Irrigation-Induced Precipitation

A wide swath of over 9 mm of irrigation-induced precipitation occurred throughout much of the northern Great Plains and Upper Midwest for the average of all

simulated years (Figure 14a). The heaviest irrigation-induced precipitation occurred over north-central Nebraska (20 mm), which was 3.6% of the average May-September control simulated precipitation. Considering the average of all simulated years, the heaviest irrigation-induced precipitation was consistently displaced slightly downwind of heavily irrigated areas, with broad swaths of irrigation-induced precipitation generally aligned with average moisture-weighted wind vectors (Figure 15e). Heavily irrigated areas in the northern Great Plains typically contributed the most irrigation-induced precipitation (Figure 15c). Cumulatively, irrigated areas in the northern Great Plains (outlined in Figure 15c) contributed 51.8% of the total irrigation-induced precipitation while irrigated areas within and adjacent to the Texas Panhandle (outlined in Figure 15d) contributed 33.7% of the total irrigation-induced precipitation. Irrigated areas in eastern Nebraska (outlined in Figure 15b) contributed 26.1% of the total irrigation-induced precipitation within the model domain, while irrigated areas in and adjacent to western Nebraska (outlined in Figure 15a) produced 25.7%. Irrigation-induced precipitation from eastern Nebraska was spread over a larger area compared with western Nebraska due to stronger 850 hPa winds over eastern Nebraska (Figure 16a).

Over the region of study, 5.12 mm and 3.00 mm of irrigation-induced precipitation fell on average from May-September and June-August, respectively (Table 5). These values were approximately 0.9% of the total simulated precipitation for both periods when considering the entire region of study, compared to up to 4% in some locations in Nebraska. For the average of all simulated years, irrigation-induced precipitation was significantly greater than zero for all months (Table 5). Irrigation-

induced precipitation was largest during May (1.28 mm) and June (1.24 mm), and lowest during July (0.79 mm; Table 5). Light irrigation-induced precipitation during July was coincident with relatively strong 850 hPa winds over irrigated areas compared to other months (Figure 17), suggesting that irrigated moisture was advected out of the region of study before falling out as precipitation. Conversely, weaker 850 hPa winds during May and June over irrigated areas meant that evapotranspired moisture from irrigated fields remained over the region of study for a longer period of time, increasing the likelihood of irrigation-induced precipitation within the region.

The concentration of irrigation also played a role in the *production* of irrigation-induced precipitation. When considering how the production of irrigation-induced precipitation changed with irrigation fraction, the more heavily irrigated grid cells produced more irrigation-induced precipitation on a per grid cell basis than the less irrigated grid cells (Figure 18a). While heavily irrigated grid cells produced more irrigation-induced precipitation, heavily irrigated grid cells also *received* more irrigation-induced precipitation (Figure 18b). Grid cells with at least 50% irrigation received 8.59 mm of irrigation-induced precipitation, compared with only 6.64 mm for grid cells with 5-10% irrigation (Figure 18b). Irrigated grid cells in general also received relatively more irrigation-induced precipitation compared with non-irrigated grid cells. Over grid cells with at least 10% irrigation within the region of study, the 7.62 mm of irrigation-induced precipitation that fell was significantly greater than the 5.11 mm of irrigation-induced precipitation that occurred over the entire region of study.

When considering the impact of antecedent soil moisture on irrigation-induced precipitation, normal years had the most irrigation-induced precipitation out of all precipitation regimes during both May-September (Figure 14c) and June-August (Table 5). Relatively weaker 850 hPa winds during normal years decreased the advection of evapotranspired moisture from irrigated fields out of the region of study, enhancing irrigation-induced precipitation. As a result, 5.43 mm of irrigation-induced precipitation fell on average during May-September in normal years (Table 5). Drought and pluvial years had lighter irrigation-induced precipitation than normal years because of stronger 850 hPa winds over the region. Surprisingly, similar amounts of irrigation-induced precipitation occurred during drought and flood years despite large differences in antecedent soil moisture. During pluvial years, very strong 850 hPa winds over the Great Plains (Figure 16d) resulted in only 4.93 mm of irrigation-induced precipitation (Table 5). Slightly weaker 850 hPa winds during drought years (Figure 16b) resulted in 4.99 mm of irrigation-induced precipitation (Table 5). During drought years, more southerly 850 hPa winds (Figure 16b) typically displaced irrigation-induced precipitation further north and west (Figure 14b). Up to 28.5 mm of irrigation-induced precipitation fell over north-central Nebraska during drought years, roughly 6% of the average May-September precipitation. While irrigation-induced precipitation was not noticeably suppressed during drought years over the entire region of study, the lightest irrigation-induced precipitation occurred over irrigated areas during drought years. Only 6.65 mm of irrigation-induced precipitation occurred over irrigated areas, compared with 8.46 mm during normal years and 7.76 mm during pluvial years. Irrigation-induced precipitation

also decreased with increasing irrigation fraction during drought years (Figure 18b), consistent with the suppression of precipitation with increasing irrigation fraction during drought years in Chapter 2. Considering the impact of irrigation intensity on the *production* of irrigation-induced precipitation during drought years, lightly irrigated grid cells produced the least irrigation-induced precipitation while heavily irrigated grid cells produced the most (Figure 18a). As a result, drought years exhibited the greatest increase in the production of irrigation-induced precipitation as the grid cell irrigation fraction increased (Figure 18a).

When considering the variability of irrigation-induced precipitation across ENSO regimes, irrigation-induced precipitation was the heaviest during neutral years (5.85 mm; Table 5; Figure 14f) and the lightest during El Niño years (4.64 mm; Table 5; Figure 14g). El Niño years had the weakest 850 hPa wind speeds over the Great Plains (Figure 16g), but significantly smaller ET increases occurred during El Niño years. The relatively lower amount of net radiation that was available during El Niño years (not shown) meant that less energy could be partitioned into latent heating, effectively limiting the amount of evapotranspired moisture that came from irrigated fields (Table 10). Conversely, greater ET increases during neutral years (Table 10) resulted in the heaviest irrigation-induced precipitation of all ENSO regimes (8.35 mm; Table 5; Figure 14f) despite relatively strong 850 hPa winds (Figure 16f).

3.4.2 Precipitation Recycling

Precipitation recycling ratios from the control simulations were significantly higher when using techniques from Brubaker et al. (2001) compared with Dominguez et

al. (2006) (Table 6; 7). While the magnitudes of recycling ratios for both methods were different, seasonal patterns were similar. Recycling ratios were highest in July and lowest in September for both methods (Table 6; 7). When considering variations in the control recycling ratio for different precipitation regimes, recycling ratios were generally the lowest during pluvial years and the highest during normal years (Table 6; 7). Strong 850 hPa wind speeds over the region of study (Figure 16d) and heavy precipitation resulted in low recycling ratios during pluvial years (Table 6; 7). Conversely, generally weak 850 hPa winds over the region of study (Figure 16c) resulted in larger recycling ratios during normal years. Using the approach of Brubaker et al. (2001), recycling ratios were larger during drought years compared with pluvial years for all months during control simulations (Table 7). Similarly, using the approach from Dominguez et al. (2006), recycling ratios were larger during drought years compared with pluvial years for all months except September (Table 6).

Irrigation resulted in an additional 6.71 mm of May-September recycled precipitation for all simulated years when considering the average of both methods (Table 10). When comparing monthly recycling ratio changes between methods, inconsistent seasonal patterns emerged. The largest recycling ratio increases during irrigation simulations occurred in September when considering both methods, but large discrepancies existed in July (Table 8; 9). Using methods from Dominguez et al. (2006) resulted in large July recycling ratio increases of 0.013, while increases of only 0.002 occurred when using methods from Brubaker et al. (2001). Despite the inconsistency in

monthly recycling ratio changes, consideration of multi-month composites for different precipitation and ENSO regimes yielded consistent results.

When considering changes in the recycling ratio from irrigation for different precipitation regimes, large differences in precipitation between different regimes meant that recycling ratio changes were generally dependent on the amount of precipitation that occurred. Years with light precipitation tended to have large increases in the recycling ratio despite small increases in recycled precipitation. For example, while the largest recycling ratio increase consistently occurred during drought years (Table 8; 9), the smallest change in recycled precipitation occurred during drought years (Table 10) because of relatively light precipitation. Considering the average of both methods, the recycling ratio increased by 0.012 and recycled precipitation increased by 6.13 mm during drought years (Table 10). During pluvial years, the recycling ratio increase was the smallest for both methods (0.008 on average), but the increase in recycled precipitation (6.35 mm) was slightly larger than during drought years because of heavier precipitation during pluvial years. The largest increase in recycled precipitation occurred during normal years (7.65 mm), because of relatively weak 850 hPa wind speeds over the region of study compared with drought and pluvial years (Figure 16).

When examining the effect of ENSO on precipitation recycling, changes in the recycling ratio and recycled precipitation were more consistent because the recycling ratio had less dependence on the amount of precipitation that occurred. Neutral years had the largest recycling ratio increase for both methods (Table 8; 9) and the largest increase in recycled precipitation (8.35 mm; Table 10), coincident with large ET increases (Table

10). Conversely, recycling ratio (Table 8; 9) and recycled precipitation (Table 10) increases were the smallest during El Niño years, despite relatively weak 850 hPa wind speeds over the region of study (Figure 16g). This likely occurred because less net radiation was available for partitioning into latent heating, leading to reduced evapotranspiration in the region of study.

3.5 Discussion

3.5.1 Comparison to previous studies

DeAngelis et al. (2010) examined the distribution of July precipitation that resulted from ET over the Ogallala Aquifer during high and low ET years using Lagrangian tracing of vapor sources. Subtracting the precipitation distribution during low ET years from the distribution during high ET years essentially represented the difference in precipitation that resulted from irrigation because a significant portion of ET over the Ogallala comes from irrigation. This precipitation distribution also will be referred to as "irrigation-induced precipitation." The distribution of July irrigation-induced precipitation presented in this study was generally similar to DeAngelis et al. (2010), except that irrigation-induced precipitation in this study was slightly farther to the north and west (not shown). Despite similar distributions, July irrigation-induced precipitation in this study was only about 25% as large as results from DeAngelis et al. (2010). Irrigation-induced precipitation from DeAngelis et al. (2010) was likely larger because it included differences in ET that resulted from precipitation discrepancies between drought

and pluvial years, likely producing greater changes in ET than would occur from irrigation alone.

Comparison of our precipitation recycling ratio findings to previous studies reveals similar results despite the fact that the region of study was larger and located over a slightly different part of the Great Plains than previous studies. Recycling ratios calculated for the region of study when using techniques from Brubaker et al. (2001) were generally similar to previous results. Higher recycling ratios during drought years compared with pluvial years in this study were consistent with higher recycling ratios during the 1988 drought compared with the 1993 flood from Brubaker et al. (2001). Over the Upper Mississippi and Missouri River Basins, Brubaker et al. (2001) reported April-July recycling ratios of 0.32 and 0.28 during 1988 and 1993, compared with our simulated May-July recycling ratios of 0.312 and 0.287 using the Brubaker et al. (2001) method during drought and pluvial years, respectively. Recycling ratios were also similar to previous studies when using techniques from Dominguez et al. (2006), despite the fact that the region of study was 25% larger than regions used in their calculations. On average, the June-August recycling ratio over the region of study was 0.23, compared with 0.14 over the Great Plains from Dominguez et al. (2006). When considering all seven overlapping years between this study and Dominguez et al. (2006), 1993 had the lowest recycling ratio over the Great Plains for both studies, with a recycling ratio of 0.16 in this study and 0.12 in Dominguez et al. (2006) (using their Region 12). Considering overlapping years, 1988 had the largest recycling ratio in Dominguez et al. (2006) but only the third largest in this study. When considering previous studies, the recycling ratio

discrepancy that was found between methods from Brubaker et al. (2001) and Dominguez et al. (2006) in this study was consistent with previous results.

3.5.2 Discussion of Model Results

Irrigation-induced precipitation was generally controlled by the strength of the 850 hPa wind field and the change in ET from irrigation. When 850 hPa wind speeds were relatively weak, greater irrigation-induced precipitation occurred because evapotranspired moisture from irrigated fields remained over the region of study longer, increasing the likelihood of falling out as precipitation before being advected out of the region. This is supported by the fact that the heaviest irrigation-induced precipitation out of all precipitation regimes occurred during normal years when 850 hPa winds were the weakest (Figure 16c). Conversely, the lightest irrigation-induced precipitation fell during pluvial years when 850 hPa winds were the strongest (Figure 16d). When considering the monthly variability, the least irrigation-induced precipitation occurred during July when 850 hPa wind speeds were the strongest (Figure 17c), consistent with the annual maximum in the Great Plains low level jet (GPLLJ) (DeAngelis et al. 2010; Weaver et al. 2009). Conversely, the heaviest irrigation-induced precipitation occurred during May and June when 850 hPa winds were the weakest (Figures 17a; 17b). While the strength of the low-level wind field contributed significantly to the variability of irrigation-induced precipitation, the ET change due to irrigation was also a factor. Considering the variation in irrigation-induced precipitation for the set of ENSO regimes, El Niño years had the lowest irrigation-induced precipitation because only a small amount of net radiation was available for partitioning into latent heating, resulting in meager changes in ET during

irrigation simulations. As a result, only light irrigation-induced precipitation occurred despite the fact that El Niño years had the weakest 850 hPa wind speeds (Figure 16g), which were inconsistent with findings from Weaver et al. (2009) that suggest a positive correlation between equatorial Pacific sea surface temperatures and the strength of the GPLLJ.

Because irrigation-induced precipitation is simply a subset of recycled precipitation (irrigation-induced precipitation that falls within the region of study is also recycled precipitation), changes in recycled precipitation were also controlled by the strength of the 850 hPa wind field and changes in ET due to irrigation. When considering how recycled precipitation varied for different precipitation regimes and on a monthly basis for all simulated years, the strength of the 850 hPa wind field played a prominent role. The strongest increase in recycled precipitation occurred during normal years when 850 hPa winds over the region of study were weakest (Figure 16c). For all simulated years, increases in recycled precipitation were lowest during the months of July and August, when 850 hPa winds were stronger over the region of study compared to other months (Figure 17). When considering the variability of changes in recycled precipitation for ENSO regimes, changes in ET from irrigation appeared to be primarily responsible. The largest increase in recycled precipitation occurred during neutral years due to large ET increases, despite strong 850 hPa winds over the region of study. Conversely, El Niño years had the smallest increase in recycled precipitation due to small ET increases, despite the fact that the weakest 850 hPa winds were present over the region study.

Changes in recycled precipitation were controlled by the same factors as irrigation-induced precipitation. Comparison of irrigation-induced precipitation to changes in recycled precipitation in Table 10 shows that irrigation-induced precipitation accounted for 76% of the change in recycled precipitation. Moderately strong correlation ($R^2 = 0.493$ for June-August, $R^2 = 0.211$ for May-September) between irrigation-induced precipitation and changes in recycled precipitation suggest that the change in recycled precipitation during irrigation simulations was primarily due to precipitation of evapotranspired water from irrigated fields. Similarly, comparison of the average May-September irrigation-induced precipitation (5.12 mm) to the average change in precipitation during irrigation simulations (4.97 mm; Table 10) implies that irrigation-induced precipitation accounted for the entire change in precipitation that occurred due to irrigation. This is supported by the fact that irrigation-induced precipitation was the primary cause of recycled precipitation changes and by strong correlation between recycled precipitation changes and total precipitation changes ($R^2 = 0.692$ for June-August, $R^2 = 0.547$ for May-September). Therefore, the increase in precipitation that occurred during irrigation simulations was primarily due to ET over irrigated fields (irrigation-induced precipitation) when considering the average of all simulated years. Because precipitation increases were due to ET over irrigated fields, precipitation increases during irrigation simulations cannot be attributed to increases in moisture advection from external sources. Furthermore, the average increase in recycled precipitation (6.71 mm) was greater than the average increase in precipitation (4.97 mm)

during irrigation simulations, suggesting that precipitation from external moisture sources (non-recycled precipitation) was actually reduced with irrigation.

While irrigation-induced precipitation and changes in precipitation during the irrigation simulations were closely related when considering weighted area averages of the region of study, comparison of their distributions also yielded interesting results. In north-central Nebraska, the heaviest average May-September irrigation-induced precipitation for all simulated years (Figure 19a) was coincident with a broad swath of average simulated precipitation increases (Figure 19b). Analysis of Cooperative Weather Observation Network (COOP) observations from the National Climatic Data Center (NCDC) over the region outlined in Figure 19 show that an additional 22.28 mm of May-September precipitation (not significant) fell between 1951-2000 (after the implementation of irrigation in this region) compared with the period of 1901-1950 (before irrigation). While the average precipitation increase after irrigation in this region was not statistically significant, 22 of the 26 counties outlined in Figure 19c had more precipitation after the implementation of irrigation and eight of them were statistically significant with 95% confidence with two-tailed, unpaired t-tests (Figure 19c). This suggests that precipitation increased over north-central Nebraska because of the implementation of irrigation in the second half of the 20th century. Considering the weighted area average over the area of counties outlined in Figure 19a, 9.11 mm of irrigation-induced precipitation was simulated, slightly more than the 8.96 mm average precipitation increase during irrigation simulations. Because the average irrigation-induced precipitation was approximately the same magnitude as the average precipitation

change, the change in precipitation over this area can be attributed to water that was evapotranspired over irrigated fields. When considering the source of irrigation-induced precipitation (and inherently the average precipitation change) over this area, 39.7% was from irrigated areas in eastern Nebraska (outlined in Figure 15b), 27.8% was from irrigated areas in and adjacent to western Nebraska (outlined in Figure 15a), and 26.3% was from irrigated areas in and adjacent to the Texas Panhandle (outlined in Figure 15d). The combination of heavily concentrated irrigation-induced precipitation, simulated precipitation increases, and observed precipitation increases in the majority of counties in north-central Nebraska suggest that evapotranspired water from irrigated fields was responsible for the observed increase in precipitation over north-central Nebraska during the latter half of the 20th century.

While irrigation-induced precipitation was shown to be responsible for precipitation increases over the region of study, and especially over north-central Nebraska, much of the evapotranspired water from irrigated fields was advected out of the region without falling out as precipitation. Comparison of ET from irrigated fields (not shown) with irrigation-induced precipitation shows that only a small percentage of evapotranspired water (15.8%) from irrigated fields fell out as precipitation over the region of study. When considering the change in *total* ET over the entire region of study (22.26 mm) to the weighted average of irrigation-induced precipitation (5.12 mm), irrigation-induced precipitation was only 23% as large as the increase in ET during irrigation simulations (Table 10). Similarly, recycled precipitation increases were only 30.1% as large as the ET increase due to irrigation (Table 10). Whether considering

irrigation-induced precipitation or changes in recycled precipitation, greater increases in ET over the Great Plains from irrigation clearly resulted in a loss of water out of the region. This was compounded by the fact that precipitation of externally advected moisture (non-recycled precipitation) decreased during irrigation simulations, as evidenced by greater increases in recycled precipitation compared with total precipitation (Table 10). During drought years, not only was the difference between changes in ET and recycled precipitation the largest, but the greatest decrease in non-recycled precipitation also occurred. Therefore, drought years experienced the greatest loss of water from irrigated fields as well as the greatest decrease in precipitation of advected moisture, resulting in large losses of water over the Great Plains during drought years. Heavily irrigated areas experienced the greatest losses of water during drought years because of large ET increases and light irrigation-induced precipitation (Figure 18b), which was consistent with the overall suppression of precipitation that occurred over heavily irrigated grid cells due to large decreases in the PBL height as noted in Chapter 2.

3.6 Conclusions

This study has demonstrated that evapotranspired water from irrigated fields in the Great Plains falls out as precipitation over much of the Great Plains and Upper Midwest, resulting in localized and region-wide increases in precipitation. On average, irrigation-induced precipitation is primarily responsible for precipitation increases of 1% over the Great Plains and 1.6% over north-central Nebraska. The distribution and magnitude of irrigation-induced precipitation has been shown to be dependent on the

strength of the 850 hPa wind field and the amount of available net radiation for partitioning into latent heating.

While a significant amount of evapotranspired water from irrigated fields results in an increase in precipitation recycling and total precipitation over the Great Plains, a large majority of evapotranspired water from irrigated fields is advected out of the region before falling out as precipitation. Similarly, increases in recycled precipitation are greater than the average increases in precipitation during irrigation simulations, suggesting that precipitation of advected moisture (non-recycled precipitation) is reduced in the presence of irrigation. As a result, irrigation diminishes the replenishment of groundwater supplies from externally advected moisture. The advection of large amounts of irrigated water out of the region combined with decreases in precipitation from external moisture sources suggests that irrigation could result in an additional depletion of regional groundwater supplies through a positive feedback mechanism. The large loss of groundwater out of the region due to irrigation results in drier soil moisture and likely promotes increased use of water for irrigation, most of which is evapotranspired and advected out of the region, thereby resulting in further reductions in total soil moisture.

Because simulations showed that water loss due to irrigation is the most prevalent during drought years, depletion of the Ogallala Aquifer from irrigation could be the most severe during periods of sustained drought. Future projections of increased drought likelihood due to climate change (Gregory et al. 1997; IPCC 2007; Kumar 2007; Manabe et al. 2004; Rind et al. 1990; Wang 2005; Wetherald and Manabe 1995, 1999), suggest that the depletion of groundwater supplies in the Ogallala Aquifer with irrigation will

likely be accelerated. More sophisticated water management in the Great Plains may be necessary in the future because water extraction costs are expected to continue to rise. As the Great Plains is one of the most critical agricultural regions in the world, more sophisticated water management of the Ogallala Aquifer in the future will likely benefit food security and economic stability in a world of rising food and energy prices.

3.7 Acknowledgments

Support for this project provided by the University of Minnesota Grant-in-Aid Program (#21601). This work was carried out in part using computing resources at the University of Minnesota Supercomputing Institute. We thank Dr. Mutlu Ozdogan for providing the fractional irrigation dataset, Dr. Francina Dominguez for providing her precipitation recycling code, and Dr. Stefan Liess for help in implementing the irrigation algorithm in WRF.

Chapter 4

Conclusion

The methods employed in this study provide a new and unique look into the impact of irrigation on the atmospheric branch of the hydrologic cycle. The inclusion of sub-grid scale irrigation in a high-resolution coupled land-atmospheric model allowed for an examination of the full atmospheric impact of irrigation in the Great Plains. In addition, a modified backward trajectory technique was used to determine where evapotranspired water from irrigated fields in the Great Plains generally falls out as precipitation and how irrigation affects precipitation recycling in the region. In this study, irrigation has been shown to impact the hydrologic cycle of the Great Plains by altering the rates of evapotranspiration and precipitation. Increases in convective available potential energy (CAPE) due to surface moisture enhancement overcame decreases in the planetary boundary layer height from surface cooling, resulting in the enhancement of summer rainfall over the Great Plains. On average, May-September rainfall over the Great Plains increased by 4.97 mm (0.91%) as a result of irrigation, with localized increases of up to 20% over parts of Nebraska, Kansas, and Oklahoma. Precipitation increases were the largest during pluvial years (6.14 mm; 0.98%) and the smallest during drought years (2.85 mm; 0.63%). Over irrigated areas, large precipitation increases occurred during pluvial (9.97 mm; 1.77%) and normal years (14.87 mm; 3.01%) while decreases occurred during drought years (-1.26 mm; -0.31%) because of strong decreases in PBL height over irrigated areas. The suppression of precipitation over irrigated areas

during drought years suggests that an antecedent soil moisture threshold likely exists where irrigation suppresses precipitation at low soil moisture levels and enhances precipitation at relatively high soil moisture levels over irrigated areas. Additional simulations using WRF with varying soil moisture levels may provide additional insight into the existence of an antecedent soil moisture threshold.

While changes in precipitation with irrigation had a significant impact on the hydrologic cycle of the Great Plains, identification of the source of increased rainfall provided additional insight into the impact that irrigation has on the hydrologic cycle. Increases in summertime rainfall and precipitation recycling (6.71 mm) that occurred with irrigation were attributed to evapotranspired water from irrigated fields (i.e. irrigation-induced precipitation). The average May-September irrigation-induced precipitation was 5.11 mm, slightly more than the increase in precipitation that occurred during simulations that included irrigation. Irrigation-induced precipitation was largest during normal precipitation years (5.43 mm) when the 850 hPa wind field was relatively weak, and smallest during pluvial years (4.93 mm) when the 850 hPa wind field was relatively strong. These results suggest that the magnitude of irrigation-induced precipitation is strongly dependent on the strength of the low-level wind field. The heaviest irrigation-induced precipitation occurred over north-central Nebraska, coincident with simulated and observed precipitation increases. That is, observed precipitation increases that occurred over north-central Nebraska since the implementation of irrigation are likely from evapotranspired water over irrigated fields.

While irrigation results in localized and region-wide enhancements in summer rainfall over the Great Plains, increases in evapotranspiration from irrigation are much larger than increases in precipitation. Therefore, irrigation results in a large net loss of water during the warm season in the Great Plains. This is supported by the fact that only 16% of evapotranspired water from irrigated fields fell out as precipitation over the Great Plains in the irrigation simulations. Additionally, increases in recycled precipitation were greater than increases in overall precipitation, suggesting that a decrease in precipitation of externally advected moisture occurs when irrigation is present in the Great Plains. The large loss of irrigated moisture out of the region and the decrease in precipitation from external moisture sources likely combine to drive large annual water deficits from irrigation in the Great Plains. The fact that the largest loss of irrigated moisture out of the region and the greatest decrease in precipitation from external moisture sources occurred during drought years suggests that the largest water losses from irrigation likely occur during drought years in the Great Plains. Because future droughts are expected to increase in severity and prevalence in the Great Plains with climate change (Gregory et al. 1997; IPCC 2007; Kumar 2007; Manabe et al. 2004; Rind et al. 1990; Wang 2005; Wetherald and Manabe 1995, 1999), annual water losses from irrigation are expected to increase.

An increase in water loss in this century will likely accelerate depletion of the Ogallala Aquifer, a critical supplier of groundwater for agriculture in the semi-arid Great Plains. The addition of high-resolution future climate scenarios in WRF will be required to determine the expected future impact of irrigation on the hydrologic cycle of the Great

Plains. These simulations would provide some insight into possible mitigation strategies to address the predicted widespread water shortages. Since the Great Plains is part of the most productive agricultural region in the world, management of groundwater supplies is critical for food security and economic stability in a world of rising food and energy prices. Effective management of the groundwater supplies from the Ogallala Aquifer can forge a delicate balance between supporting irrigated agriculture and preventing depletion of this finite source of paleowater, thus preserving an important source of groundwater for future generations.

4.1 Future Work

A number of possible research directions involving the impact of irrigation on the atmospheric branch of the hydrologic cycle have emerged as a result of the findings reported in this study. The discovery of a possible soil moisture threshold in Chapter 2 warrants further investigation. Simulations using varying levels of soil moisture over the Great Plains could be used to determine the presence and magnitude of an antecedent soil moisture threshold whereby irrigation suppresses convection over irrigated areas during low soil moisture conditions and enhances convection when antecedent soil moisture is reasonably high. This knowledge could be applied in future water management strategies for mitigation of possible extreme events.

While understanding the current impact of irrigation in the hydrologic cycle is important, determining the future impact of irrigation with climate change allows for more guided water management. In this study, the smallest precipitation increases occurred during drought years, coincident with the largest increase in evapotranspiration.

Therefore, the largest loss of water over irrigated areas and the region of study occurred during drought years. Because the prevalence and severity of droughts are expected to increase in the Great Plains with climate change, increased water losses from irrigation will likely occur in the future. Future regional simulations forced with data from climate model scenarios could be used to determine whether accelerated water losses from irrigation will occur over the Great Plains in the remainder of the 21st century. Knowledge of the future impact of irrigation on the hydrologic cycle would provide better insight into future management of the Ogallala Aquifer.

While the modified backward trajectory analysis in this study provided a new and unique look into the precipitation of irrigated water in the Great Plains, using the same approach with small changes to the model domain could allow for an even more detailed analysis. Because the model domain was constrained to only cover the middle third of the contiguous United States, the full atmospheric transport of irrigated water could not be realized because a large majority of evapotranspired water from irrigated fields left the model domain without falling out as precipitation. An eastward expansion of the model domain in future studies could be used to examine how far irrigated water from the Great Plains travels before it falls out as precipitation. Similarly, southward expansion of the model domain could allow for the identification of changes in the advection of Gulf moisture into the region. Implementing these modifications would require greater computing power, but would allow for an even more detailed look into the hemispheric impact of irrigation on the hydrologic cycle. Further knowledge into the full impact of

irrigation on the hydrologic cycle would allow for more effective management of regional water supplies in a world where water is quickly becoming a limited resource.

Tables

Simulations	Precipitation and ENSO Regimes		
	Drought	**Normal**	**Pluvial**
Current Vegetation, Irrigated (IRRIG)	El Niño: 1983 Neutral: 2000 La Niña:1988	El Niño: 1997 Neutral: 1990 La Niña: 1985	El Niño: 1993 Neutral: 2008 La Niña: 2007
Current Vegetation, Non-Irrigated (CONTROL)	El Niño: 1983 Neutral: 2000 La Niña:1988	El Niño: 1997 Neutral: 1990 La Niña: 1985	El Niño: 1993 Neutral: 2008 La Niña: 2007

Table 1. Summary of simulated years, precipitation regimes, and ENSO regimes.

	Region of Study (RoS) Averages		10%+ Irrigated Grid Cells within RoS	
	May-September	**JJA**	**May-September**	**JJA**
Irrigated Area (km^2)	6.39×10^4	6.39×10^4	5.0×10^4	5.0×10^4
Soil Moisture Difference ($m^3\ m^{-3}$)	0.014 [5.68%]***	0.014 [5.75%]***	0.059 [27.0%]***	0.059 [27.3%]***
Latent Heat Flux Change ($W\ m^{-2}$)	4.293 [4.29%]***	4.332 [4.04%]***	20.745 [22.6%]***	21.182 [21.6%]***
Sensible Heat Flux Change ($W\ m^{-2}$)	-3.235 [-7.74%]***	-3.353 [-7.86%]***	-14.542 [-30.2%]***	-14.846 [-30.3%]***
Net Radiation Change ($W\ m^{-2}$)	0.107 [0.06%]	0.056 [0.03%]	1.580 [0.94%]**	1.645 [0.93%]*
2-m Temperature Change (^oC)	-0.159*	-0.234***	-0.485***	-0.573***
2-m Dew Point Change (^oC)	0.295***	0.286***	0.786***	0.777***
Precipitable Water Change (mm)	0.137 [0.50%]***	0.135 [0.47%]***	0.186 [0.74%]***	0.181 [0.69%]***
CAPE Change ($J\ kg^{-1}$)	16.128 [5.01%]***	17.896 [4.91%]***	45.099 [16.0%]***	50.057 [15.9%]***
CIN Change ($J\ kg^{-1}$)	0.214 [0.61%]	0.379 [0.95%]	2.091 [5.71%]*	2.604 [6.29%]*
PBL Height Change (m)	-23.533 [-2.88%]***	-25.364 [-3.09%]***	-67.854 [-7.80%]***	-71.534 [-8.14%]***
Convergence Change (s^{-1})	-3.27×10^{-9} [-4.75%]*	-3.24×10^{-9} [-5.13%]	-8.87×10^{-7} [-84.2%]***	-9.08×10^{-7} [-88.5%]***
Precipitation Change (mm)	4.974 [0.91%]**	4.245 [1.29%]*	7.861 [1.61%]	4.494 [1.45%]

Table 2. May-September and June-July-August (JJA) weighted averages of differences between control and irrigated simulations for all simulated years. Weighted averages were calculated for the region of study and for grid cells with at least 10% irrigation within the region of study. Significance values for paired t-tests are as follows: * ($p < 0.1$), ** ($p < 0.05$), *** ($p < 0.01$).

	Region of Study				10%+ Irrigated Grid Cells in Region of Study			
	All	**Drought**	**Normal**	**Pluvial**	**All**	**Drought**	**Normal**	**Pluvial**
Irrigated Area (km^2)	6.39×10^4	6.39×10^4	6.39×10^4	6.39×10^4	5.0×10^4	5.0×10^4	5.0×10^4	5.0×10^4
Soil Moisture ($m^3\ m^{-3}$)	0.0138 [5.68%]***	0.0145 [6.40%]***	0.0138 [5.53%]***	0.0130 [5.19%]***	0.0588 [27.0%]***	0.0623 [30.2%]***	0.0580 [26.1%]***	0.0560 [25.0%]***
Latent Heat Flux ($W\ m^{-2}$)	4.293 [4.29%]***	4.508 [4.60%]***	3.940 [3.84%]***	4.431 [4.44%]**	20.745 [22.6%]***	22.291 [24.6%]***	19.695 [20.9%]***	20.250 [22.5%]**
Sensible Heat Flux ($W\ m^{-2}$)	-3.235 [-7.74%]***	-3.587 [-7.68%]***	-2.842 [-7.00%]***	-3.276 [-8.59%]**	-14.542 [-30.2%]***	-16.115 [-31.1%]***	-12.948 [-27.8%]***	-14.562 [-31.8%]***
Net Radiation ($W\ m^{-2}$)	0.107 [0.06%]	-0.081 [-0.04%]	0.181 [0.11%]	0.223 [0.13%]	1.580 [0.94%]**	1.171 [0.68%]	2.452 [1.45%]***	1.118 [0.68%]
2-m Temperature (^oC)	-0.159*	-0.247***	-0.023	-0.206**	-0.485***	-0.611***	-0.326	-0.519***
2-m Dew Point (^oC)	0.295***	0.317***	0.322***	0.244***	0.786***	0.854***	0.841***	0.665***
Precipitable Water Change (mm)	0.137 [0.50%]***	0.115 [0.42%]**	0.159 [0.62%]	0.136 [0.46%]	0.186 [0.74%]***	0.177 [0.71%]***	0.224 [0.94%]*	0.156 [0.59%]***
CAPE ($J\ kg^{-1}$)	16.128 [5.01%]***	18.963 [5.85%]**	13.949 [5.71%]***	15.470 [3.90%]**	45.099 [16.0%]***	50.971 [19.4%]**	40.456 [18.8%]***	43.870 [12.0%]**
CIN ($J\ kg^{-1}$)	0.214 [0.61%]	0.743 [2.14%]	0.394 [1.32%]	-0.495 [-1.22%]	2.091 [5.71%]*	3.147 [9.12%]	3.024 [9.44%]	0.104 [0.24%]
PBL Height (m)	-23.533 [-2.88%]***	-26.579 [-3.15%]***	-20.333 [-2.61%]***	-23.687 [-2.85%]**	-67.854 [-7.80%]***	-75.017 [-8.37%]***	-61.835 [-7.44%]***	-66.711 [-7.55%]**
Convergence ($10^{-9}\ s^{-1}$)	-3.27×10^{-9} [-4.75%]*	-4.08×10^{-9} [-5.68%]	-3.46×10^{-9} [-17.5%]	-2.29×10^{-9} [-1.99%]	-8.87×10^{-8} [-84.2%]***	-8.16×10^{-8} [-114%]***	-9.63×10^{-8} [-188%]***	-8.81×10^{-8} [-45.5%]**
Precipitation Change (mm)	4.974 [0.91%]**	2.850 [0.63%]	5.935 [1.06%]	6.136 [0.98%]*	7.861 [1.61%]	-1.258 [-0.31%]	14.866 [3.01%]**	9.973 [1.77%]

Table 3. May-September weighted averages of differences between control and irrigated simulations for all, drought, normal, and pluvial years. Weighted averages were calculated for the region of study and for grid cells with at least 10% irrigation within the region of study. Significance values for paired t-tests are as follows: * ($p < 0.1$), ** ($p < 0.05$), *** ($p < 0.01$).

	Region of Study				10%+ Irrigated Grid Cells in Region of Study			
	All	**El Niño**	**Neutral**	**La Niña**	**All**	**El Niño**	**Neutral**	**La Niña**
Irrigated Area (km^2)	6.39×10^4	6.39×10^4	6.39×10^4	6.39×10^4	5.0×10^4	5.0×10^4	5.0×10^4	5.0×10^4
Soil Moisture Difference ($m^3\ m^{-3}$)	0.0138 [5.68%]***	0.0127 [4.85%]***	0.0144 [6.11%]***	0.0142 [6.20%]***	0.0588 [27.0%]***	0.0532 [22.3%]***	0.0627 [31.2%]***	0.0603 [28.3%]***
Latent Heat Flux ($W\ m^{-2}$)	4.293 [4.29%]***	3.386 [3.29%]***	4.804 [4.74%]***	4.690 [4.88%]***	20.745 [22.6%]***	16.480 [17.3%]***	23.663 [26.3%]***	22.092 [24.7%]***
Sensible Heat Flux ($W\ m^{-2}$)	-3.235 [-7.74%]***	-2.612 [-7.05%]***	-3.557 [-8.40%]***	-3.537 [-7.68%]***	-14.542 [-30.2%]***	-11.771 [-27.6%]***	-16.343 [-31.2%]***	-15.511 [-31.5%]***
Net Radiation ($W\ m^{-2}$)	0.107 [0.06%]	-0.121 [-0.07%]	0.245 [0.14%]	0.199 [0.12%]	1.580 [0.94%]**	0.926 [0.56%]	2.050 [1.20%]***	1.764 [1.05%]
2-m Temperature (^oC)	-0.159*	-0.188***	-0.220***	-0.068	-0.485***	-0.470***	-0.594***	-0.392
2-m Dew Point (^oC)	0.295***	0.279***	0.318***	0.287***	0.786***	0.727**	0.872***	0.760***
Precipitable Water (mm)	0.137 [0.50%]***	0.125 [0.49%]***	0.166 [0.60%]	0.120 [0.41%]	0.186 [0.74%]***	0.176 [0.74%]***	0.214 [0.87%]*	0.168 [0.62%]***
CAPE ($J\ kg^{-1}$)	16.128 [5.01%]***	13.285 [5.19%]***	17.889 [4.86%]*	17.209 [5.04%]**	45.099 [16.0%]***	33.456 [14.7%]***	50.188 [16.6%]**	51.652 [16.5%]***
CIN ($J\ kg^{-1}$)	0.214 [0.61%]	0.108 [0.47%]	0.675 [1.55%]	-0.142 [-0.37%]	2.091 [5.71%]*	0.805 [3.17%]	3.388 [7.39%]	2.081 [5.38%]
PBL Height (m)	-23.533 [-2.88%]***	-19.791 [-2.53%]***	-24.684 [-2.92%]***	-26.125 [-3.16%]***	-67.854 [-7.80%]***	-56.613 [-6.80%]***	-74.728 [-8.24%]***	-72.221 [-8.28%]***
Convergence (s^{-1})	-3.27×10^{-9} [-4.75%]*	-1.84×10^{-9} [-5.61%]	-1.69×10^{-9} [-2.18%]	-6.30×10^{-9} [-6.53%]**	-8.87×10^{-8} [-84.2%]***	-7.70×10^{-8} [-96.3%]**	-8.76×10^{-8} [-75.1%]***	-1.01×10^{-7} [-85.2%]**
Precipitation (mm)	4.974 [0.91%]**	4.570 [0.77%]	5.776 [1.10%]*	4.575 [0.89%]**	7.861 [1.61%]	3.395 [0.61%]	12.199 [2.84%]	7.989 [1.64%]

Table 4. May-September weighted averages of differences between control and irrigated simulations for all, El Niño, neutral, and La Niña years. Weighted averages were calculated for region of study and for grid cells with at least 10% irrigation within region of study. Significance values for paired t-tests are as follows: * ($p < 0.1$), ** ($p < 0.05$), *** ($p < 0.01$).

Regime	May	June	July	August	September	May-September	JJA
All	1.284***	1.237***	0.789***	0.973***	0.834***	5.117***	3.000***
Drought	1.273*	1.097**	0.768***	0.725	1.131***	4.993***	2.590**
Normal	1.438**	1.519***	0.760***	1.013***	0.704**	5.434***	3.292***
Pluvial	1.143***	1.095*	0.839	1.182***	0.666*	4.925***	3.116**
El Niño	1.092**	0.992***	0.973**	0.732	0.851*	4.641***	2.698**
Neutral	1.728***	1.683***	0.890***	0.872***	0.674*	5.847***	3.445***
La Niña	1.033*	1.036**	0.505	1.316***	0.976***	4.865***	2.856***

Table 5. Weighted area average of irrigation-induced precipitation (mm) over the region of study from grid cells with at least 10% irrigation fraction. Significance values for paired t tests are as follows: * ($p < 0.1$), ** ($p < 0.05$), *** ($p < 0.01$).

Regime	May	June	July	August	September	May-September	JJA
All	0.203	0.220	0.244	0.227	0.148	0.208	0.230
Drought	0.200	0.236	0.249	0.220	0.128	0.207	0.235
Normal	0.218	0.217	0.246	0.242	0.167	0.218	0.235
Pluvial	0.191	0.207	0.238	0.217	0.148	0.200	0.220
El Niño	0.211	0.223	0.216	0.236	0.150	0.208	0.225
Neutral	0.198	0.219	0.249	0.248	0.169	0.216	0.238
La Niña	0.201	0.218	0.267	0.196	0.125	0.201	0.227

Table 6. Recycling ratio calculated from control simulations using the approach of Dominguez et al. (2006). Recycling ratio calculated for the domain shown in Figure 3b.

Regime	May	June	July	August	September	May-September	JJA
All	0.302	0.293	0.355	0.350	0.211	0.293	0.312
Drought	0.300	0.273	0.363	0.408	0.235	0.298	0.312
Normal	0.355	0.337	0.362	0.305	0.226	0.317	0.334
Pluvial	0.251	0.269	0.341	0.336	0.172	0.264	0.289
El Niño	0.324	0.287	0.341	0.322	0.263	0.306	0.310
Neutral	0.288	0.315	0.313	0.334	0.178	0.280	0.312
La Niña	0.295	0.276	0.412	0.394	0.192	0.293	0.314

Table 7. Recycling ratio calculated from control simulations using the approach of Brubaker et al. (2001). Recycling ratio calculated for the domain shown in Figure 3b.

Regime	May	June	July	August	September	May-September	JJA
All	0.011 [5.42%]***	0.009 [3.64%]***	0.013 [5.33%]***	0.011 [4.41%]***	0.013 [8.78%]***	0.011 [5.29%]***	0.011 [4.78%]***
Drought	0.009 [4.59%]***	0.009 [3.79%]*	0.014 [5.77%]**	0.014 [6.24%]**	0.016 [12.9%]**	0.013 [6.05%]**	0.012 [5.23%]**
Normal	0.015 [6.85%]**	0.010 [4.40%]	0.015 [6.23%]*	0.006 [2.55%]	0.013 [7.86%]*	0.012 [5.41%]*	0.010 [4.41%]**
Pluvial	0.008 [4.16%]**	0.007 [3.47%]*	0.009 [3.85%]**	0.013 [5.93%]*	0.010 [6.45%]*	0.009 [4.70%]**	0.010 [4.45%]**
El Niño	0.010 [4.52%]**	0.005 [2.37%]**	0.009 [4.27%]**	0.005 [1.94%]	0.009 [6.04%]*	0.008 [3.63%]**	0.006 [2.82%]**
Neutral	0.012 [6.26%]*	0.014 [6.31%]***	0.015 [6.16%]**	0.014 [5.53%]***	0.016 [9.73%]**	0.014 [6.64%]***	0.014 [6.02%]***
La Niña	0.010 [5.07%]*	0.007 [3.01%]*	0.014 [5.34%]	0.015 [7.43%]*	0.014 [11.0%]*	0.012 [5.88%]***	0.012 [5.19%]**

Table 8. Difference in recycling ratio (Irrigation (IRRIG) minus control (CONTROL)) using the approach of Dominguez et al. (2006). Recycling ratio calculated for the domain shown in Figure 3b. Significance values for paired t tests are as follows: * ($p < 0.1$), ** ($p < 0.05$), *** ($p < 0.01$).

Regime	May	June	July	August	September	May-September	JJA
All	0.012 [3.97%]***	0.010 [3.41%]**	0.002 [0.56%]	0.004 [1.14%]	0.014 [6.64%]***	0.009 [3.07%]***	0.007 [2.24%]***
Drought	0.013 [4.30%]	0.016 [6.05%]	0.001 [0.23%]	0.007 [1.61%]	0.017 [7.13%]*	0.011 [3.85%]**	0.010 [3.12%]
Normal	0.014 [4.07%]**	0.007 [1.95%]	0.003 [0.81%]	0.007 [2.27%]	0.012 [5.25%]***	0.009 [2.74%]**	0.005 [1.57%]
Pluvial	0.008 [3.12%]*	0.008 [2.86%]	0.002 [0.65%]	-0.002 [-0.70%]	0.012 [7.15%]	0.007 [2.54%]**	0.006 [2.02%]
El Niño	0.009 [2.78%]**	0.002 [0.55%]	0.002 [0.70%]	0.009 [2.80%]	0.014 [5.24%]	0.006 [2.11%]**	0.004 [1.27%]
Neutral	0.010 [3.46%]*	0.020 [6.51%]**	0.013 [4.24%]*	-0.003 [-0.94%]	0.009 [5.11%]**	0.010 [3.73%]**	0.011 [3.36%]
La Niña	0.016 [5.51%]	0.009 [3.14%]*	-0.010 [-2.35%]	0.005 [1.33%]	0.018 [9.39%]*	0.010 [3.40%]**	0.006 [2.04%]

Table 9. Difference in recycling ratio (IRRIG minus CONTROL) using the approach of Brubaker et al. (2001). Recycling ratio calculated for the domain shown in Figure 3b. Significance values for paired t tests are as follows: * ($p < 0.1$), ** ($p < 0.05$), *** ($p < 0.01$).

	May-September				June-August			
Regime	**Precipitation Change (mm)**	**Irrigation-Induced Precipitation (mm)**	**Recycled Precipitation Change (mm)**	**ET Change (mm)**	**Precipitation Change (mm)**	**Irrigation-Induced Precipitation (mm)**	**Recycled Precipitation Change (mm)**	**ET Change (mm)**
All	4.974 [0.91%]**	5.117***	6.707 [4.97%]***	22.701 [4.29%]***	4.245 [1.29%]*	3.000***	4.011 [4.59%]***	13.775 [4.04%]***
Drought	2.850 [0.63%]	4.993***	6.126 [5.34%]**	23.837 [4.60%]***	0.583 [0.21%]	2.590**	3.143 [4.19%]	14.111 [4.27%]***
Normal	5.935 [1.06%]	5.434***	7.650 [5.45%]**	20.834 [3.84%]***	5.758 [1.69%]	3.292***	4.496 [4.65%]***	12.926 [3.73%]***
Pluvial	6.136 [0.98%]*	4.925***	6.346 [4.48%]**	23.432 [4.44%]**	6.395 [1.72%]***	3.116**	4.395 [4.85%]**	14.286 [4.14%]**
El Niño	4.570 [0.77%]	4.641***	5.262 [3.58%]**	17.904 [3.29%]***	5.012 [1.32%]	2.698**	3.321 [3.46%]	10.537 [3.05%]***
Neutral	5.776 [1.10%]*	5.847***	8.347 [6.23%]***	25.403 [4.74%]***	3.935 [1.25%]	3.445***	4.974[5.78%]***	16.144 [4.60%]***
La Niña	4.575 [0.89%]**	4.865***	6.514 [5.24%]**	24.797 [4.88%]***	3.788 [1.29%]**	2.856***	3.739 [4.67%]***	14.643 [4.50%]***

Table 10. Difference (IRRIG minus CONTROL) in simulated precipitation, irrigation-induced precipitation, recycled precipitation, and ET averaged over June-August and May-September. All values are calculated over the recycling region as depicted in Figure 3b. Recycled precipitation change is the average recycled precipitation change based on approaches from Dominguez et al. (2006) and Brubaker et al. (2001). Significance values for paired t tests are as follows: * ($p < 0.1$), ** ($p < 0.05$), *** ($p < 0.01$).

Figures

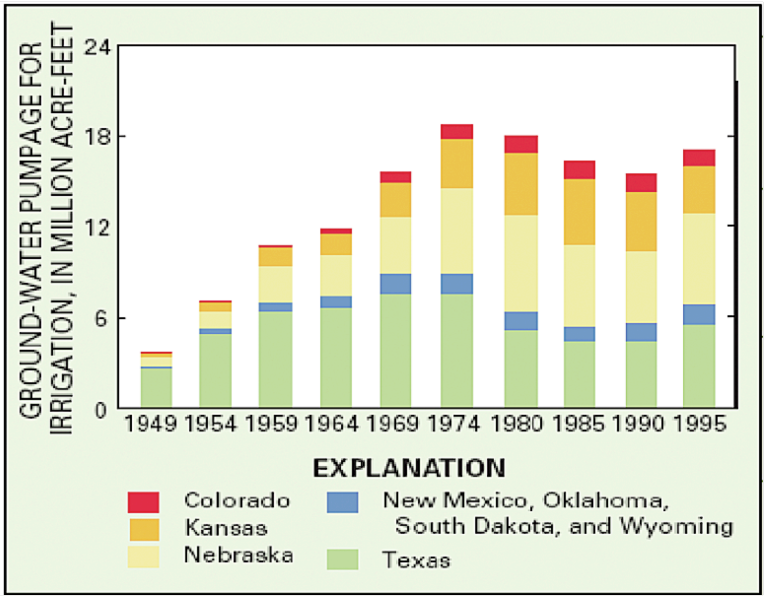

Figure 1. Groundwater pumpage for irrigation from 1949 to 1995 in the Great Plains states (McGuire et al. 2003).

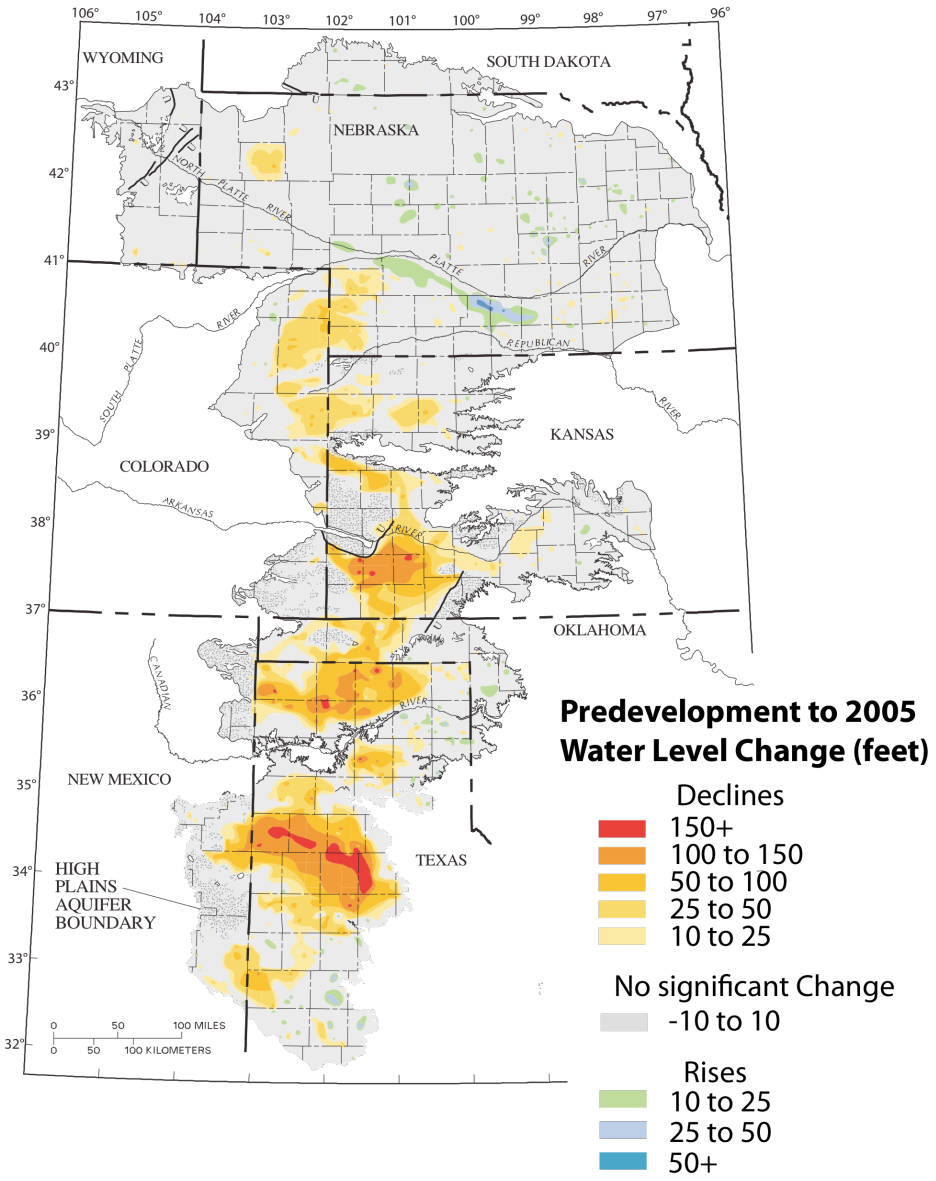

Figure 2. Water level changes in the Ogallala Aquifer, predevelopment to 2005 (McGuire 2007).

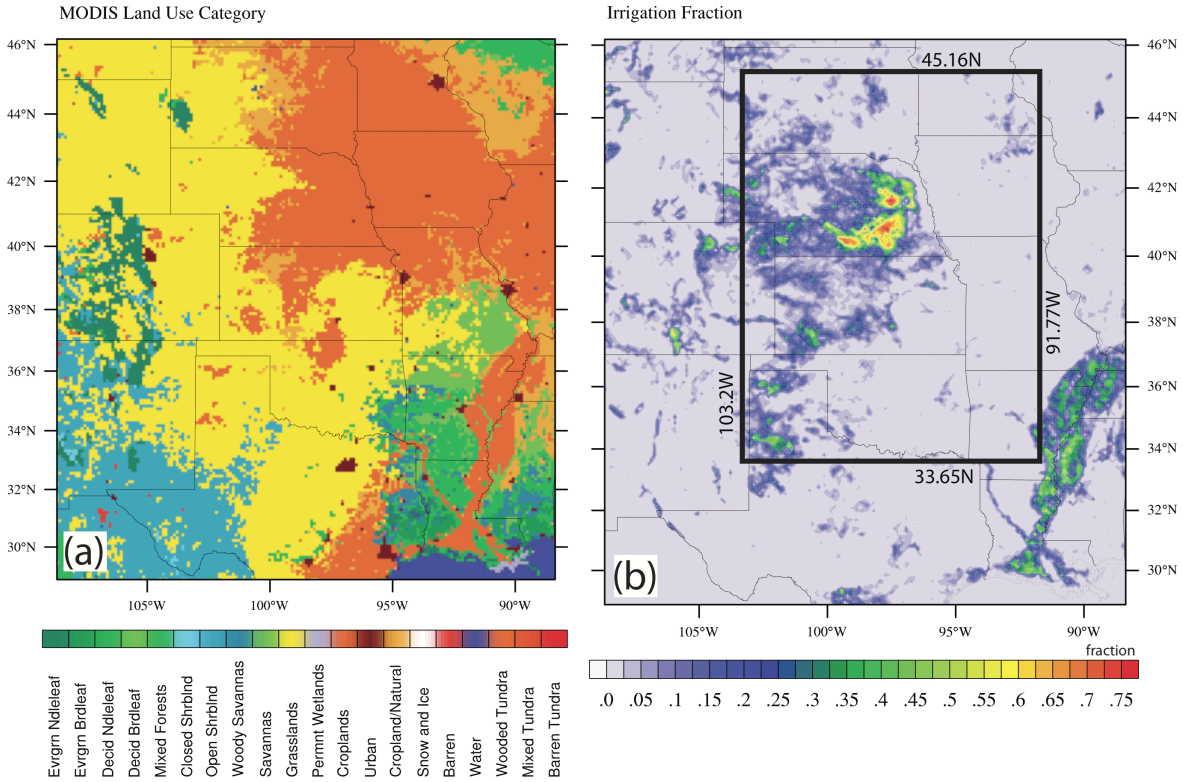

Figure 3. (a) MODIS Land Use Category that is input to WRF model and (b) irrigated fraction from Ozdogan and Gutman (2008) for WRF Model Domain. The region of study, shown in (b), is a subset of the WRF domain to minimize model edge effects and concentrate the impacts of irrigation.

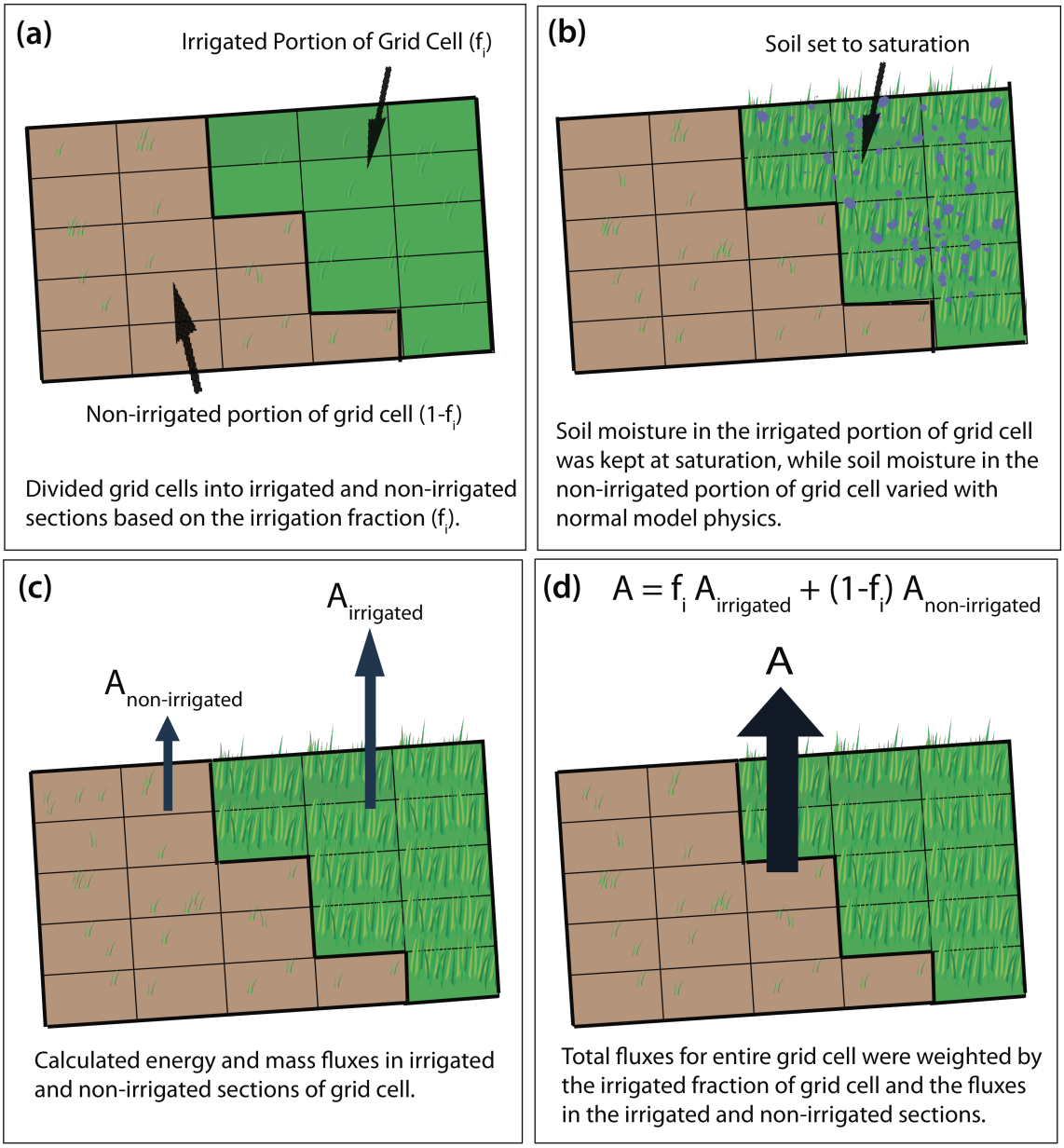

Figure 4. Irrigation representation in the WRF Model.

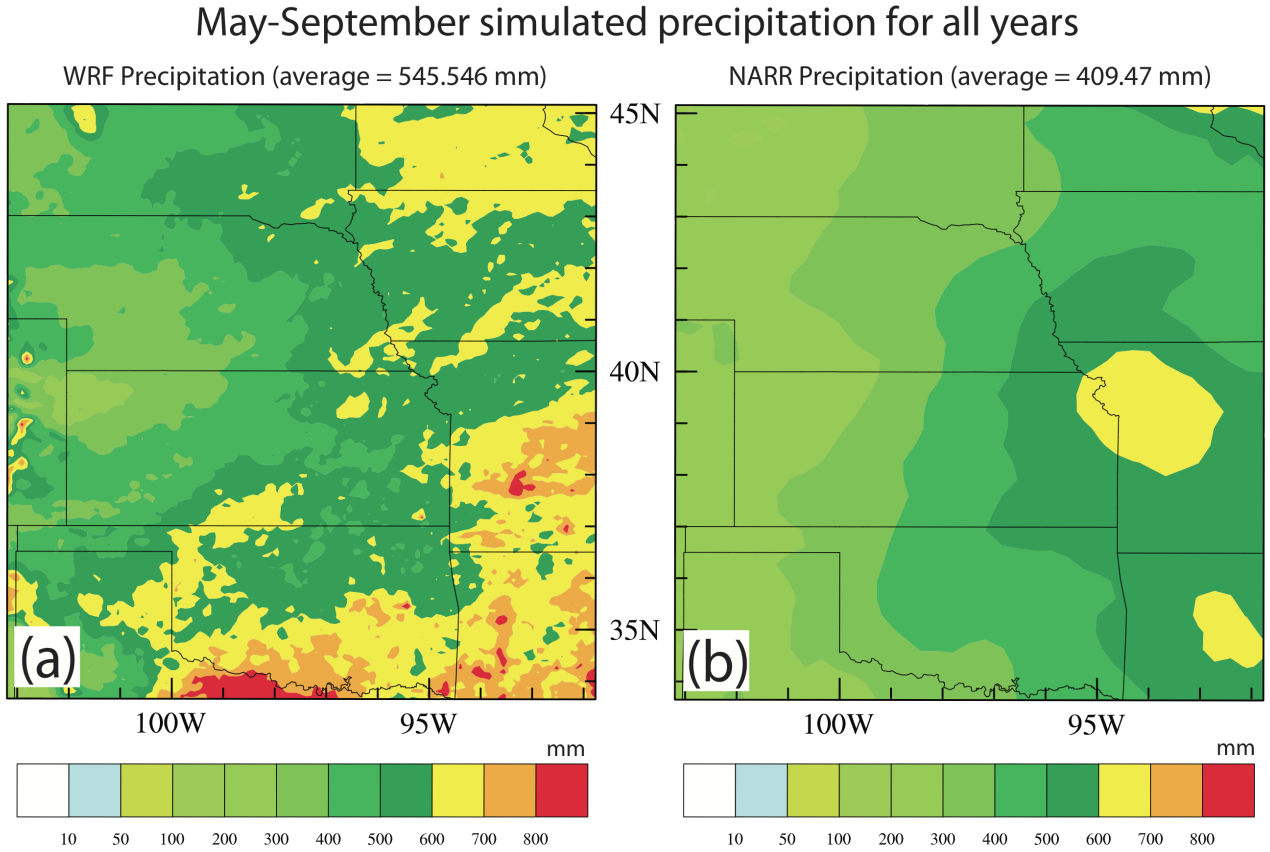

Figure 5. (a) Average May-September simulated precipitation from WRF for all simulated years. (b) As (a) but for NARR observed precipitation.

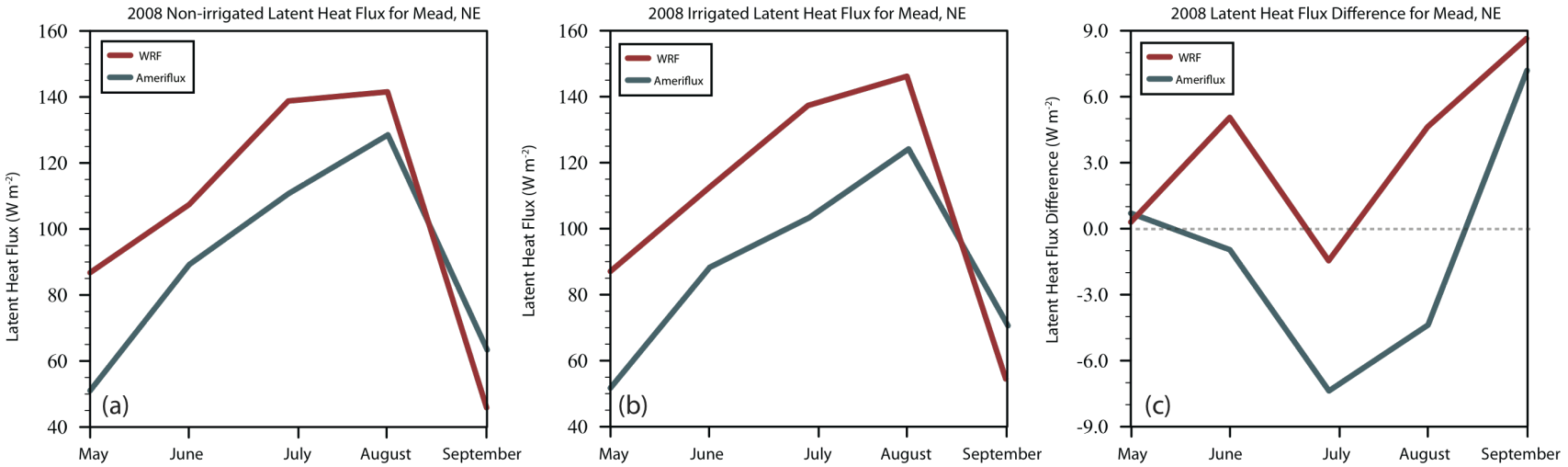

Figure 6. (a) Latent heat flux observed at Ameriflux Mead Rainfed Site and simulated from WRF Model for 2008. (b) As (a) but observed at Ameriflux Mead Irrigated Rotation Site and simulated by WRF Model with irrigation. (c) Latent heat flux difference between Ameriflux Mead Irrigated Rotation and Rainfed sites (blue) and WRF irrigated and control simulations (red) for 2008.

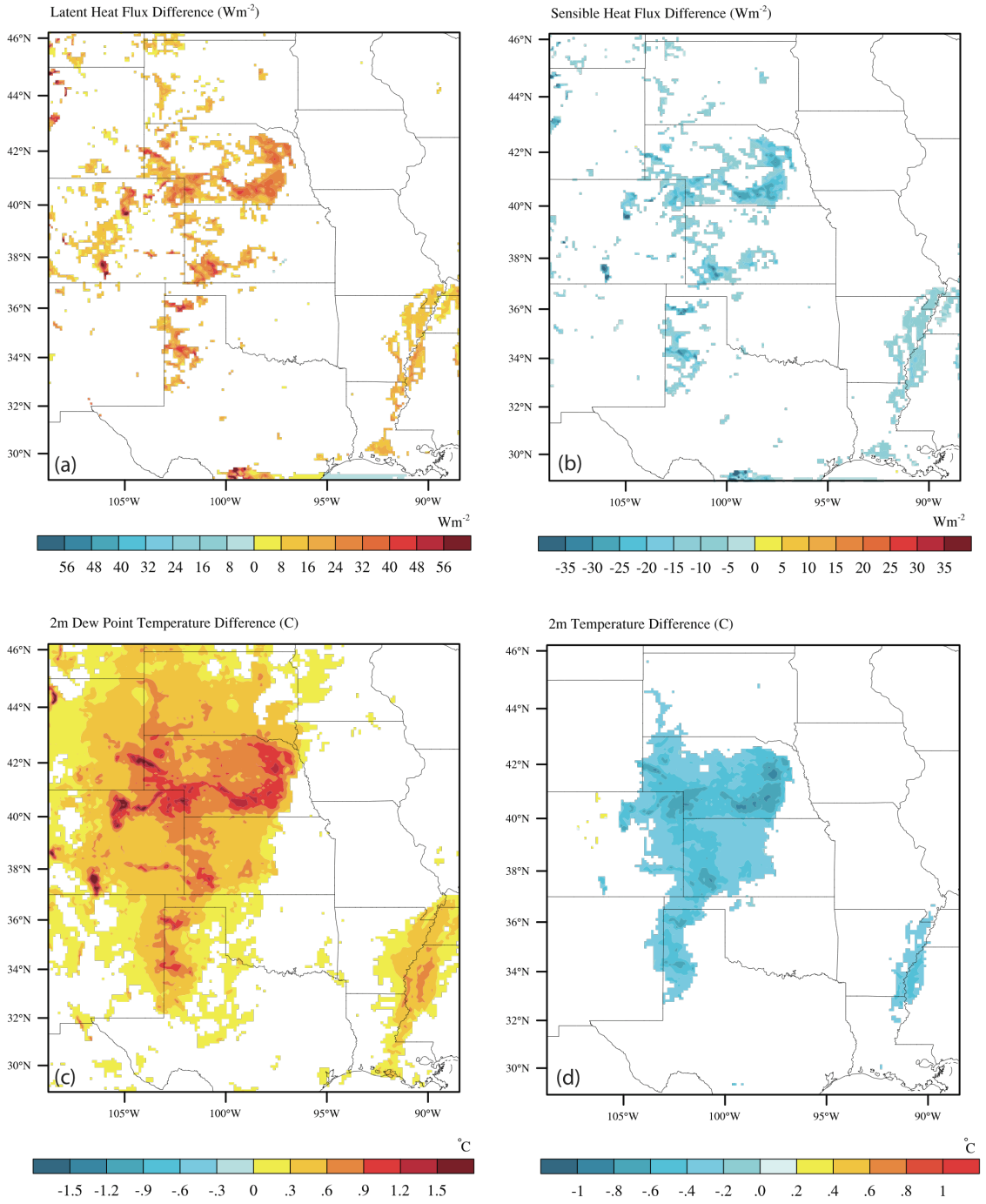

Figure 7. (a) Average May-September irrigated (IRRIG) minus control (CTRL) simulated latent heat flux for all years. (b) As (a) but for sensible heat flux. (c) As (a) but for 2-m dew point temperature. (d) As (a) but for 2-m temperature. Differences are shown only for grid cells found to be significant using a two-tailed paired t-test at the 95% confidence level.

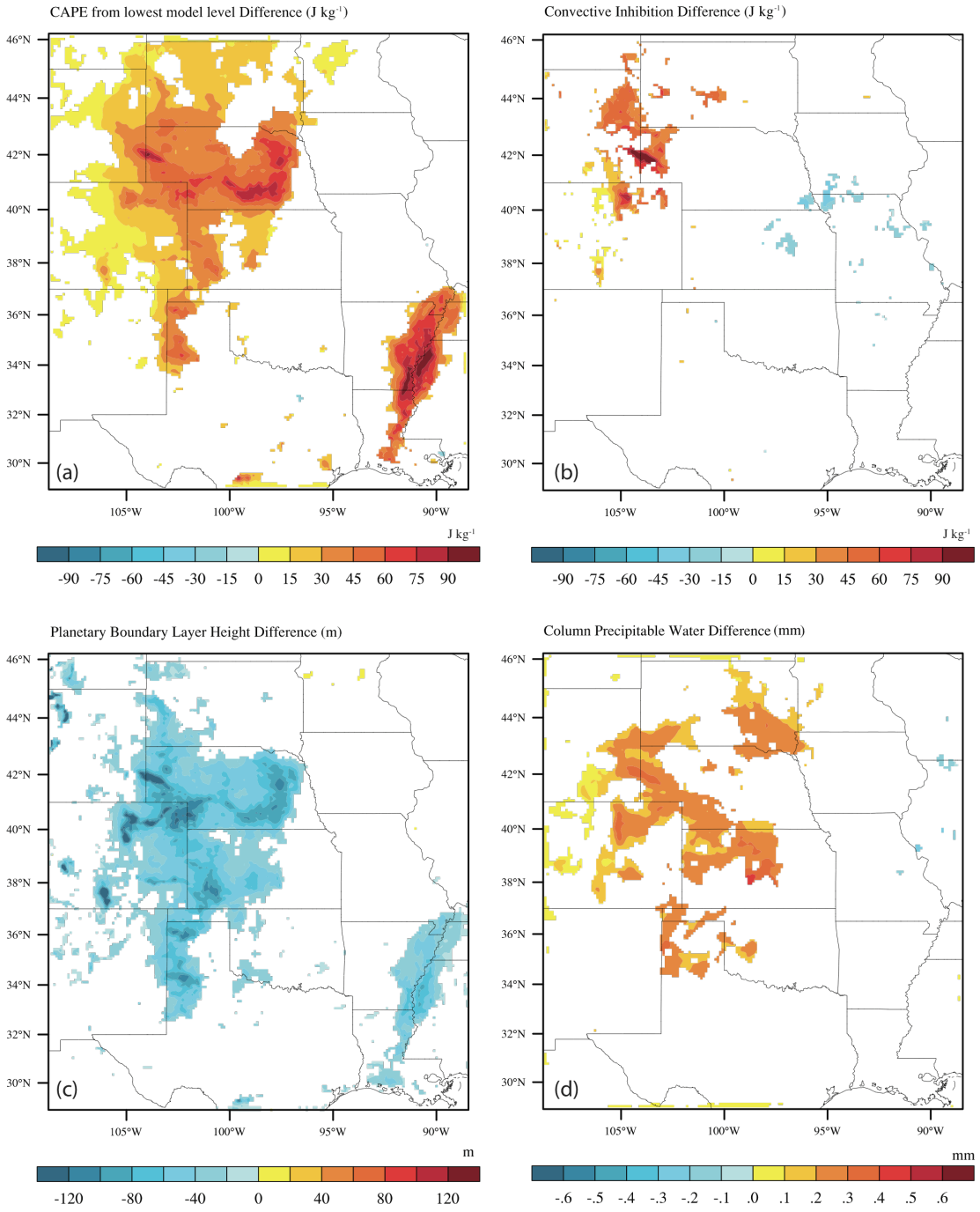

Figure 8. (a) Average May-September IRRIG minus CTRL simulated convective available potential energy (CAPE) for all years. (b) As (a) but for convective inhibition (CIN). (c) As (a) but for planetary boundary layer (PBL) height. (d) As (a) but for column precipitable water. Differences are shown only for grid cells found to be significant using a two-tailed, paired t-test at the 95% confidence level.

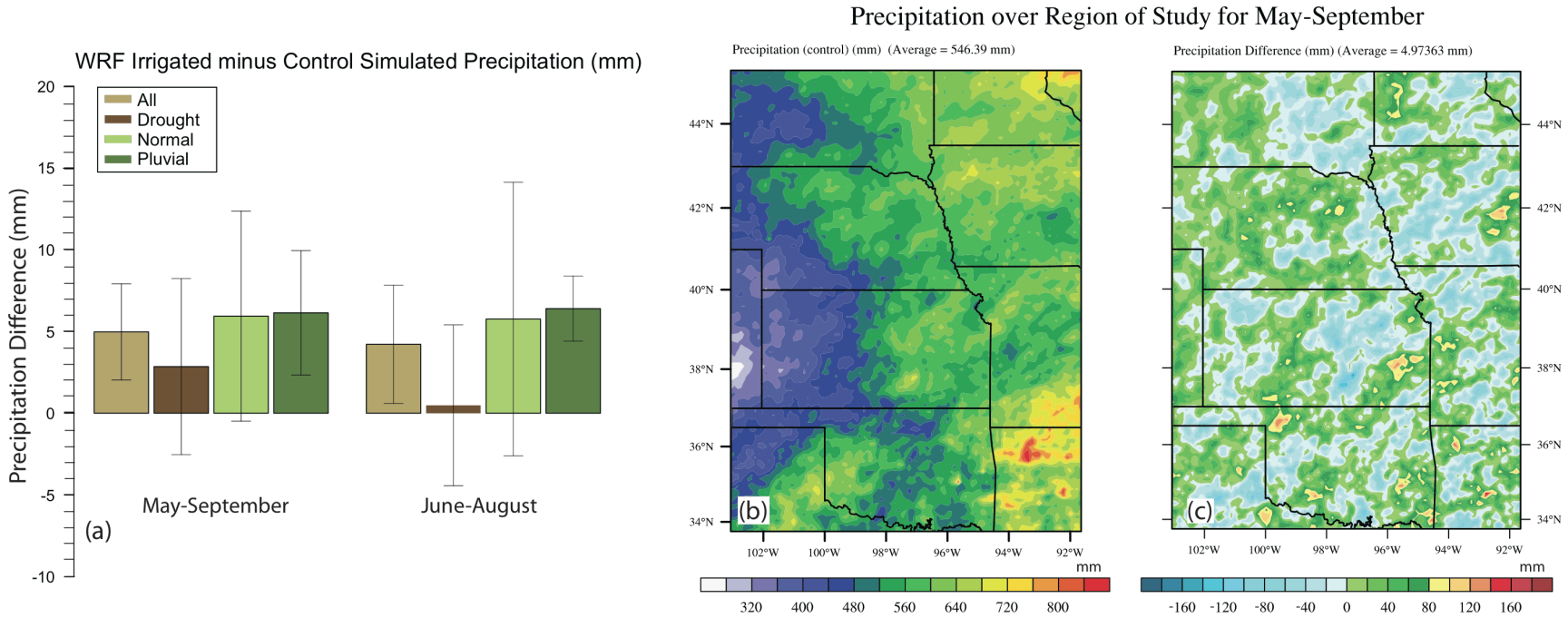

Figure 9. (a) Weighted average of IRRIG minus CTRL simulated precipitation (mm) in region of study (defined in Figure 3b) during JJA and May-September for drought, normal, pluvial, and all years. Error bars denote 95% confidence interval. (b) Average May-September CTRL simulated precipitation for all years. (c) Average May-September IRRIG minus CTRL simulated precipitation for all years. No differences in (c) were found to be statistically significant with 95% confidence from a two-tailed, paired t-test.

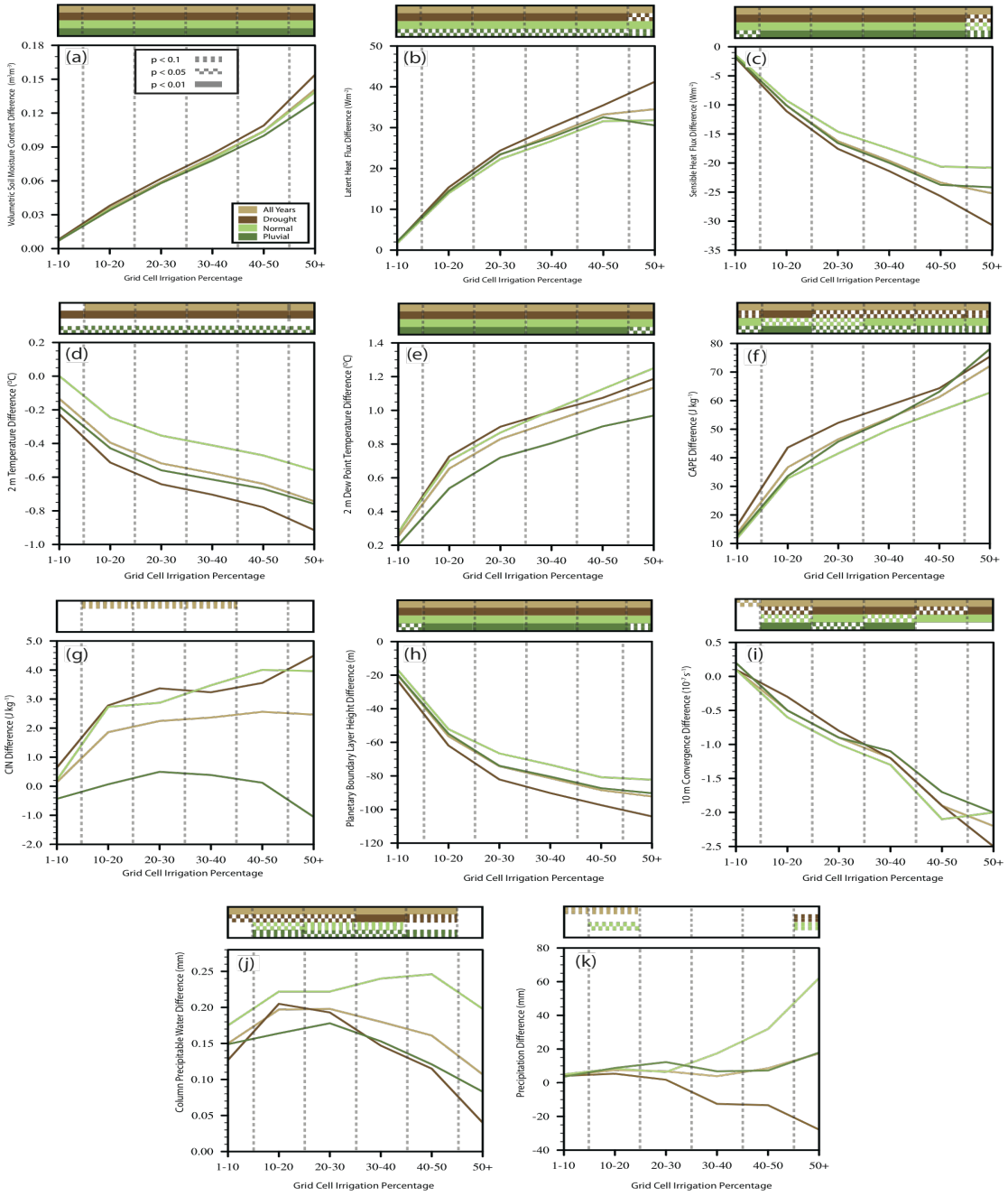

Figure 10. Weighted average of IRRIG minus CTRL simulated (a) volumetric soil moisture content, (b) latent heat flux, (c) sensible heat flux, (d) 2-m temperature, (e) 2-m dew point, (f) convective available potential energy (CAPE), (g) convective inhibition (CIN) (h) planetary boundary layer (PBL) height, (i) 10-m convergence, (j) column precipitable water, and (k) precipitation as a function of grid cell irrigation fraction. Drought, normal, pluvial (flood), and all years are plotted as described in (a). Levels of statistical significance are noted on bars above each plot as described in (a). Only grid cells within the region of study were considered.

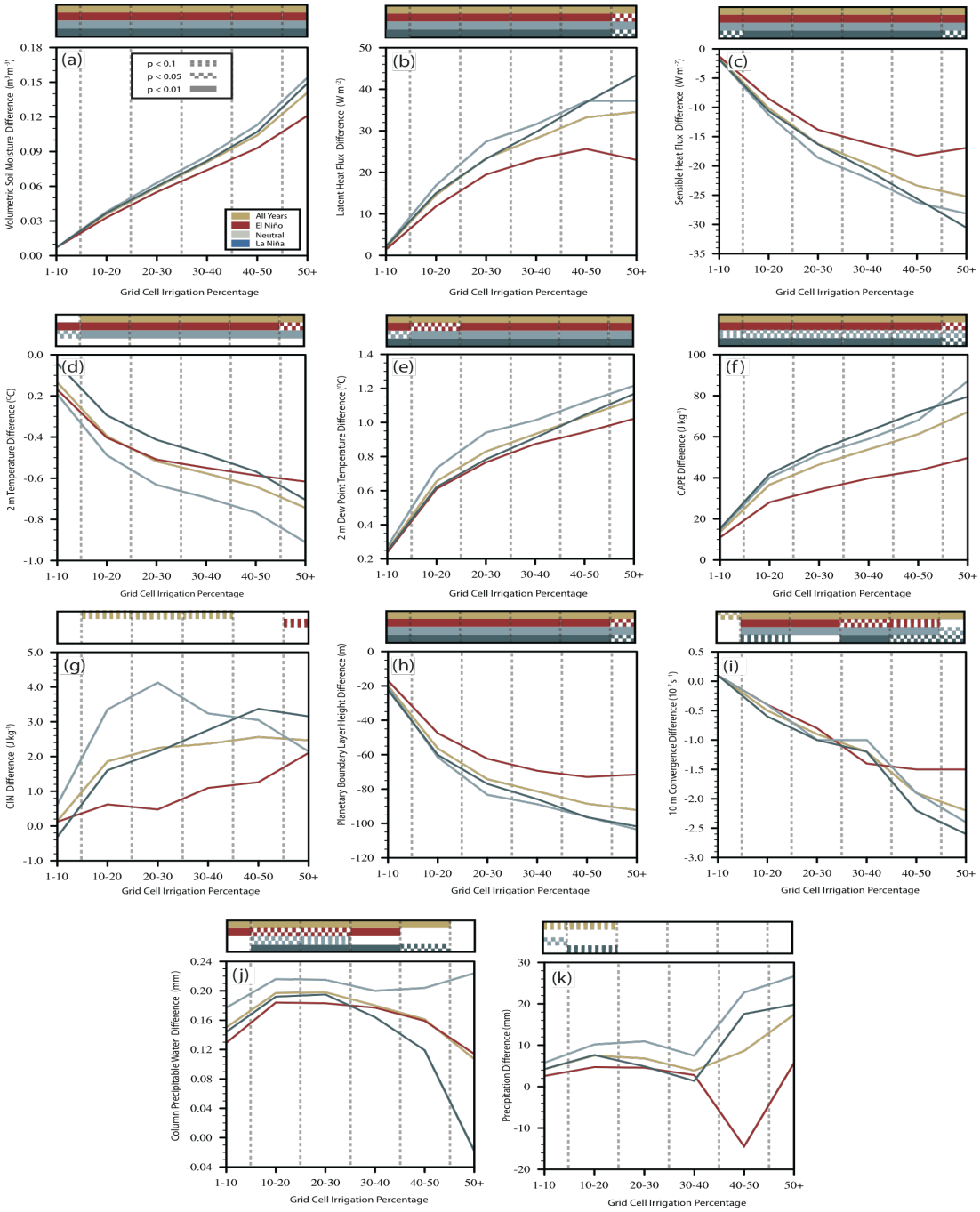

Figure 11. Weighted average of IRRIG minus CTRL simulated (a) volumetric soil moisture content, (b) latent heat flux, (c) sensible heat flux, (d) 2-m temperature, (e) 2-m dew point, (f) CAPE, (g) CIN, (h) planetary boundary layer height, (i) 10-m convergence, (j) column precipitable water, and (k) precipitation as a function of grid cell irrigation fraction. El Niño, neutral, La Niña, and all years are plotted as described in (a). Levels of statistical significance are noted on bars above each plot as described in (a). Only grid cells within the region of study were considered.

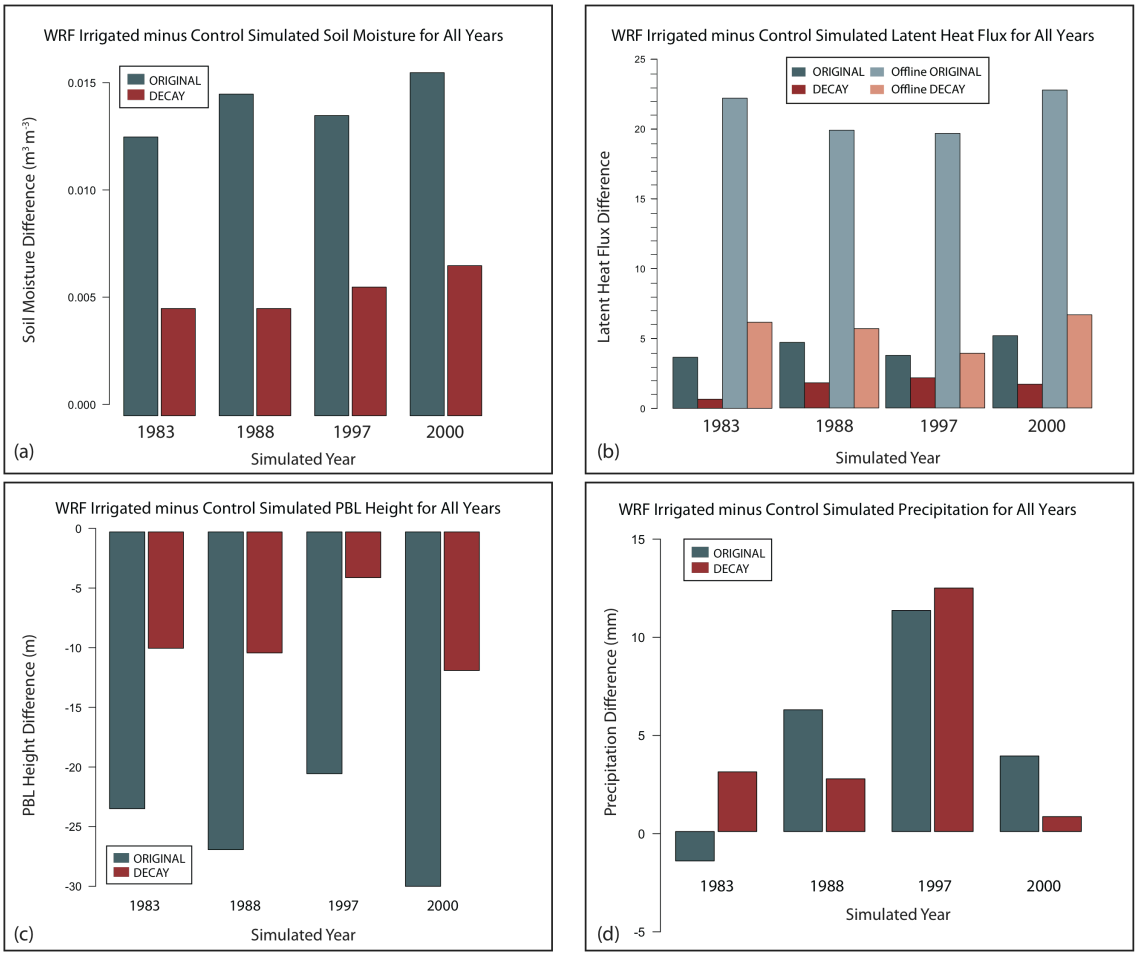

Figure 12. Weighted average of IRRIG minus CTRL simulated (a) volumetric soil moisture within the region of study for simulations of original irrigation method (ORIGINAL) and time-decay irrigation method (DECAY). (b) As (a) but for latent heat flux with the inclusion of offline simulations as described in section 2.5.2. (c) As (a) but for planetary boundary layer (PBL) height. (d) As (a) but for precipitation.

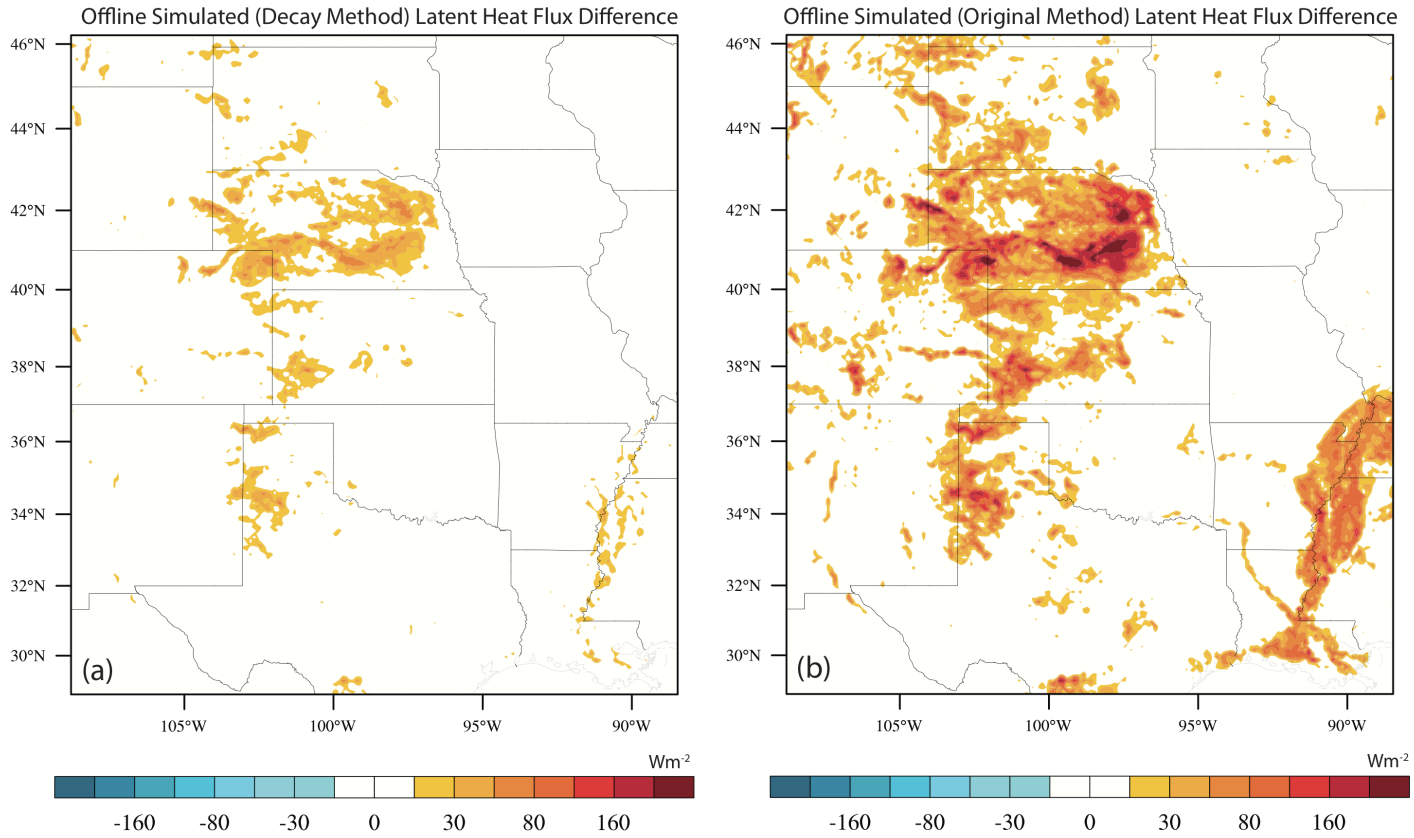

Figure 13. Average May-September IRRIG minus CTRL simulated latent heat flux for all simulated years using offline simulations that employed (a) the DECAY irrigation technique from section 2.4.5 and (b) the ORIGINAL irrigation technique from section 2.3.2.

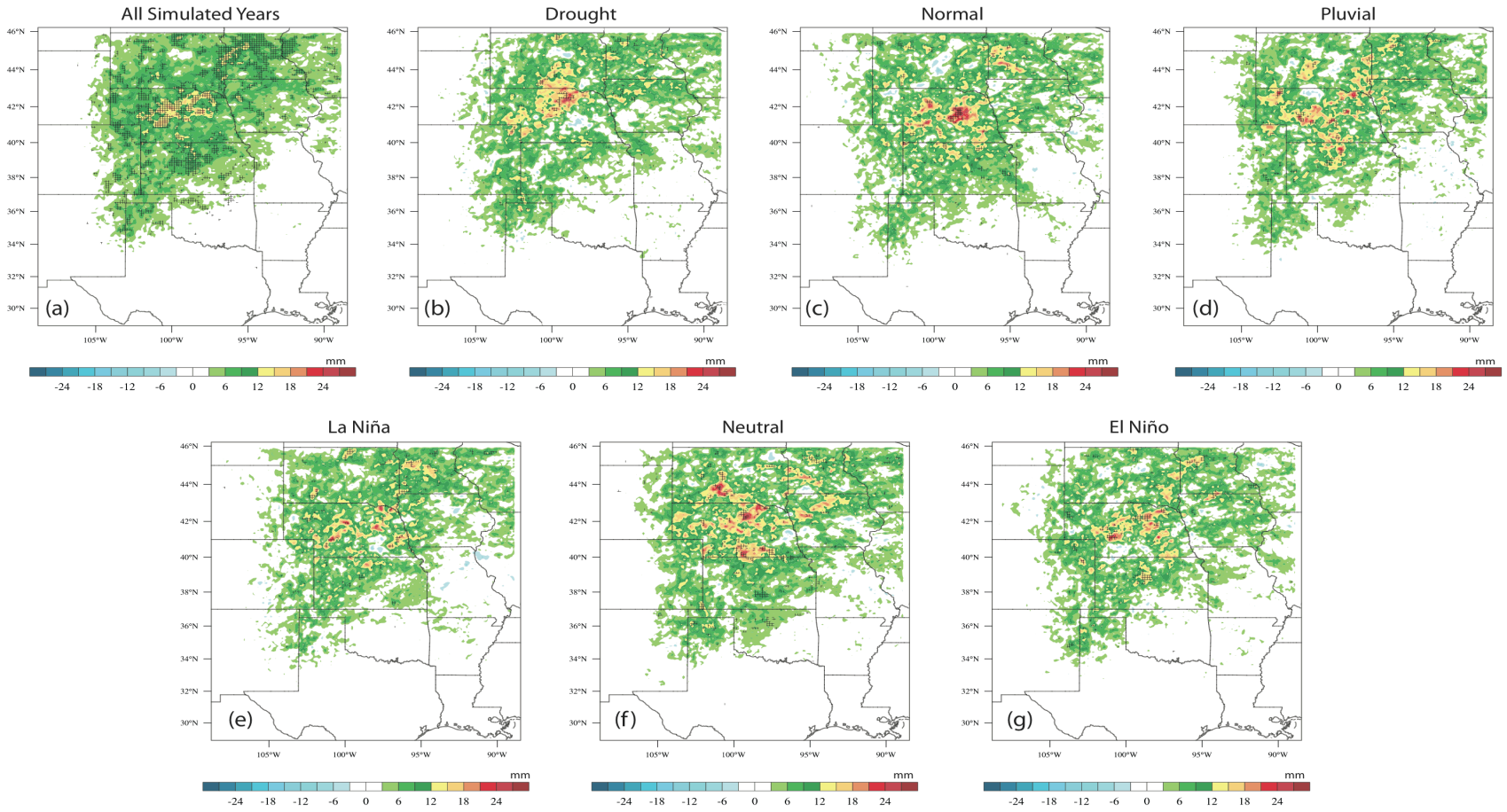

Figure 14. Average May-September irrigation-induced precipitation (mm) from grid cells with at least 10% irrigation fraction for (a) all simulated years, (b) drought years, (c) normal precipitation years, (d) pluvial years, (e) La Niña years, (f) neutral years, and (g) El Niño years. Hatched areas represent locations where irrigation-induced precipitation is significantly different than zero at the 95% confidence level.

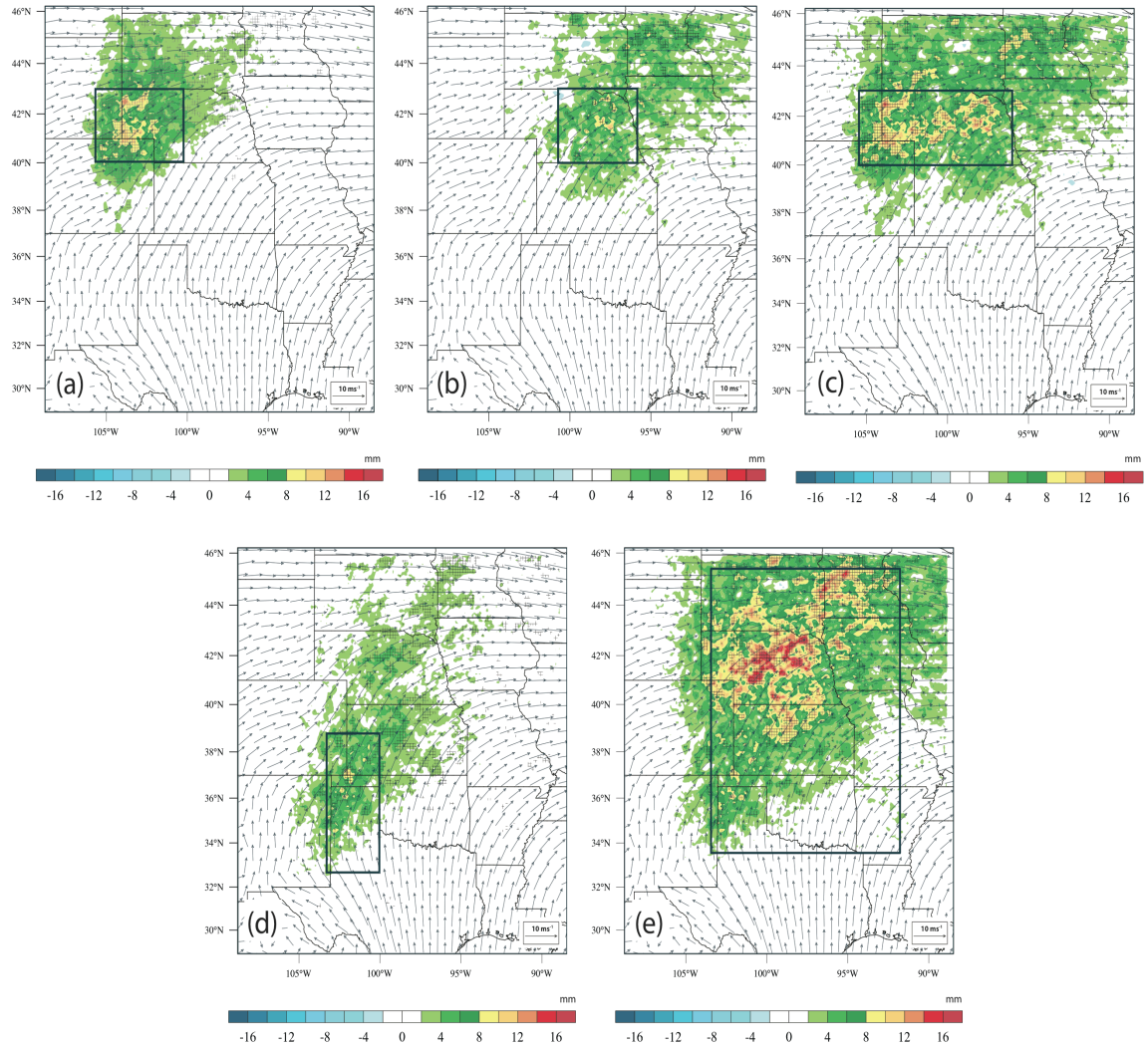

Figure 15. May-September average moisture-weighted wind vectors and average irrigation-induced precipitation (mm) that originated from grid cells with at least 10% irrigation for all simulated years within the regions outlined in black in (a) through (e). Hatched areas represent locations where irrigation-induced precipitation is significantly different than zero at the 95% confidence level.

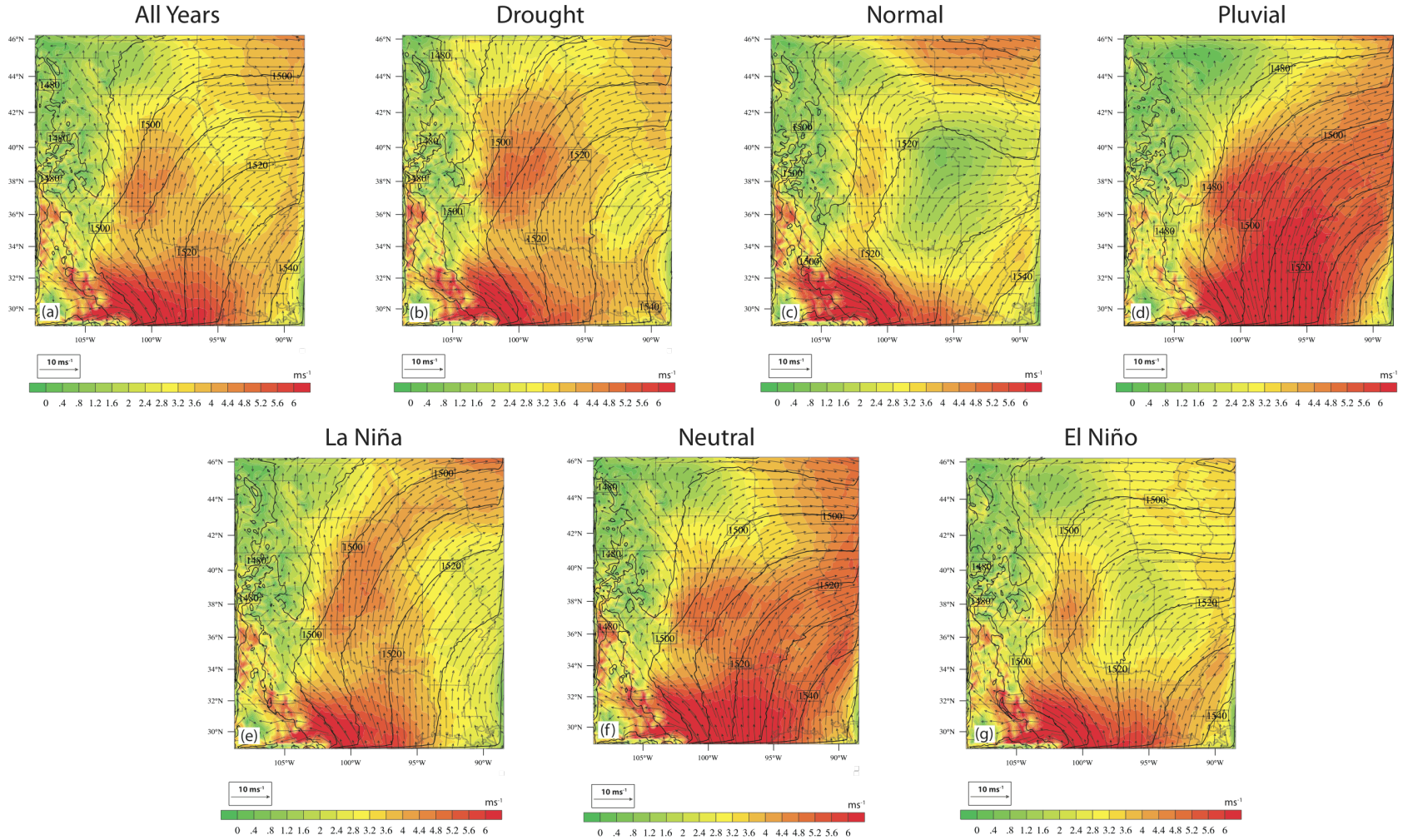

Figure 16. Average May-September 850 hPa wind speed (filled; ms^{-1}), geopotential height (contours; meters), and wind vectors (ms^{-1}) from irrigation simulations of (a) all, (b) drought, (c) normal, (d) pluvial, (e) La Niña, (f) neutral, and (g) El Niño years.

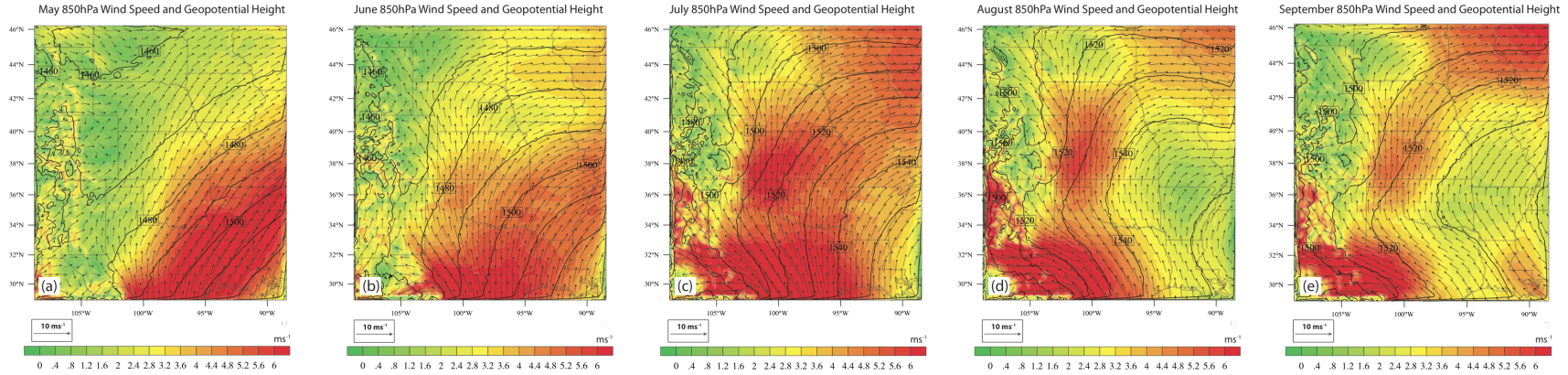

Figure 17. Average 850 hPa wind speed (filled; ms^{-1}), geopotential height (contours; meters), and wind vectors (ms^{-1}) from irrigation simulations of all years for (a) May, (b) June, (c) July, (d) August, (e) September.

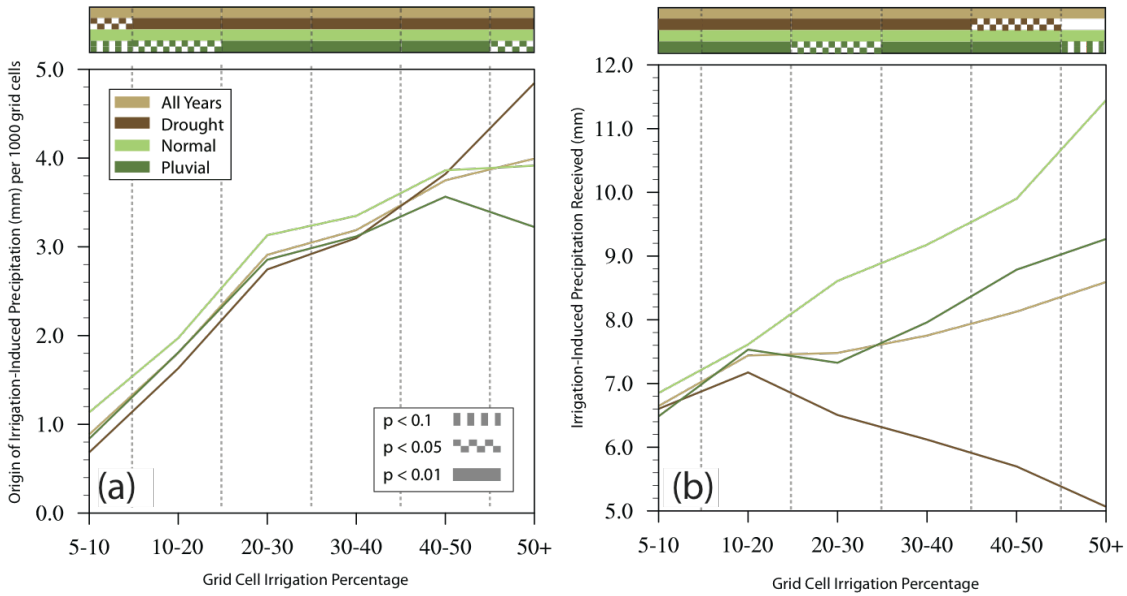

Figure 18. (a) Weighted average of the *origin* of irrigation-induced precipitation (mm) over the region of study as a function of grid cell irrigation percentage during May-September for all, drought, normal, and pluvial years. Values from each range of irrigation percentages represent the amount of precipitation that originated from ET in grid cells within that irrigation percentage range. Precipitation values are shown per 1000 grid cells to normalize values for each irrigation percentage group and give equal weight to groups with fewer grid cells. (b) Weighted average of the amount of irrigation-induced precipitation *received* as a function of grid cell irrigation percentage during May-September for all, drought, normal, and pluvial years.

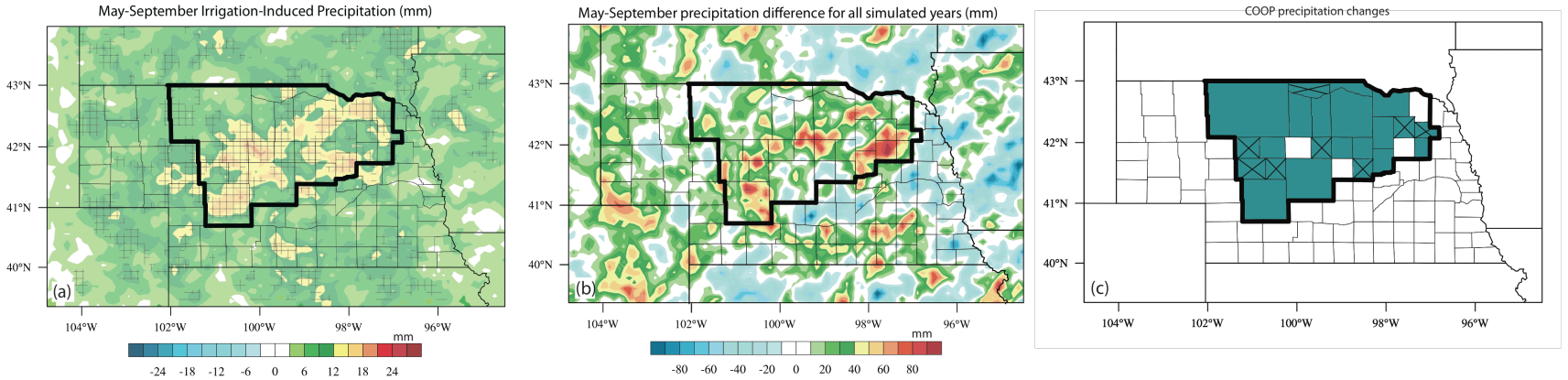

Figure 19. (a) May-September average irrigation-induced precipitation over Nebraska (areal average of 9.11 mm over outlined area). (b) Simulated May-September average irrigated minus control precipitation over Nebraska (areal average of 8.96 mm over outlined area). (c) North-central Nebraska analysis region for COOP observed precipitation comparisons. The shaded region represents counties where the 1951-2000 precipitation is larger than the 1901-1950 precipitation using the COOP precipitation dataset from NCDC. The hatched regions represent counties where the difference is statistically significant at the 95% confidence level.

Bibliography

Adegoke, J. O., R. Pielke, and A. M. Carleton, 2007: Observational and modeling studies of the impacts of agriculture-related land use change on planetary boundary layer processes in the central US. *Agricultural and Forest Meteorology*, **142,** 203-215.

Adegoke, J. O., R. A. Pielke, J. Eastman, R. Mahmood, and K. G. Hubbard, 2003: Impact of irrigation on midsummer surface fluxes and temperature under dry synoptic conditions: A regional atmospheric model study of the U.S. high plains. *Mon Weather Rev*, **131,** 556-564.

Baidya Roy, S., G. C. Hurtt, C. P. Weaver, and S. W. Pacala, 2003: Impact of historical land cover change on the July climate of the United States. *J Geophys Res-Atmos*, **108,** 4793.

Barnston, A. G., and P. T. Schickedanz, 1984: The Effect of Irrigation on Warm Season Precipitation in the Southern Great Plains. *Journal of Climate and Applied Meteorology*, **23,** 865-888.

Betts, R. A., P. M. Cox, S. E. Lee, and F. I. Woodward, 1997: Contrasting physiological and structural vegetation feedbacks in climate change simulations. *Nature*, **387,** 796-799.

Bisselink, B., and A. J. Dolman, 2008: Precipitation Recycling: Moisture Sources over Europe using ERA-40 Data. *J Hydrometeorol*, **9,** 1073-1083.

Bosilovich, M. G., and S. D. Schubert, 2001: Precipitation recycling over the central United States diagnosed from the GEOS-1 Data Assimilation System. *J Hydrometeorol*, **2,** 26-35.

Boucher, O., G. Myhre, and A. Myhre, 2004: Direct human influence of irrigation on atmospheric water vapour and climate. *Climate Dynamics*, **22,** 597-603.

Brubaker, K. L., D. Entekhabi, and P. S. Eagleson, 1993: Estimation of Continental Precipitation Recycling. *J Climate*, **6,** 1077-1089.

Brubaker, K. L., P. A. Dirmeyer, A. Sudradjat, B. S. Levy, and F. Bernal, 2001: A 36-yr climatological description of the evaporative sources of warm-season precipitation in the Mississippi River basin. *J Hydrometeorol*, **2,** 537-557.

Changnon, S. A., 2001: Thunderstorm rainfall in the conterminous United States. *B Am Meteorol Soc*, **82,** 1925-1940.

Chen, F., and J. Dudhia, 2001: Coupling an advanced land surface-hydrology model with the Penn State-NCAR MM5 modeling system. Part I: Model implementation and sensitivity. *Mon Weather Rev*, **129,** 569-585.

Chen, F., K. W. Manning, D. N. Yates, M. A. LeMone, S. B. Trier, R. Cuenca, and D. Niyogi, 2004: Development of high resolution land data assimilation system and its application to WRF. *16th Conf. on Numerical Weather Prediction*, A. M. Soc., Ed.

De Ridder, K., and H. Gallee, 1998: Land surface-induced regional climate change in southern Israel. *J Appl Meteorol*, **37,** 1470-1485.

DeAngelis, A., F. Dominguez, Y. Fan, A. Robock, M. D. Kustu, and D. Robinson, 2010: Evidence of enhanced precipitation due to irrigation over the Great Plains of the United States. *J Geophys Res-Atmos*, **115,** 1-14.

Dirmeyer, P. A., and K. L. Brubaker, 1999: Contrasting evaporative moisture sources during the drought of 1988 and the flood of 1993. *J Geophys Res-Atmos*, **104,** 19383-19397.

Dirmeyer, P. A., and K. L. Brubaker, 2007: Characterization of the global hydrologic cycle from a back-trajectory analysis of atmospheric water vapor. *J Hydrometeorol*, **8,** 20-37.

Dirmeyer, P. A., C. A. Schlosser, and K. L. Brubaker, 2009: Precipitation, Recycling, and Land Memory: An Integrated Analysis. *J Hydrometeorol*, **10,** 278-288.

Dominguez, F., P. Kumar, X. Z. Liang, and M. F. Ting, 2006: Impact of atmospheric moisture storage on precipitation recycling. *J Climate*, **19,** 1513-1530.

Eltahir, E. A. B., and R. L. Bras, 1994: Precipitation Recycling in the Amazon Basin. *Quarterly Journal of the Royal Meteorological Society*, **120,** 861-880.

Friedl, M., and Coauthors, 2002: Global land cover mapping from MODIS: algorithms and early results. *Remote Sens Environ***,** 287-302.

Gregory, J. M., J. F. B. Mitchell, and A. J. Brady, 1997: Summer drought in northern midlatitudes in a time-dependent CO2 climate experiment. *J Climate*, **10,** 662-686.

Hong, S. B., V. Lakshmi, E. E. Small, F. Chen, M. Tewari, and K. W. Manning, 2009: Effects of vegetation and soil moisture on the simulated land surface processes from the coupled WRF/Noah model. *J Geophys Res-Atmos*, **114,** D18118.

Hutson, S. S., N. L. Barber, J. F. Kenny, K. S. Linsey, D. S. Lumia, and M. A. Maupin, 2004: Estimated Use of Water in the United States in 2000.

IPCC, 2007: Climate Change 2007: The Physical Science Basis. Contribution of Working Group I to the Fourth Assessment Report of the Intergovernmental Panel on Climate Change.

Jacquemin, B., and J. Noilhan, 1990: Sensitivity Study and Validation of a Land Surface Parameterization Using the Hapex-Mobilhy Data Set. *Bound-Lay Meteorol*, **52,** 93-134.

Jódar, J., J. Carrera, and A. Cruz, 2010: Irrigation enhances precipitation at the mountains downwind. *Hydrol Earth Syst Sc*, **14,** 2003-2010.

Koster, R. D., and Coauthors, 2004: Regions of strong coupling between soil moisture and precipitation. *Science*, **305,** 1138-1140.

Kueppers, L. M., M. A. Snyder, and L. C. Sloan, 2007: Irrigation cooling effect: Regional climate forcing by land-use change. *Geophysical Research Letters*, **34,** L03703.

Kumar, S., 2007: Fourth assessment report of the Intergovernmental Panel on Climate Change: Important observations and conclusions. *Curr Sci India*, **92,** 1034-1034.

Lee, E., W. Sacks, T. Chase, and J. Foley, 2011: Simulated impacts of irrigation on the atmospheric circulation over Asia. *J Geophys Res-Atmos***,** D08114.

Lin, Y., and K. Mitchell, 2005: The NCEP stage II/IV hourly precipitation analyses: Development and applications. *19th Conference on Hydrology*, San Diego, CA, American Meteorological Society.

Lobell, D. B., G. Bala, and P. B. Duffy, 2006: Biogeophysical impacts of cropland management changes on climate. *Geophysical Research Letters*, **33,** L06708.

Lobell, D. B., C. J. Bonfils, L. M. Kueppers, and M. A. Snyder, 2008: Irrigation cooling effect on temperature and heat index extremes. *Geophysical Research Letters*, **35,** L09705.

Mahmood, R., K. G. Hubbard, and C. Carlson, 2004: Modification of growing-season surface temperature records in the northern Great Plains due to land-use transformation: Verification of modelling results and implication for global climate change. *Int J Climatol*, **24,** 311-327.

Mahmood, R., S. A. Foster, T. Keeling, K. G. Hubbard, C. Carlson, and R. Leeper, 2006: Impacts of irrigation on 20th century temperature in the northern Great Plains. *Global Planet Change*, **54,** 1-18.

Manabe, S., R. Wetherald, P. Milly, T. Delworth, and R. Stouffer, 2004: Century-scale change in water availability: CO2-quadrupling experiment. *Climatic Change***,** 59-76.

McGuire, V. L., 2007: Water-Level Changes in the High Plains Aquifer, Predevelopment to 2005 and 2003 to 2005: U.S. Geological Survey Scientific Investigations Report 2006-5324, 7 pp.

McGuire, V. L., M. R. Johnson, R. L. Schieffer, J. S. Stanton, S. K. Sebree, and I. M. Verstraeten, 2003: Water in Storage and Approaches to Ground-Water Management, High Plains Aquifer, 2000. U. S. G. S. C. 1243, Ed., 51 p.

Merrill, J., and R. Bleck, 1986: Isentropic Trajectory Analysis of Long-Range Transport over the Pacific. *Atmos Environ*, **20,** 2072-2073.

Merrill, J. T., R. Bleck, and D. Boudra, 1986: Techniques of Lagrangian Trajectory Analysis in Isentropic Coordinates. *Mon Weather Rev*, **114,** 571-581.

Mesinger, F., and Coauthors, 2006: North American regional reanalysis. *B Am Meteorol Soc*, **87,** 343-360.

Moore, N., and S. Rojstaczer, 2001: Irrigation-induced rainfall and the great plains. *J Appl Meteorol*, **40,** 1297-1309.

NASS, 2002: 2002 Census of Agriculture - Volume 1 - Geographic Area Series - Farm & Ranch Irrigation Survey.

Noilhan, J., and S. Planton, 1989: A Simple Parameterization of Land Surface Processes for Meteorological Models. *Mon Weather Rev*, **117,** 536-549.

Ozdogan, M., and G. Gutman, 2008: A new methodology to map irrigated areas using multi-temporal MODIS and ancillary data: An application example in the continental US. *Remote Sens Environ*, **112,** 3520-3537.

Ozdogan, M., M. Rodell, H. K. Beaudoing, and D. L. Toll, 2010: Simulating the Effects of Irrigation over the United States in a Land Surface Model Based on Satellite-Derived Agricultural Data. *J Hydrometeorol*, **11,** 171-184.

Pielke, R. A., 2001: Influence of the spatial distribution of vegetation and soils on the prediction of cumulus convective rainfall. *Reviews of Geophysics*, **39,** 151-177.

Pielke, R. A., T. J. Lee, J. H. Copeland, J. L. Eastman, C. L. Ziegler, and C. A. Finley, 1997: Use of USGS-provided data to improve weather and climate simulations. *Ecol Appl*, **7,** 3-21.

Puma, M. J., and B. I. Cook, 2010: Effects of irrigation on global climate during the 20th century. *J Geophys Res-Atmos*, **115,** D16120.

Rasmusson, E. M., 1968: Atmospheric Water Vapor Transport and the Water Balance of North America. Part 2. Large-scale water balance investigations. *Mon Weather Rev*, **96,** 720-734.

Rind, D., R. Goldberg, J. Hansen, C. Rosenzweig, and R. Ruedy, 1990: Potential Evapotranspiration and the Likelihood of Future Drought. *J Geophys Res-Atmos*, **95,** 9983-10004.

Sacks, W. J., B. I. Cook, N. Buenning, S. Levis, and J. H. Helkowski, 2009: Effects of global irrigation on the near-surface climate. *Climate Dynamics*, **33,** 159-175.

Segal, M., Z. Pan, R. W. Turner, and E. S. Takle, 1998: On the potential impact of irrigated areas in North America on summer rainfall caused by large-scale systems. *J Appl Meteorol*, **37,** 325-331.

Skamarock, W. C., and Coauthors, 2008: A description of the Advanced Research WRF version 3.

Trenberth, K. E., A. Dai, R. M. Rasmussen, and D. B. Parsons, 2003: The changing character of precipitation. *B Am Meteorol Soc*, **84,** 1205-1217.

Twine, T. E., and Coauthors, 2000: Correcting eddy-covariance flux underestimates over a grassland. *Agricultural and Forest Meteorology*, **103,** 279-300.

Verma, S., and Coauthors, 2005: Annual carbon dioxide exchange in irrigated and rainfed maize-based agroecosystems. *Agricultural and Forest Meteorology***,** 77-96.

Wang, G., 2005: Agricultural drought in a future climate: results from 15 global climate models participating in the IPCC 4th assessment. *Climate Dynamics***,** 739-753.

Weaver, S. J., S. Schubert, and H. Wang, 2009: Warm Season Variations in the Low-Level Circulation and Precipitation over the Central United States in Observations, AMIP Simulations, and Idealized SST Experiments. *J Climate*, **22,** 5401-5420.

Wetherald, R. T., and S. Manabe, 1995: The mechanisms of summer dryness induced by greenhouse warming. *J Climate*, **8,** 3096-3108.

Wetherald, R. T., and S. Manabe, 1999: Detectability of summer dryness caused by greenhouse warming. *Climatic Change*, **43,** 495-511.

Wilson, K., and Coauthors, 2002: Energy balance closure at FLUXNET sites. *Agricultural and Forest Meteorology*, **113,** 223-243.

Wolter, K., and M. S. Timlin, 1998: Measuring the strength of ENSO events - how does 1997/98 rank? *Weather*, **53,** 315-324.

Zangvil, A., D. H. Portis, and P. J. Lamb, 2004: Investigation of the large-scale atmospheric moisture field over the Midwestern United States in relation to summer precipitation. Part II: Recycling of local evapotranspiration and association with soil moisture and crop yields. *J Climate*, **17,** 3283-3301.